


August 2015

Tunable Photonic Multilayers from Stimulus-Responsive, Photo-Crosslinkable Polymers

Maria C. Chiappelli
University of Massachusetts - Amherst

Follow this and additional works at: https://scholarworks.umass.edu/dissertations_2

 Part of the [Materials Chemistry Commons](#), [Nanoscience and Nanotechnology Commons](#), [Polymer and Organic Materials Commons](#), and the [Polymer Chemistry Commons](#)

Recommended Citation

Chiappelli, Maria C., "Tunable Photonic Multilayers from Stimulus-Responsive, Photo-Crosslinkable Polymers" (2015). *Doctoral Dissertations*. 353.
https://scholarworks.umass.edu/dissertations_2/353

This Open Access Dissertation is brought to you for free and open access by the Dissertations and Theses at ScholarWorks@UMass Amherst. It has been accepted for inclusion in Doctoral Dissertations by an authorized administrator of ScholarWorks@UMass Amherst. For more information, please contact scholarworks@library.umass.edu.

**TUNABLE PHOTONIC MULTILAYERS FROM STIMULUS-RESPONSIVE,
PHOTO-CROSSLINKABLE POLYMERS**

A Dissertation Presented

By

Maria C. Chiappelli

Submitted to the Graduate School of the
University of Massachusetts Amherst in partial fulfillment
of the requirements for the degree of

DOCTOR OF PHILOSOPHY

May 2015

Polymer Science and Engineering

© Copyright by Maria C. Chiappelli
2015
All Rights Reserved

**TUNABLE PHOTONIC MULTILAYERS FROM STIMULUS-RESPONSIVE,
PHOTO-CROSSLINKABLE POLYMERS**

A Dissertation Presented

By

MARIA C. CHIAPPELLI

Approved as to style and content by:

Ryan C. Hayward, Chair

Kenneth R. Carter, Member

Anthony D. Dinsmore, Member

David Hoagland, Department Head
Polymer Science and Engineering

DEDICATION

To my parents, John and JoAnn Chiappelli.

ACKNOWLEDGEMENTS

I would like to express my sincere gratitude to my thesis advisor, Professor Ryan Hayward, for his endless scientific guidance throughout my Ph.D. Thanks to his genuine commitment to advancing science and encouragement to discuss and explore, I have grown to be a better scientist than I would have thought possible. I would like to express my thanks to Professor Kenneth Carter and Professor Anthony Dinsmore for being active members of my committee and for their constructive advice and support over the entire duration of my Ph.D. I would also like to acknowledge the faculty and staff in the Polymer Science and Engineering Department for their excellent teaching, insight and advice. Many thanks especially to Lisa Groth, Sophia Hsu, Maria Farrington, Alyssa Kristek and Lisa McNamara for their invaluable administrative assistance and kindness.

I would like to express my great appreciation to Dr. Alexander Ribbe, Louis Raboin, Dr. Sekar Thirunavukkarasu and Jacob Hirsch for their experimental assistance, our many fruitful conversations and their genuine interest in my thesis work.

I would like to acknowledge the funding agencies which supported the work presented in this thesis: Defense Threat Reduction Agency (Award #HDTRA1-10-1-0099) and NSF Materials Research Facilities Network (DMR-1121053).

I would like to specifically thank my co-workers and collaborators both for work that directly contributed to this thesis and for helpful conversations: Dr. Scott Christensen, Dr. Cheol Hee Lee, Dr. Thomas Mates, Adam Hauser and, of course, Prof. Jinhwan Yoon, an excellent mentor and teacher. I will be forever grateful for the mentorship of my undergraduate research advisor, Prof. John McMahon. I would like to thank all the Hayward group members, past and present, for their support and friendship

along the way; I wish you all great happiness in your futures. Personal thanks especially for the friendships of former group members Dr. Felicia Bokel, Dr. Scott Christensen and Dr. Dayong Chen...wonderful scientists, dear friends and truly good people. I would like to thank my fellow classmates and all of my friends in and out of the department. Particularly to the Class of 2009, I thank you for the ever-present support and friendship as we traveled this journey together through many shared difficulties and accomplishments.

I am especially thankful for the friendships of Rachel Letteri, Armagan Bayram, Polina Ware, Jinhye Bae “JB”, Yujie Liu, Xiaobo Shen, Catherine Walker, Anesia Auguste, Daniel King, Jon Pham, Angela Cugini, and Guler Yavuz; I could not have imagined a better group of people to share these past several years with, and I know no amount of distance will lessen the strength of our friendships. Special thanks to our “Farm-Share Group”: Yujie Liu, Daniel King and Jon Pham for such great memories cooking and eating together and, most importantly, their invaluable friendship and companionship in times of struggle and celebration. Thank you, Irem Bolukbasi, for being a true best friend and most kind-hearted person from the very first day of our graduate school adventure. Thank you to Rabeka Alam, a fellow Fordham alum, graduate school comiserator and life-long friend. I am also grateful for the friendship of Phil Pineau, Katie Leonard, Kristen Malesardi, Brittany Vellucci, Marie Vitello and Lauren Linnell; supporting each other through each new phase of life.

I would like to thank my family, my mom JoAnn Chiappelli, my dad John Chiappelli, and my sister (and friend), Adriana Chiappelli, for their unconditional love, strength and support through all of my endeavors in life, and especially over the past 5

years; without you I could never have journeyed to this point. I am blessed to have these people in my life, and there are simply no words to capture what they mean to me. I would also like to acknowledge the love and support of my grandma, Josephine Cavallo, and my uncle, Frank Ferrante. To my grandparents, Nedo Chiappelli and Ada Chiappelli, though no longer with us on Earth, their strength, perseverance and love is always with me. Finally, endless gratitude and love for our dog, Chex, my lovable “little pup”, always there to happily welcome me home.

ABSTRACT

TUNABLE PHOTONIC MULTILAYERS FROM STIMULUS-RESPONSIVE, PHOTO-CROSSLINKABLE POLYMERS

MAY 2015

MARIA C. CHIAPPELLI, B.S., FORDHAM UNIVERSITY

M.S., UNIVERSITY OF MASSACHUSETTS AMHERST

PH.D., UNIVERSITY OF MASSACHUSETTS AMHERST

Directed by: Professor Ryan C. Hayward

This dissertation describes the synthesis of photo-crosslinkable copolymers and their utilization for the fabrication and testing of tunable and responsive one-dimensional (1D) photonic multilayers. Photonic multilayers exhibit structural color due to the interference of incident light at layer interfaces, providing a convenient route towards optically responsive materials that do not rely on potentially light- or oxygen-sensitive chromophore-containing pigments and dyes. A fabrication technique based on sequential spin-coating and crosslinking of photo-crosslinkable polymers is used to assemble tunable and responsive photonic multilayers.

Chapter One introduces the fundamental underlying principles of 1D photonic structures and explores their importance in a variety of areas, including sensors, responsive films, as well as the necessity of their optimization through routes such as the incorporation of nanocomposites for enhanced refractive index. This chapter also details the experimental approach used here for fabricating tunable and responsive 1D photonic multilayers utilizing sequential spin-coating and crosslinking of photo-crosslinkable polymers. Chapter Two describes the use of these multilayer photonic films as

thermochromic materials using poly(N-isopropylacrylamide) (PNIPAM) as the low-refractive index, stimulus responsive layers and poly(*p*-methyl styrene) (PpMS) as the high-refractive index, hydrophobic layers. Temperature is utilized as an analyte to validate this platform as a feasible and flexible approach for the fabrication of a variety of tunable and responsive structures. Building upon the knowledge developed in Chapters 1 and 2, this photonic sensing platform is next expanded to detect additional analytes and further optimize sensor performance by improving reflectance efficiency, response and exploring various multilayer geometries and arrays. Chapter 3 describes the utilization of polymeric photonic multilayers for colorimetric sensing of ionizing radiation. Chapter 4 explores a method of enhancing the reflectance efficiency of multilayers through the incorporation of high refractive index zirconia nanoparticles. The utilization of nanoparticles also enables the fabrication of all-gel multilayers for flexible, potentially mechanochromatic, photonic materials by eliminating the necessity of the high refractive index, but brittle, PpMS. Chapter 5 explores in detail the kinetic response of photonic multilayers with a variety of responsive polymer materials during the swelling and de-swelling phases. Chapter 6 details how this approach can be expanded to create new multilayer geometries, including Bragg filters, as well as multifunctional sensors and arrays on a single substrate. Chapter 7 introduces preliminary work studying the electrochromic response of photonic multilayers. Applied voltage triggers the reversible de-swelling of the responsive layers and subsequently a blue-shift in the wavelength of reflected light. Finally, Chapter 8 provides a summary of this dissertation and proposes future directions for photonic polymer multilayers.

TABLE OF CONTENTS

	Page
ACKNOWLEDGEMENTS.....	v
ABSTRACT.....	viii
LIST OF TABLES.....	xiii
LIST OF FIGURES.....	xiv
LIST OF SCHEMES.....	xviii
CHAPTER	
1. INTRODUCTION.....	1
1.1 Photonic crystals and responsive materials.....	1
1.1.1 Overview of 1-dimensional photonic structures.....	1
1.1.2 Approaches in literature.....	2
1.2 Experimental approach.....	6
1.2.1 1-dimensional responsive photonic crystal fabrication.....	6
1.2.2 Photochemistry of benzophenone.....	8
1.3 References.....	10
2. THERMOCHROMIC PHOTONIC MULTILAYERS.....	14
1.1 Introduction and design.....	14
1.2 Experimental methods.....	15
1.2.1 Materials.....	15
1.2.2 Polymer and monomer synthesis.....	16
1.2.3 Sample preparation and analysis.....	17
1.2.4 Sensor fabrication.....	17
1.2.5 Instruments and measurements.....	18
1.2.6 Reflectance calculations.....	19
1.3 Temperature responsive swelling and reversibility.....	20
1.4 Kinetics.....	22
1.5 Structure analysis.....	24

1.5.1	Interfacial & surface characterization.....	24
1.6	Comparison to reflectivity calculations.....	27
1.7	Conclusions.....	29
1.8	References.....	30
3.	COLORIMETRIC RADIATION SENSING USING PHOTONIC POLYMER MULTILAYERS.....	32
3.1	Introduction.....	32
3.1.2	Approaches in literature.....	32
3.2	Experimental methods.....	35
3.2.1	Polymer synthesis.....	35
3.3	Sensor preparation and characterization.....	36
3.4	Results and discussion.....	38
3.5	Conclusions and future outlook.....	43
3.6	References.....	44
4.	NANOCOMPOSITE POLYMER FILMS AND PHOTONIC MULTILAYERS WITH ENHANCED REFLECTANCE EFFICIENCY.....	46
4.1	Introduction.....	46
4.2	Experimental methods.....	50
4.2.1	Polymer synthesis.....	50
4.2.2	Photonic multilayer preparation and characterization.....	51
4.2.3	Reflectance calculations.....	53
4.3	Results and discussion.....	53
4.4	Conclusions and outlook.....	60
4.5	References.....	61
5.	KINETIC RESPONSE OF PHOTONIC POLYMER MULTILAYERS.....	63
5.1	Introduction.....	63
5.2	Experimental methods.....	65
5.3	Results and discussion.....	67
5.4	Conclusions and future outlook.....	75

5.5 References.....	76
6. NEW GEOMETRIES AND SENSOR DESIGNS: DYNAMIC FILTERS, MIRRORS AND ARRAYS.....	78
6.1 Introduction and motivation.....	78
6.2 Experimental methods.....	80
6.3 Results and discussion.....	82
6.3.1 Demonstration of tunable Bragg filter.....	82
6.3.2 Multifunctional sensors and arrays.....	83
6.4 Conclusions and future directions.....	86
6.5 References.....	87
7. ELECTROCHROMIC RESPONSE OF PHOTONIC MULTILAYER FILMS.....	89
7.1 Introduction and motivation.....	89
7.2 Experimental methods.....	91
7.3 Results and discussion.....	92
7.4 Conclusions and future directions.....	97
7.5 References.....	98
8. SUMMARY AND OUTLOOK.....	100
BIBLIOGRAPHY.....	102

LIST OF TABLES

Table	Page
Table 3.1 Electron-beam irradiation processing applications. Table reproduced and modified from E-Beam Services, Inc.....	34
Table 5.1 Range of swelling for non-charge containing responsive multilayers, from $\lambda_{\max}(\text{dry})$ to $\lambda_{\max}(\text{swell, RT water})$	67
Table 5.2 Time constants for λ_{\max} vs. time curves best fit with either a single or bi-exponential.....	71

LIST OF FIGURES

Figure	Page
Figure 1.1 1-D photonic multilayer (left) with alternating layers of high (red) and low (blue) refractive indices reflect a characteristic wavelength of light, or Bragg peak, (right).....	2
Figure 1.2 Design of 3-D responsive photonic gels by Asher and co-workers which rely on analyte-induced changes in d-spacing of a crystalline colloidal array in a gel matrix (a) to shift the wavelength of reflected light (b). Figure reproduced and modified with permission from Ref. 9, 13.....	3
Figure 1.3 1-D responsive photonic structures by Thomas and co-workers rely on the self-assembly of (a) a hydrophobic-block-hydrophilic polyelectrolyte block copolymer to access b) the full range of the visible spectrum. Figure reproduced and modified with permission from Ref. 14, 19.....	4
Figure 1.4 Figure shows (left) sequential deposition of nanoparticles by Miguez and co-workers used to fabricate 1-D photonic multilayers with (b) reflectance peaks responsive to solvent analytes. Figure reproduced and modified with permission from Ref. 27.....	5
Figure 2.1 Structures of polymers used in thermochromic photonic multilayers.....	14
Figure 2.2 Peak reflectance wavelength (left) and photographs of sensors (right) swelled in water show clear colorimetric changes with temperature.....	20
Figure 2.3 Reflectance spectra during a series of 5 cycles of (a) heating to 50 °C to de-swell and (b) cooling to 20 °C to re-swell the multilayer.....	21
Figure 2.4 (a) Multiple cycles of swelling/de-swelling induced by rapid switching of temperature between 20 and 50°C show the sensor response is highly reproducible. (b) An enlargement of a single swelling/de-swelling cycle, as denoted by the box in (a), along with comparison of multilayer swelling in c) water and ethanol.....	22
Figure 2.5 d-SIMS analysis of deuterium ($m/z = 2.1$) and cyano ($m/z = 26$) signals for 6 layer alternating PpMS/PNIPAM films reveal excellent layer uniformity and minimal interfacial broadening.....	25
Figure 2.6 d-SIMS analysis of deuterium ($m/z = 2.1$) and cyano ($m/z = 26$) signals from a two-layer sample (PpMS, PNIPAM) on Si prepared from (a, left) pyridine, a good solvent for both polymers and (b, left) from selective solvents, as in the main text, with interfacial widths of 10 nm and 20 nm, respectively. AFM height images (right) of a) PpMS ($R_{\text{rms}} = 0.346$ nm), PNIPAM (0.648 nm), c) 4 layers (0.478 nm) and d) 6 layers (0.563 nm). Scale bars are 500 nm.....	26

Figure 2.7 Comparison of experimental (a) and calculated (b) reflectance curves at various degrees of swelling with temperature shows c) high reflectance efficiency of thermochromic materials compared to the ideal case.....	28
Figure 2.8 Volume fraction of polymer with temperature at various degrees of swelling used to calculate reflectance.....	29
Figure 3.1 Chemical structures of responsive materials a) P(OEGMA-BP) and b) P(MMA-BP) and c) schematic of multilayer radiation exposure setup and dimensions.....	35
Figure 3.2 Optical micrographs of swelled multilayers after exposure to radiation within the regions denoted by the dotted square for preferentially a) crosslinking and d) degrading systems. Corresponding reflectance spectra show a c) blue shift and f) red shift from the unexposed areas (b, e) of the crosslinked and degraded sensors, respectively, upon swelling.....	40
Figure 3.3 Graphs showing change in peak wavelength of reflected light with increasing radiation dose demonstrating a blue-shift for a) a preferentially crosslinking sensor and a red-shift for b) a preferentially degrading sensor. Data shown is a representative sample of sensor response with error bars depicting typical uncertainty in λ_{\max} , $\pm 0.5\%$ and $\pm 1\%$, respectively.....	41
Figure 3.4 Reflectance spectrum of a 7-layer flexible sensor with a photograph (inset) showing the flexibility of such a multilayer fabricated on a Mylar sheet.....	42
Figure 4.1 Tunability of refractive index of both a) hydrophobic PpMS and b) hydrophilic PNIPAM is achieved by adjusting weight % of zirconia.....	54
Figure 4.2 a) Experimental spectra showing enhanced reflectance of photonic multilayers with particles (solid line) versus without (dashed line) and supported by b) calculated reflectance spectra based on the experimental thickness and refractive index parameters for each system. AFM images reveal d) nanocomposite films maintain homogeneity with minimal increase in surface roughness compared to c) polymer-only film. Scale bar = 5 μm	55
Figure 4.3 Blue shift of reflected light with increasing temperature observed for both a) P(pMS-BP) + 70 wt% ZrO ₂ /P(NIPAM-BP)-based nanocomposite multilayer and b) P(pMS-BP)/P(NIPAM-BP) polymer-only based multilayers in deionized water, and c) reflectance spectra at comparable degrees of swelling showing enhanced intensity of composite multilayer (solid line) versus polymer-only multilayer (dashed line). Data plotted in a,b are λ_{\max} of primary reflectance peak, $m = 1$, calculated based on the higher order harmonics, $m = 2$, if $m = 1$ was not visible in the accessible spectral range of the instrument during experiment.....	56

Figure 4.4 Reflectance spectra of an all-gel P(NIPAM-BP)-based composite photonic multilayer in the dry state. b) Plot showing blue shift of reflected light with increasing temperature for all-gel composite immersed in deionized water. $m = 2,3,4$ corresponds to the harmonic used to calculate λ_{\max} of primary peak, $m = 1$. Data plotted are λ_{\max} of primary reflectance peak, $m = 1$, calculated based on c) the higher order harmonics, $m = 2,3,4$, visible in d) the accessible spectral range of the instrument during experiment.....	58
Figure 5.1 Chemical structures of responsive monomers used for kinetics studies of temperature sensitive systems.....	66
Figure 5.2 Monitoring change in λ_{\max} for multilayers of equivalent optical thickness with different temperature responsive layers based on, P(NIPAM-BP), P(DEAM-BP) or P(OEGMA-BP), swelled in deionized water from the dry state.....	69
Figure 5.3 a) Reflectance spectra of P(NIPAM-BP)-based multilayer swelling in water at room temperature. For analysis of initial swelling at shorter time scales, b) transmittance spectra of swelling P(NIPAM-5%AAc-1%BP)-based multilayer are shown. A well-defined characteristic Bragg peak is observed at all time points, which is red-shifted with increasing degree of swelling.....	70
Figure 5.4 a) Monitoring swelling of λ_{\max} with time in various salt concentrations and b) corresponding time constants for kinetic data best fit with either a single or bi-exponential shows fast kinetic response which slows with increasing salt concentration.....	72
Figure 5.5 Optical profilometry showing the surface morphology of a de-swelling P(OEGMA)-based multilayer. Similar delamination scars are evident on a dried P(SPMA)-based multilayer (bottom left).....	74
Figure 6.1 Schematic of a Bragg filter geometry (left) and a dynamic mirror-filter multilayer achieved by tuning the chemistry of the central layer to selectively swell (mirror, center) or de-swell (filter, right) in response to a particular analyte.....	78
Figure 6.2 Demonstration of a Bragg filter with a high refractive index central cavity layer. The filter character is retained with swelling, and the transmittance peak shifts with swelling of the P(NIPAM-BP) responsive layers in room temperature water.....	82
Figure 6.3 Reflectance spectra showing the transition from filter to mirror with increasing salt concentration from a) DI water, b) 0.05 M, c) 0.3 M to d) 4M.....	83
Figure 6.4 a) Structure of polyelectrolyte, P(SPMS-BP), used as b) a salt-sensitive material for multilayers with c) rapid response time through the visible spectrum.....	84

Figure 6.5 Structure of a) neutral and b) MPC-containing PNIPAM. Addition of zwitterionic MPC c) enhances the degree of swelling two-fold d) without imparting any salt sensitivity to multilayers when swelled in up to 100 mM salt.....	85
Figure 6.6 Two sensors patterned in parallel on a single substrate are Bragg mirrors in the dry state (solid lines) and transition to a filter (left) or mirror (right) with a design wavelength of 550 nm upon swelling in water.....	86
Figure 7.1 Demonstration of photonic multilayers successfully fabricated and swelled on silane-treated ITO substrate with well defined reflectance peaks and no evidence of delamination.....	92
Figure 7.2 Reflectance spectra reveal multilayers fabricated on ITO do demonstrate a reversible blue-shift in λ_{max} under an applied voltage of 3V, indicating the voltage-induced de-swelling of P(NIPAM-AAc-BP) layers in the film stack.....	93
Figure 7.3 a) Reversibility of electrochromic behavior where 3V triggers a blue-shift in the “on” state with b) typical equilibration times for “on” and “off” cycles on the order of tens of minutes.....	94
Figure 7.4 a) Reflectance spectra reveal faster swelling in regions to which voltage was previously applied according to the setup in b). After voltage-cycling, swelling of the previously cycled region shows fast kinetics, displaying a further red-shift (yellow color) than the outside region (blue-green) not previously cycled.....	96

LIST OF SCHEMES

Scheme	Page
Scheme 1.1 Multilayer fabrication based on sequential spin-coating, crosslinking and developing of alternating layers of high and low refractive index polymers.....	6
Scheme 1.2 Synthetic route for copolymerization of BP by conventional free-radical polymerization.....	7
Scheme 1.3 Reaction scheme of photo-excitation of benzophenone followed by H-abstraction and subsequent radical recombination.....	8
Schematic 1.4 Synthesis of acrylamidobenzophenone from acryloyl chloride and 4-aminobenzophenone.....	9
Scheme 4.5 Nanocomposite photonic multilayer schematic of PNIPAM-based multilayers with a) P(pMS-BP) + 70 wt% zirconia and b) P(NIPAM-BP) + 85 wt% zirconia as the high-refractive index layers.....	50

CHAPTER 1

INTRODUCTION

1.1 Photonic crystals and responsive materials

1.1.1 Overview of 1-dimensional photonic structures

Photonic materials, which consist of two different dielectric materials arranged periodically in one or more dimensions, offer many opportunities for controlling the propagation of light.¹ The simplest case of a photonic structure is that of a Bragg mirror, where alternating layers of high and low-refractive index materials are arranged in a periodic one-dimensional (1D) stack. Light in a certain wavelength range is reflected by constructive interference at each interface, with maximum reflectance when the optical thickness of each layer is one quarter of the wavelength of light, as in a quarter-wave film stack, according to the following¹⁻³:

$$n_h d_h = n_l d_l = \frac{\lambda_0}{4} \quad 1.1$$

The intensity of the Bragg peak reflected from this period stack can be increased by increasing the number of layers in the stack or by increasing the refractive index contrast between layers.

An area of particular interest is the use of photonic crystals for responsive materials.⁴⁻⁶ Such devices are typically designed such that the analyte alters the domain spacing and/or refractive index of one component of the photonic material, thereby shifting the wavelength and intensity of reflected or diffracted light. A reliance on purely structural color provides photonic materials with a unique advantage over many existing colorimetric detection techniques which rely on light- or oxygen-sensitive chromophores

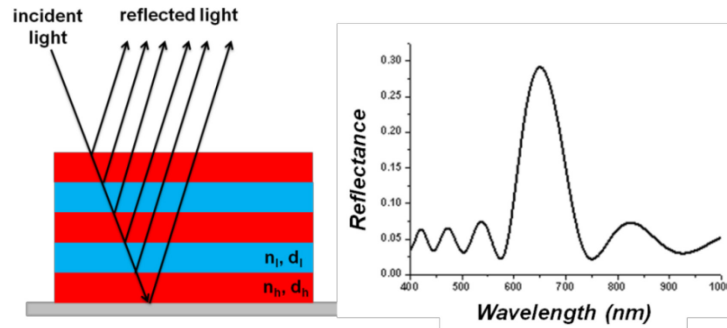


Figure 1.1 1-D photonic multilayer (left) with alternating layers of high (red) and low (blue) refractive indices reflect a characteristic wavelength of light, or Bragg peak, (right).

and thus may often require stringent storage and containment conditions and have a limited shelf-life. Pioneering work in photonic sensing utilized three-dimensional (3D) structures, periodic in three directions, and is of great significance to the field. In comparison to their 3D counterparts, 1D photonic crystals, the focus of this work, offer several advantages as responsive materials, including simplicity of fabrication, reduced directional sensitivity in their optical properties and the necessity to undergo dimensional changes in only one direction.

1.1.2 Approaches in literature

Asher and co-workers pioneered the concept of 3D photonic sensors based on diffraction from an ordered crystalline colloidal array embedded within analyte-responsive hydrogel matrices.⁷⁻¹³ The hydrogel matrix, functionalized with a responsive moiety, swells or de-swells in the presence of an external stimulus, causing the domain spacing of the colloidal array to expand or contract and thus the wavelength of diffracted light is red-shifted or blue-shifted, respectively. This concept has since been used to detect a range of stimuli including pH, ionic strength, temperature and specific biological

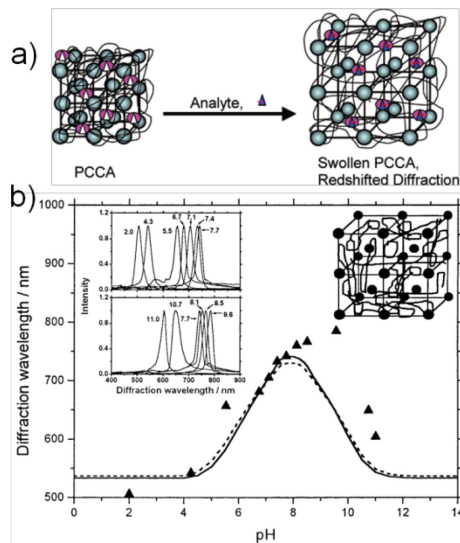


Figure 1.2 Design of 3-D responsive photonic gels by Asher and co-workers which rely on analyte-induced changes in d-spacing of a crystalline colloidal array in a gel matrix (a) to shift the wavelength of reflected light (b). Figure reproduced and modified with permission from Ref. 9, 13.

or chemical targets, with the general approach and example of pH sensitivity illustrated in Figure 1.2.

As discussed previously, 1D photonic crystals offer several advantages as sensors over the 3D case but to date have been explored to a lesser extent. Progress thus far can be classified into two main approaches; self-assembly of block copolymers and sequential layer deposition. Thomas and co-workers, have utilized the self-assembly of hydrophobic block-hydrophilic polyelectrolyte block copolymers into lamellar stacks with appropriate periodicities to reflect visible light, providing sensors for stimuli including humidity, salt, temperature and strain.^{14–19} The refractive index contrast is not sufficient to be visible in the dry state, however color becomes apparent upon the analyte-induced swelling, and subsequent decrease of the effective refractive index, of the hydrophilic block. While the use of a self-assembling block copolymer is attractive, the flexibility of this approach is limited by the need to synthesize a modest-to-high

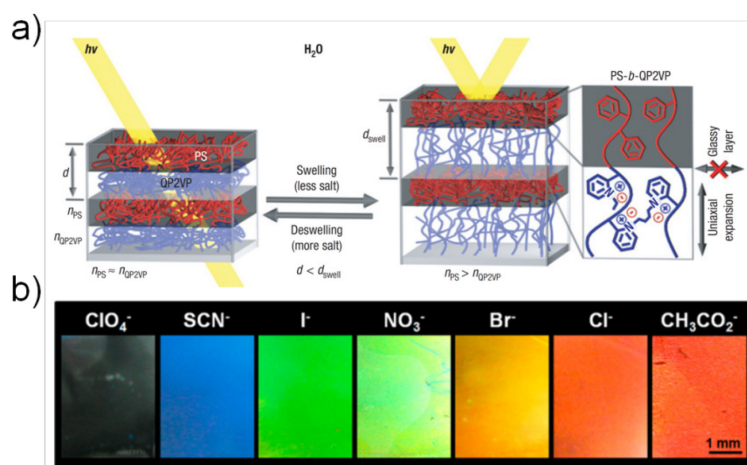


Figure 1.3 1-D responsive photonic structures by Thomas and co-workers rely on the self-assembly of (a) a hydrophobic-block-hydrophilic polyelectrolyte block copolymer to access b) the full range of the visible spectrum. Figure reproduced and modified with permission from Ref. 14, 19.

molecular weight block copolymer with appropriate stimuli-responsiveness for each sensor design. In addition, the covalent linkage between blocks makes it impossible to independently control the material properties or thickness of a single layer or selective number of layers.

A number of methods based on sequential layer deposition to yield 1D photonic structures have been previously described.^{20,21} For example, Ozin and co-workers^{22–26} and Míguez and co-workers^{27,28} have independently developed platforms based on spin-casting of nanoparticles to fabricate 1D photonic sensors. The use of metal oxide nanoparticles can provide enhanced refractive index contrast and subsequently 1D photonic structures with high reflectance intensity. However, in contrast to polymer multilayers, nanoparticle based approaches rely on changes in refractive index due to the

infiltration of an analyte into a porous layer network, rather than swelling of one of the layers, thus providing only modest shifts in the wavelength of peak reflection.

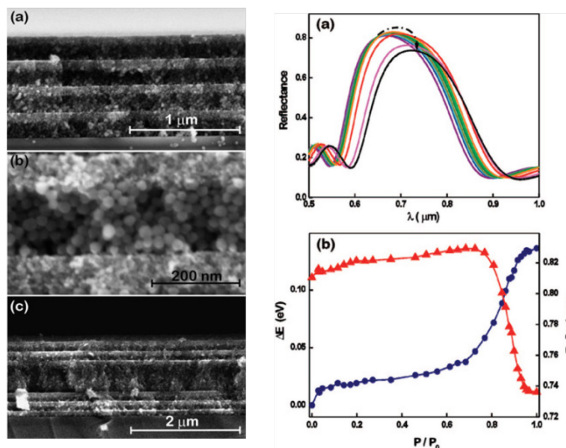


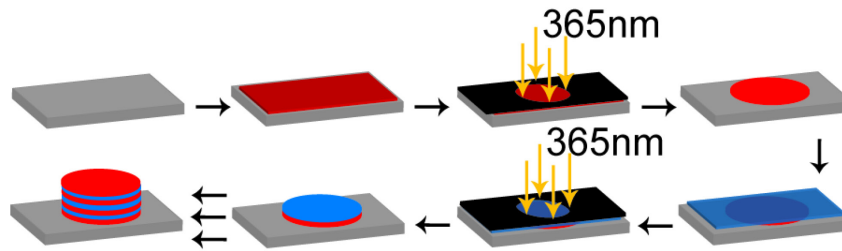
Figure 1.4 Figure shows (left) sequential deposition of nanoparticles by Miguez and co-workers used to fabricate 1-D photonic multilayers with (b) reflectance peaks responsive to solvent analytes. Figure reproduced and modified with permission from Ref. 27.

The approach detailed in this thesis involves photo-crosslinking utilizing benzophenone, discussed in more detail in the following section, to fabricate tunable and responsive photonic multilayers from sequentially spin-cast polymer films. This work serves to develop responsive photonic structures which possess both the high reflectance efficiency afforded by metal oxide particles and the dynamic breadth of accessible wavelengths afforded by a block-copolymer approach. We note that R uhe and co-workers have previously demonstrated a closely related approach to fabricate tunable Bragg mirrors and filters from polymer multilayers, though their work did not focus on responsive structures or sensor development.²¹

1.2 Experimental approach

1.2.1 1-D responsive photonic crystal fabrication

This work utilizes a facile approach to fabricating photonic multilayer sensors, whereby alternating layers of high- and low-refractive index photo-crosslinkable polymers are sequentially spin-cast, crosslinked and developed in a marginal solvent. The



Scheme 1.6 Multilayer fabrication based on sequential spin-coating, crosslinking and developing of alternating layers of high and low refractive index polymers.

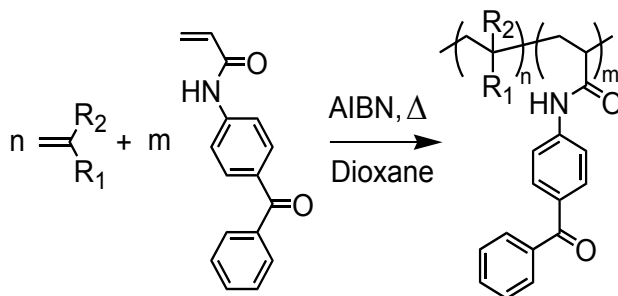
low refractive index layer is stimulus-responsive and will swell (or de-swell) in the presence of an analyte, altering the domain spacing of the multilayer and thus shifting the wavelength of reflected light. The preparation of multilayers is a robust technique and broadly applicable to a library of photo-crosslinkable polymers with sensitivities to a range of analytes. Appropriate layer thicknesses for each polymer, easily tuned from tens to hundreds of nanometers by varying the concentration of copolymer in solution and spin speed, are chosen to achieve a Bragg reflectance peak (λ_{\max}) within the visible range for light incident normal to the surface, according to:

$$\lambda_{\max} = 2(n_{\text{high}}d_{\text{high}} + n_{\text{low}}d_{\text{low}}) \quad 1.2$$

where n_{high} , d_{high} and n_{low} , d_{low} are the refractive indices and thicknesses of the high-refractive index, non-swelling layer and low-refractive index, stimulus-responsive layers, respectively.

This fabrication approach provides great flexibility over the wavelength range and sensitivity of the resulting sensors. The work described in Chapter 2 utilizes thermochromic multilayers to validate this approach as a straight-forward and robust method of making reversible and responsive polymer multilayers, and focuses specifically on the design of multilayers that cover the full visible spectrum for colorimetric read-out. This fabrication technique also allows the low index, stimuli responsive layer, to be easily interchanged or possibly combined to change the nature of the sensor simply by selecting from a library of previously synthesized copolymers.

In addition, as the only requirement is that the monomer can be readily



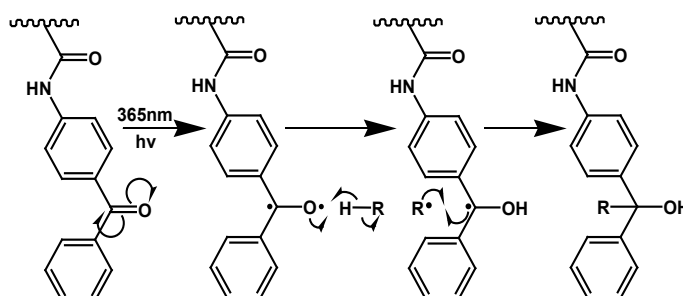
Scheme 1.7 Synthetic route for copolymerization of BP by conventional free-radical polymerization.

copolymerized by conventional free-radical polymerization with 1 to 10 mol% photo-crosslinker, acrylamidobenzophenone (BP), this technique can be applied to a broad range of materials even beyond the scope of the work presented herein. Subsequent chapters of this thesis explore the responsivity and tunability of photonic multilayers with

independent variations in thickness, chemistry and material properties of the high and low index layers.

1.2.2 Photochemistry of benzophenone

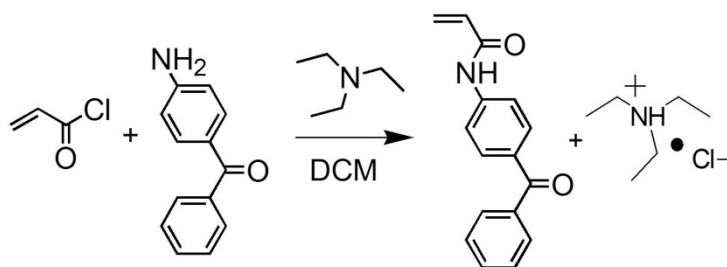
Covalently incorporating a photo-active moiety into a polymer is a useful means toward efficient formation of networks in a straight-forward manner via irradiation with light. The copolymers presented in this thesis all contain benzophenone for photo-crosslinking.



Scheme 1.8 Reaction scheme of photo-excitation of benzophenone followed by H-abstraction and subsequent radical recombination.

Benzophenone is a widely utilized, versatile photoactive molecule. Upon excitation with 250 – 365 nm UV light, benzophenone becomes a diradical after undergoing a transition to an $n-\pi^*$ triplet.²⁹ This triplet is reactive and will abstract an aliphatic hydrogen from a neighboring molecule.³⁰ Rates of hydrogen abstraction are highly dependent upon the chemical environment, including monomer and solvent chemistry, sterics, and temperature.^{31,32} In the event of polymer photo-crosslinking, the focus of this work, benzophenone abstracts a hydrogen from a nearby polymer chain and a crosslink is formed upon radical recombination, as depicted in Schematic 1.3.³³

Many studies have used benzophenone as a dopant for facilitating photo-initiation as well as photo-crosslinking, particularly in the field of polymers.³⁴ While small molecule doping is experimentally simple, the drawback of this method is the risk of phase separation and migration of benzophenone. In the case of photo-crosslinking polymer materials, the disadvantages of doping could result in inhomogeneously and incompletely crosslinked samples. In addition, for poly(methyl methacrylate), in comparison to an equivalently small molecule doped system, covalently incorporated benzophenone was shown to have significantly higher crosslinking efficiencies due to the presence of more crosslinking routes, most significantly the recombination of aliphatic- and AAmBP-centered radicals.³⁵ A solution to the issues of doping is the covalent incorporation of benzophenone directly on the polymer chain, creating a one-component system and thereby eliminating the risk of small molecule migration and phase



Schematic 1.9 Synthesis of acrylamidobenzophenone from acryloyl chloride and 4-aminobenzophenone.

separation, and providing alternate means of crosslink formation, thus boosting efficiency.³⁶ All photo-crosslinkable polymers discussed in this thesis contain the crosslinking monomer acrylamidobenzophone, synthesized according to a previously reported literature procedure via reaction of acryloyl chloride and 4-amino benzophenone.³⁷ The benzophenone chemistry was chosen due to the good efficiency and control of crosslinking for the systems studied here.^{35,38,39}

1.3 References

1. Born, M. Wolf, E. *Principles of Optics*. (Cambridge University Press, 2002).
2. Joannopoulos, J. D., Villeneuve, P. R. & Fan, S. Photonic crystals: putting a new twist on light. *Nature* **386**, 143–149 (1997).
3. Winn, J. N., Fink, Y., Fan, S. & Joannopoulos, J. D. Omnidirectional reflection from a one-dimensional photonic crystal. *Opt. Lett.* **23**, 1573–5 (1998).
4. Ge, J. & Yin, Y. Responsive photonic crystals. *Angew. Chem. Int. Ed. Engl.* **50**, 1492–522 (2011).
5. Fenzl, C., Hirsch, T. & Wolfbeis, O. S. Photonic crystals for chemical sensing and biosensing. *Angew. Chem. Int. Ed. Engl.* **53**, 3318–35 (2014).
6. Nair, R. V. & Vijaya, R. Photonic crystal sensors: An overview. *Prog. Quantum Electron.* **34**, 89–134 (2010).
7. Holtz, J. H. & Asher, S.A. Polymerized colloidal crystal hydrogel films as intelligent chemical sensing materials. *Nature* **389**, 829–32 (1997).
8. Goponenko, A. V & Asher, S. a. Modeling of stimulated hydrogel volume changes in photonic crystal Pb²⁺ sensing materials. *J. Am. Chem. Soc.* **127**, 10753–9 (2005).
9. Weissman, J., Sunkara, H., Tse, A. & Asher, S. Thermally Switchable Periodicities and Diffraction from Mesoscopically Ordered Materials. *Science* **274**, 959–60 (1996).
10. Asher, S. a, Kimble, K. W. & Walker, J. P. Enabling Thermoreversible Physically Cross-Linked Polymerized Colloidal Array Photonic Crystals. *Chem. Mater.* **20**, 7501–7509 (2008).
11. Reese, E., Baltusavich, M. E., Keim, J. P. & Asher, S. a. Development of an intelligent polymerized crystalline colloidal array colorimetric reagent. *Anal. Chem.* **73**, 5038–42 (2001).
12. Lee, K. & Asher, S.A. Photonic Crystal Chemical Sensors: pH and Ionic Strength. *J. Am. Chem. Soc.* **122**, 9534–9537 (2000).
13. Walker, J. P. & Asher, S.A. Nerve Agent Sensing Photonic Crystal (PCCA) photonic crystal sensing material that senses the. *Test* **77**, 1596–1600 (2005).

14. Yoon, J., Lee, W. & Thomas, E. L. Thermochromic Block Copolymer Photonic Gel. *Macromolecules* **41**, 4582–4584 (2008).
15. Kim, E., Kang, C. Baek, H., Hwang, K., Kwak, D., Lee, E., Kang, Y., Thomas, E.L. Control of Optical Hysteresis in Block Copolymer Photonic Gels: A Step Towards Wet Photonic Memory Films. *Adv. Funct. Mater.* **20**, 1728–1732 (2010).
16. Walish, J. J., Kang, Y., Mickiewicz, R. a. & Thomas, E. L. Bioinspired Electrochemically Tunable Block Copolymer Full Color Pixels. *Adv. Mater.* **21**, 3078–3081 (2009).
17. Kang, Y., Walish, J. J., Gorishnyy, T. & Thomas, E. L. Broad-wavelength-range chemically tunable block-copolymer photonic gels. *Nat. Mater.* **6**, 957–60 (2007).
18. Kang, C, Kim, E., Baek, H., Hwang, K., Kwak, D., Kang, Y., Thomas, E.L. Full color stop bands in hybrid organic/inorganic block copolymer photonic gels by swelling-freezing. *J. Am. Chem. Soc.* **131**, 7538–9 (2009).
19. Lim, H. S., Lee, J.-H., Walish, J. J. & Thomas, E. L. Dynamic swelling of tunable full-color block copolymer photonic gels via counterion exchange. *ACS Nano* **6**, 8933–9 (2012).
20. Guldin, S., Kolle, M., Stefik, M., Langford, R., Eder, D., Wiesner, U., Steiner, U. Tunable mesoporous bragg reflectors based on block-copolymer self-assembly. *Adv. Mater.* **23**, 3664–8 (2011).
21. Mönch, W., Dehnert, J., Prucker, O., Rühle, J. & Zappe, H. Tunable Bragg filters based on polymer swelling. *Appl. Opt.* **45**, 4284–90 (2006).
22. Redel, E., Mirtchev, P., Huai, C., Petrov, S. & Ozin, G. a. Nanoparticle films and photonic crystal multilayers from colloidally stable, size-controllable zinc and iron oxide nanoparticles. *ACS Nano* **5**, 2861–9 (2011).
23. Bonifacio, L. D., Puzzo, L.P., Breslav, S., Willey, B.M., McGeer, A., Ozin, G.A. Towards the photonic nose: a novel platform for molecule and bacteria identification. *Adv. Mater.* **22**, 1351–4 (2010).
24. Lotsch, B. V., Scotognella, F., Moeller, K., Bein, T. & Ozin, G. a. Stimuli-responsive Bragg stacks for chemo-optical sensing applications. **7713**, 77130V–77130V–10 (2010).
25. Kobler, J., Lotsch, B. V, Ozin, G. a & Bein, T. Vapor-sensitive bragg mirrors and optical isotherms from mesoporous nanoparticle suspensions. *ACS Nano* **3**, 1669–76 (2009).

26. Choi, S. Y., Mamak, M., von Freymann, G., Chopra, N. & Ozin, G. a. Mesoporous bragg stack color tunable sensors. *Nano Lett.* **6**, 2456–61 (2006).
27. Colodrero, S., Ocaña, M., González-Elipe, a R. & Míguez, H. Response of nanoparticle-based one-dimensional photonic crystals to ambient vapor pressure. *Langmuir* **24**, 9135–9 (2008).
28. Colodrero, S., Ocaña, M. & Míguez, H. Nanoparticle-based one-dimensional photonic crystals. *Langmuir* **24**, 4430–4 (2008).
29. Rabek, J. F. *Mechanisms of Photophysical Processes and Photochemical Reactions in Polymers: Theory and Applications*. (John Wiley & Sons, Inc., 1987).
30. Dorman, G. & Prestwich, G. D. Benzophenone Photophores in Biochemistry. *Biochemistry* **33**, (1994).
31. Griller, D., Howard, J. A., Marriott, P. R. & Scaiano, J. C. Absolute Rate Constants for the Reactions of tert-Butoxyl, tert-Butylperoxyl, and Benzophenone Triplet with Amines: The Importanc of a Stereoelectronic Effect. *J. Am. Chem. Soc.* **103**, 619–623 (1981).
32. Shoute, L. C. T. & Huie, R. E. Reactions of Triplet Decafluorobenzophenone with Alkenes . A Laser Flash Photolysis Study. **5639**, 3467–3471 (1997).
33. Higuchi, H., Yamashita, T., Horie, K. & Mitai, I. Photo-Cross-Linking Reaction of Benzophenone-Containing Polyimide and Its Model Compounds. *Chem. Mater.* **3**, 188–194 (1991).
34. Doytcheva, M., Dotcheva, D., Stamenova, R., Orahovats, A. & Leder, J. Ultraviolet-Induced Crosslinking of Solid Poly (ethylene oxide). *J. Appl. Polym. Sci.* **64**, 2299–2307 (1996).
35. Christensen, S. K., Chiappelli, M. C. & Hayward, R. C. Gelation of Copolymers with Pendent Benzophenone Photo-Cross-Linkers. *Macromolecules* **45**, 5237–5246 (2012).
36. Toomey, R., Freidank, D. & Rùhe, J. Swelling Behavior of Thin, Surface-Attached Polymer Networks. *Macromolecules* **37**, 882–887 (2004).
37. Jia, J., Sarker, M., Steinmetz, M. G., Shukla, R. & Rathore, R. Photochemical elimination of leaving groups from zwitterionic intermediates generated via electrocyclic ring closure of alpha,beta-unsaturated anilides. *J. Org. Chem.* **73**, 8867–79 (2008).

38. Kim, J., Hanna, J.A., Byun, M., Santangelo, C. D. & Hayward, R. C. Designing Responsive Buckled Surfaces by Halftone Gel Lithography. *Science*. **335**, 1201–1205 (2012).
39. Kim, J., Hanna, J.A., Hayward, R. C. & Santangelo, C. D. Thermally responsive rolling of thin gel strips with discrete variations in swelling. *Soft Matter* **8**, 2375 (2012).

CHAPTER 2

THERMOCHROMIC PHOTONIC MULTILAYERS

2.1 Introduction and design

To validate the platform previously described in Chapter 1 as an efficient and robust means to fabricating 1-d photonic sensors, poly(N-isopropylacrylamide) (PNIPAM) ($n \sim 1.5$), a well-characterized thermally-responsive polymer, was chosen as a water-swallowable, stimulus-responsive component of a thermochromic material.^{1,2} In its crosslinked form, PNIPAM is a hydrogel which will de-swell due to a volume phase transition above a lower critical solution temperature. In this sensor, as well as in all subsequent multilayers, unless otherwise noted, a random copolymer of poly(*p*-methyl styrene) (PpMS) ($n \sim 1.6$) and acrylamidobenzophenone photo-crosslinker was chosen as the high-refractive index, non-swallowable layer rather than polystyrene due to the much more efficient crosslinking of the former material by benzophenone upon irradiation with 365 nm light.^{3,4} Acrylic acid (AAc) was also incorporated into the NIPAM-based random copolymer to enhance swelling. Appropriate layer thicknesses for each polymer, easily tuned from tens to hundreds of nanometers by varying the concentration of copolymer in solution and spin speed, are chosen to achieve a Bragg reflectance peak (λ_{\max}) within the visible range for light incident normal to the surface, according to Equation 1.2.

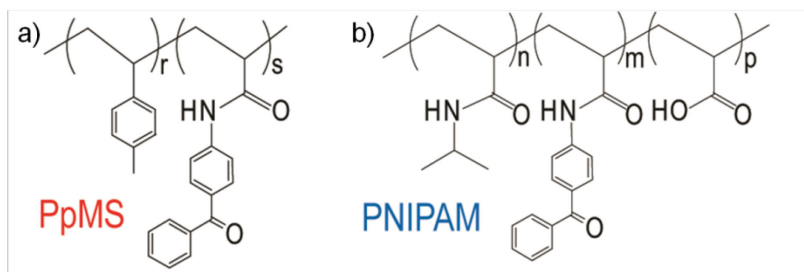


Figure 2.1 Structures of polymers used in thermochromic photonic multilayers.

To validate the proposed fabrication approach, PNIPAM-based thermochromic multilayers were created which cover the full visible spectrum upon changing from ~ 20 to $50\text{ }^{\circ}\text{C}$ in water.⁵ While the use of a large number of layers increases the amount of reflected light and also narrows the width of the reflectance peak, it also requires a longer fabrication process.⁶ For the polymers used here, color is observable even for 5 layer stacks. Sensors with 11 layers were found to show a clearly visible violet-blue color ($\lambda_{\text{max}} = 410\text{ nm}$) even in the dry state, for respective PpMS and PNIPAM layer thicknesses of 90 and 40 nm.

2.2 Experimental methods

Multilayers were fabricated on glass substrates and films for the calibration of thickness with solution concentration were cast onto silicon wafers. Polymer solutions were sonicated for 5 min and passed through a $0.2\text{ }\mu\text{m}$ PTFE syringe filter prior to spin-coating at 2000 rpm for 50 s. After crosslinking, films were developed in a marginal solvent mixture to remove uncrosslinked polymer. Polymer films were dried for 10 min after each spin-coating and developing cycle to completely evaporate solvent. Films were crosslinked using a 365 nm UV light source (typical dose $\approx 6\text{ J/cm}^2$). Reflectance of light normal to the substrate surface is monitored across the visible range using a microscope-integrated fiber-optics reflectance probe. Unless otherwise noted, this procedure was also followed for the preparation of multilayers subsequent chapters.

2.2.1 Materials

AIBN was obtained from Aldrich and re-crystallized from methanol prior to use. The inhibitor was removed from *d*₈-styrene (Aldrich) and *p*-methylstyrene (Acros Organics) by passing through a column of basic alumina. NIPAM and acrylic acid (AAc)

were purchased from Aldrich and used as received. Acrylamidobenzophenone (BP) monomer was synthesized using a previously reported procedure via reaction of 4-aminobenzophenone with acryloyl chloride in dichloromethane and triethylamine. For d-SIMS analysis, 5 mol% of d₈-styrene was incorporated along with pMS and AAmBP.

2.2.2 Polymer and monomer synthesis

In order to covalently attach benzophenone to the polymer chain, it must be functionalized such that copolymerization with free-radical techniques is possible. An acrylamide- functionalized benzophenone is used in all copolymers within this work. Acrylamidobenzophenone (BP) monomer was synthesized using a previously reported procedure via reaction of 4-aminobenzophenone with acryloyl chloride in dichloromethane and triethylamine (Figure 5).⁷ The organic fraction was purified by extractions with 1M HCl, NaHCO₃ and water. Product was dried under vacuum, yielding an orange solid. For d-SIMS analysis, discussed further in 2.4.1, 5 mol% of d₈-styrene was incorporated along with pMS and AAmBP.

Polymers were synthesized by free-radical polymerization at 80 °C in 1,4-dioxane for 15 hours following three freeze-pump-thaw cycles and a nitrogen purge using AIBN as initiator. Polymers were purified by precipitation into stirring diethyl ether (for PNIPAM) or methanol (for PpMS), washed by filtration and dried in a vacuum oven overnight. Solvent, monomer and initiator concentrations were chosen as follows: pMS (3 mL), AAmBP (0.451 g) and AIBN (0.015 g) in 30 mL of 1,4-dioxane, resulting in a copolymer containing 10 mol% AAmBP; NIPAM (1.503 g), AAc (0.049 mL), AAmBP (0.036 g) and AIBN (0.0046g) in 15 mL 1,4-dioxane, resulting in a copolymer with 5 mol% AAc and 1 mol% AAmBP. For comparison of swelling in water versus ethanol,

PNIPAM with a lower degree of swelling was prepared by copolymerizing: NIPAM (1.996g), AAc (0.0256 mL), AAmBP (0.142 g) and AIBN (0.008 g) in 22 mL 1,4-dioxane, resulting in a copolymer with 3 mol% AAmBP and 2 mol% AAc. For PpMS, molecular weight (M_n) was determined to be 12 kg/mol using size exclusion chromatography (SEC) with a Polymer Laboratories GPC-50 with THF as eluent and polystyrene standards. Molecular weights of PNIPAM copolymers were not determined due to interactions of the polymers with SEC columns.

2.2.3 Sample preparation & analysis

PpMS was dissolved at a concentration of 20 mg/mL in toluene, yielding film thicknesses of approximately 90 nm after crosslinking and developing. PNIPAM (5% AAc, 1% AAmBP) was dissolved at 12 mg/mL in 1-propanol, yielding film thicknesses of approximately 40 nm after crosslinking and developing. For the comparison between swelling kinetics in water and ethanol, the other PNIPAM copolymer (2% AAc, 3% AAmBP) was dissolved at 12 mg/mL in 1-propanol, yielding film thicknesses of approximately 60 nm after crosslinking and developing.

2.2.4 Sensor fabrication

Silicon, for d-SIMS and AFM analysis, and glass substrates, for 1D photonic sensors, were first cleaned by sonication for 10 min each successively in water, acetone and ethanol and treated with UV-ozone for 15 min. Substrate surfaces were then treated to promote adhesion by placing in a stirring solution of 200 μ L methacryloxypropyltrichlorosilane (Gelest) in 50 mL ethanol for a minimum of 4 h and thoroughly rinsed with ethanol prior to use. Polymer solutions were sonicated for 5 min and passed through a 0.2 μ m PTFE syringe filter prior to spin-coating (Headway

Research) at 2000 rpm for 50 s. After crosslinking, films were developed in a marginal solvent mixture (2:1 ethanol:water for PNIPAM, 1:0.65 toluene:hexanes for PpMS) to remove uncrosslinked polymer. Polymer films were dried for 10 min after each spin-coating and developing cycle to completely evaporate solvent.

2.2.5 Instruments and measurements

Polymer compositions were measured using ^1H NMR (Bruker DPX300). Films were crosslinked using a 365 nm UV light source (Lumen Dynamics, XCite 120Q or a UVP handheld lamp, typical dose $\approx 6 \text{ J/cm}^2$). Refractive indices and thicknesses of polymer films were characterized using a variable angle spectroscopic ellipsometer (Sopra) or null ellipsometer (LSE Stokes, Gaertner). All reflectance measurements were made using a Filmetrics F20 or Semiconsoft reflectometer integrated with a Zeiss Axiovert upright optical microscope using a 10x objective. Samples are placed on the microscope stage and a halogen lamp is used as a normal incidence light source. An approximately 5 mm spot size is illuminated through a Zeiss Epiplan 10x objective with 0.2 numerical aperture and reflected light is monitored by the spectrometer. A constant background of bare glass was subtracted from spectra for comparisons with calculations. Water from a Milli-Q UF Plus Ultrapure Water Purification System (Millipore) was used in all experiments. To measure changes in reflectance with temperature, sensors were placed on a temperature stage (INTEC HCS621V) with liquid nitrogen cooling and the sample surface fully covered with water for all variable temperature experiments. For equilibrium measurements, multilayers were allowed to equilibrate for 30 min at each temperature, while rapid heating and cooling ramps between 20 and 50 °C were completed in approximately 45 s and 65 s, respectively, with a slight undercooling to 17

°C followed by equilibration to 20 °C over 4 min as measured with a thermocouple (Fisher Scientific). Photographs of the sensors were taken using a Canon PowerShot A640 digital camera on a black felt background, and brightness/contrast adjustment was applied to images to best match the visual appearance of sensors. d-SIMS measurements were made using a Physical Electronics 6650 Quadrupole mass spectrometer at the University of California, Santa Barbara. A 200 μm x 200 μm area was etched by bombardment with O₂⁺ primary ions. Deuterium (²H⁺, *m/z* = 2.1), and cyano (CN⁻, *m/z* = 26), signals were monitored in a 40% x 40% gated area of the etched surface. Scanning force microscopy measurements were taken using a DI Dimension3000 instrument.

2.2.6 Reflectance calculations

MATLAB was used for all reflectance simulations. The transfer matrix method was employed for calculating reflectance assuming normal incidence, perfectly smooth interfaces parallel to the substrate and homogenous material properties (refractive index, layer thickness) through each layer of the stack in an ambient environment of air (*n* = 1.00) or water (*n* = 1.33). The refractive indices of PpMS and PNIPAM (dry-state) were taken as 1.60 and 1.50, respectively, and dispersion was ignored. Lorentz-Lorenz theory was used to calculate the refractive index of the swelled PNIPAM layers according to

$$\frac{n_{swell}^2 - 1}{n_{swell}^2 + 2} = \varphi_1 \frac{n_{water}^2 - 1}{n_{water}^2 + 2} + (1 - \varphi_1) \frac{n_{polymer}^2 - 1}{n_{polymer}^2 + 2} \quad (2.1)$$

where φ_1 and $\varphi_{polymer} = (1 - \varphi_1)$ are the volume fractions of water and PNIPAM, respectively, in the swelled system.⁸ We assume 1D swelling of PNIPAM layers perpendicular to the substrate, according to:

$$d_{swell} = \frac{d_{dry}}{1 - \varphi_1} \quad , \quad (2.2)$$

where d_{swell} and d_{dry} are the thicknesses of a single PNIPAM layer, either fully swelled or dry, in the multilayer stack. Values of φ_{polymer} used for calculated reflectance curves are summarized in Figure 2.8.

2.3 Temperature responsive swelling & reversibility

Multilayers that cover the full visible spectrum upon changing from ~ 20 to 50 °C were successfully designed and fabricated. To maximize the degree of swelling and thus wavelength range, a PNIPAM copolymer with a small content (1 mol%) of photo-crosslinker and 5 mol% of the charged monomer acrylic acid (AAc) was used, which swells extensively at room temperature and undergoes a pronounced collapse with increasing temperature. Upon immersion in room temperature water, the PNIPAM layers swell, causing a red-shift in maximum reflectance to 710 nm and also increasing the peak reflectivity to 0.49 ± 0.05 , due to both an increase in refractive index contrast and a better match between the optical thicknesses of the high- and low-index layers. Upon heating, the PNIPAM layers de-swell, causing a progressive blue shift in reflectance (Figure 2.2,

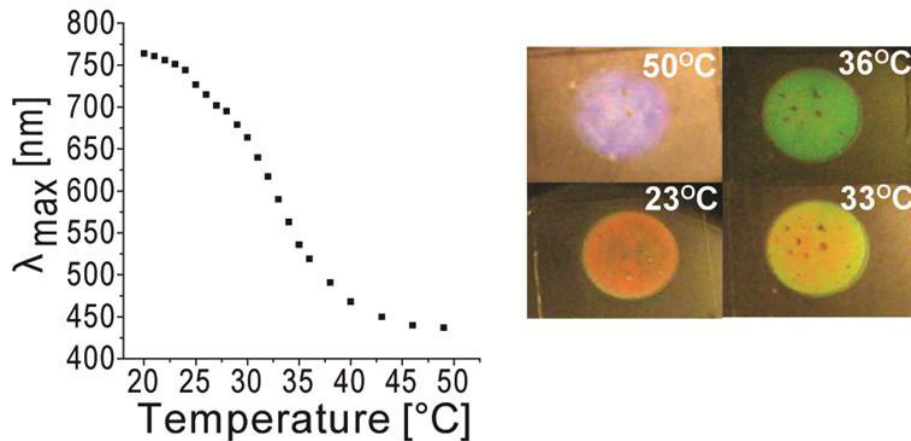


Figure 2.2 Peak reflectance wavelength (left) and photographs of sensors (right) swelled in water show clear colorimetric changes with temperature.

right) and allowing temperature to be read out colorimetrically. By 50 °C, the peak reflection occurs at 431 nm (Figure 2.2, left), only slightly greater than the value in the dry state. The temperature response was found to be fully reversible with good reproducibility (variations in λ_{max} of ± 10 nm) over at least 5 swelling/de-swelling cycles induced by rapidly switching temperature between 20 °C and 50 °C (see Figure 2.3 for reflectivity curves).

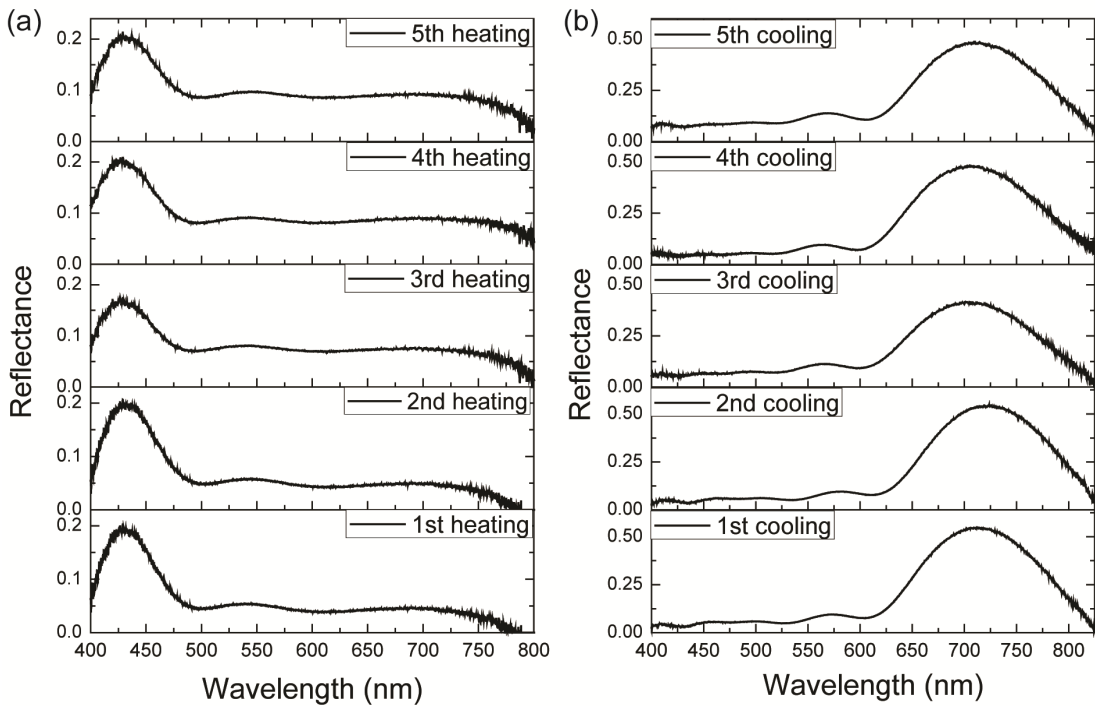


Figure 2.3 Reflectance spectra during a series of 5 cycles of (a) heating to 50 °C to de-swelling and (b) cooling to 20 °C to re-swelling the multilayer (as shown in Figure 2a).

No signs of delamination or damage to the multilayer were visible, and following a cycle of hydration and dehydration, the reflectance profile matched closely with that of the as-prepared sample. To measure changes in reflectance with temperature, sensors were placed on a temperature stage with liquid nitrogen cooling and the sample surface

fully covered with deionized water for all variable temperature experiments. For equilibrium measurements of peak reflectance with temperature, multilayers were allowed to equilibrate for 30 min at each temperature.

2.4 Kinetics

A preliminary investigation of the kinetics of swelling and de-swelling, to be discussed in expanded depth in Chapter 5, was also conducted, as seen in Figure 2.4. For

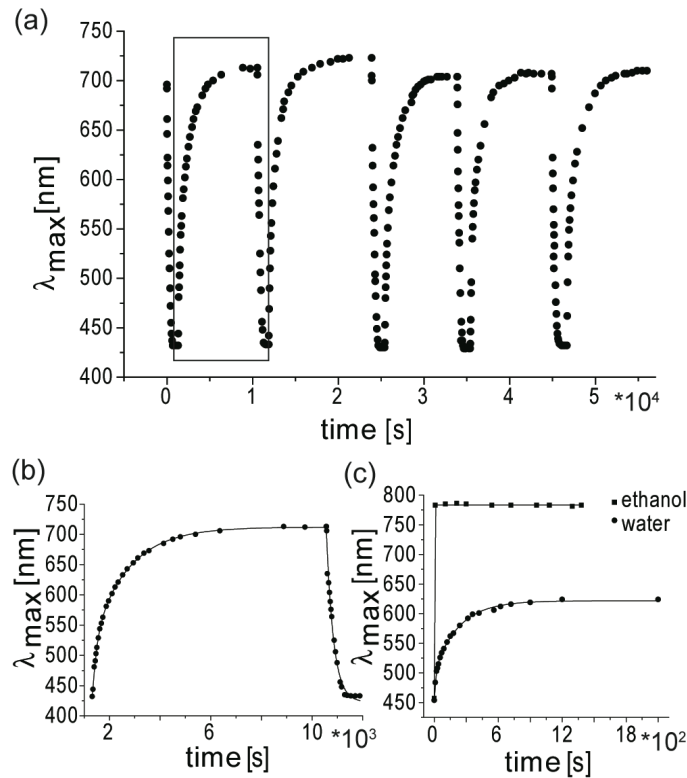


Figure 2.4 (a) Multiple cycles of swelling/de-swelling induced by rapid switching of temperature between 20 and 50°C show the sensor response is highly reproducible. (b) An enlargement of a single swelling/de-swelling cycle, as denoted by the box in (a), along with comparison of multilayer swelling in (c) water and ethanol.

equilibrium measurements, sensors were placed on a temperature stage and the surface

covered with deionized water followed by rapid heating and cooling ramps between 20 and 50 °C completed in approximately 45 s and 65 s, respectively. While the de-swelling curves can be fit with single exponentials (time constant $\tau = 270 \pm 20$ s), the swelling curves are found to be biexponential ($\tau_1 \approx 175 \pm 15$ s and $\tau_2 \approx 1400 \pm 90$ s) (Figure 2.4b).

Reflectance measurements across multiple sample spots from the edge inward reveal uniform swelling, demonstrating that the kinetics are not limited by lateral transport of water through the film. Similarly, Serpe and co-workers also find that solvent transport in the direction perpendicular to the substrate is the dominant route of exchange for microgel-based etalons.^{9,10} Using a literature value for permeability of polystyrene, we roughly estimate that permeation of water through the combined thickness of PpMS layers (~ 600 nm) would require ~ 40 s, which is even somewhat shorter than the faster of the swelling time-scales.¹¹

Swelling kinetics were also analyzed for sensors when immersed in ethanol, a much better solvent for the PNIPAM copolymer than water, but which should be transported more slowly through the glassy PpMS layers due to its larger molecular size. In this case, sensors fabricated as described above swell so extensively that the Bragg peak is shifted out of the visible range. Therefore this study was conducted using a PNIPAM copolymer containing a larger amount of AAmBP (3 mol %) to increase crosslink density, and a smaller amount of AAc (2 mol%), both factors which decrease swelling. As shown in Figure 2.4c, swelling in ethanol is complete within the time-scale of the first measurement (~ 10 s), at least 2 orders of magnitude faster than in water. This result suggests that mass transport does not limit the observed kinetics, and furthermore that swelling presumably does not occur by permeation through PpMS layers, but is

instead likely dominated by pinhole defects typically found in the glassy polymer layers (Figure 2.6a, AFM). The slow time scales for sensor response in water may instead reflect the kinetics of de-aggregation of hydrophobic benzophenone units and/or breaking of inter- and intra-molecular hydrogen bonds. In fact, the hysteresis seen in the globule-to-coil transition of PNIPAM homopolymers has been ascribed to the necessity to break hydrogen-bonds, and the same mechanism could provide a kinetic hindrance to changes in swelling of a PNIPAM gel layer.¹²⁻¹⁴ This slow sensor response may be addressed by tuning the polymer chemistry and will be discussed further in Chapter 5.

2.5 Structure analysis

It is necessary to characterize the structure of the multilayer films in order to better understand their performance as responsive photonic materials. While the use of a large number of layers increases the amount of reflected light and also narrows the width of the reflectance peak in 1-d photonic crystals, it also requires a longer fabrication process.⁶ For the polymers used here, color is observable even for 5-layer stacks. The sensors studied consist of 11 layers, which was found to provide a balance between a reasonable processing time and a clearly visible violet-blue color even in the dry state. No signs of delamination or damage to the multilayer were visible, and following a cycle of hydration and dehydration, the reflectance profile matched closely with that of the as-prepared sample, confirming the structural integrity of the sensor even after multiple swelling, de-swelling and drying cycles.

2.5.1 Interfacial & surface characterization

Dynamic secondary ion mass spectrometry (d-SIMS) was used to examine the layer uniformity and interfacial profiles as a function of etch depth using an O_2^+ beam. For these experiments, 5 mol% of d_8 -styrene is included in the PpMS copolymer to provide a clear deuterium signal (2H , $m/z = 2.1$), while the much greater density of amide groups in the PNIPAM copolymer provides contrast in the yield of cyano anions (CN^- ,

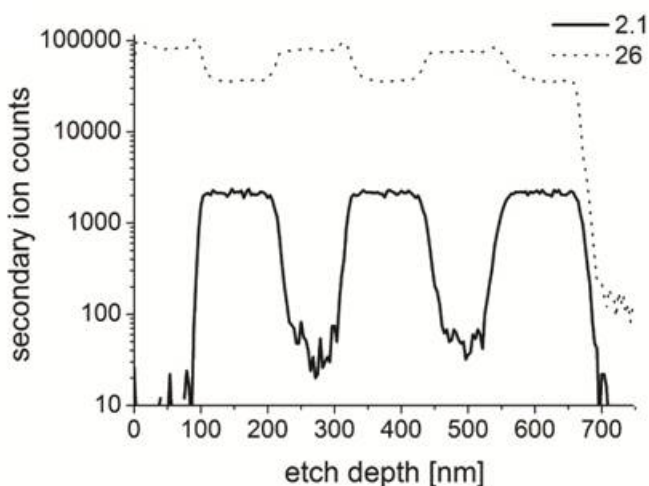


Figure 2.5 d-SIMS analysis of deuterium ($m/z = 2.1$) and cyano ($m/z = 26$) signals for 6 layer alternating PpMS/PNIPAM films reveal excellent layer uniformity and minimal interfacial broadening.

$m/z = 26$). As seen in Figure 7, the multilayers show excellent uniformity of layer thicknesses (typical variations of $\pm 5\%$) and interfacial widths between neighboring layers below 15 nm. This value is close to the estimated resolution of the spectrometer (≈ 10 nm), determined by profiling a bilayer sample consisting of a PpMS film floated on water and dry-transferred onto a previously crosslinked and developed PNIPAM film. The similarity of apparent interfacial widths in these two cases indicates that little interfacial broadening or inter-penetration of the layers occurs due to solvent-induced

swelling during the sequential spin-coating process. While this result is to be expected given the use of selective solvents for the spin-coating steps (toluene for PpMS, 1-propanol for PNIPAM), remarkably, even samples prepared using the same solvent (pyridine) for each layer showed similar interfacial widths.

This finding suggests that even when the coating solvent substantially swells the pre-existing layers, significant penetration of copolymers from solution into the swelled film does not occur, at least over the time scale of several seconds. In addition, both single and multiple layer spin-coated films showed values of surface roughness below 1 nm (rms) by atomic force microscopy (AFM) (Figure 9). The low surface roughness and

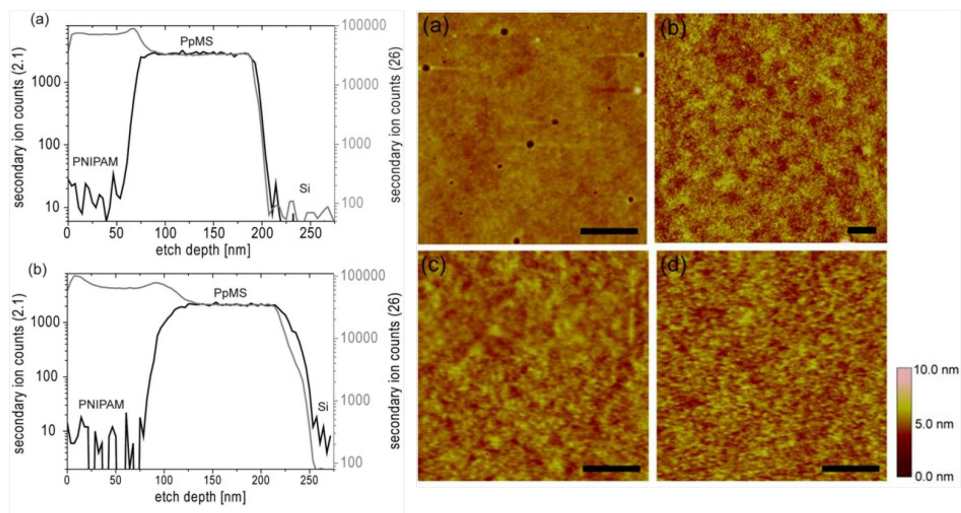


Figure 2.6 d-SIMS analysis of deuterium ($m/z = 2.1$) and cyano ($m/z = 26$) signals from a two-layer sample (PpMS, PNIPAM) on Si prepared from (a, left) pyridine, a good solvent for both polymers and (b, left) from selective solvents, as in the main text, with interfacial widths of 10 nm and 20 nm, respectively. AFM height images (right) of a) PpMS ($R_{\text{rms}} = 0.346$ nm), PNIPAM (0.648 nm), c) 4 layers (0.478 nm) and d) 6 layers (0.563 nm). Scale bars are 500 nm.

uniform layer thicknesses show that this fabrication approach is a feasible route for sensor fabrication, even beyond this model PNIPAM-PpMS system. Macroscopic defects were apparent in most samples, as evident in Figure 6, however, this was primarily due to dust deposited during sample preparation and could be eliminated or greatly diminished by preparation in a clean room environment. To obtain even higher reflectance efficiencies of these thermochromic materials, the process can easily be extended to a greater number of layers, however, for these materials, 11 layers provided a clear colorimetric signal even in the fully de-swelled state.

2.6 Comparison to reflectivity calculations

In addition to structural analysis, a useful way of analyzing the efficiency of the multilayer design is by comparison to the calculated reflectance values. To do so, the experimentally measured reflectance curves were compared to calculations based on the transfer matrix method for ideal multilayers with perfectly sharp interfaces, zero roughness, and uniform layer thicknesses using MATLAB. A homogenous dielectric film can be described by the following characteristic matrix:

$$\mathbf{M}(z) = \begin{bmatrix} \cos(k_0 n z \cos\theta) & \frac{-i}{p} \sin(k_0 n z \cos\theta) \\ -i p \sin(k_0 n z \cos\theta) & \cos(k_0 n z \cos\theta) \end{bmatrix} \quad (2.3)$$

$$\text{where } k_0 = \frac{2\pi}{\lambda}, p = \sqrt{\frac{\varepsilon}{\mu}} \cos\theta, z = \text{layer thickness}$$

Refractive index, film thickness and wavelength are known variables and for light incident normal to the surface ($\theta = 0$), the case for all reflectivity measurements made in this thesis, and the matrix is further simplified as $\cos(\theta) = 1$. The characteristic matrix of

a multilayer is thus computed by multiplying the matrices of each component film (Eq. 2).

$$\mathbf{M} = \prod_{j=1}^N \mathbf{M}_j = \begin{bmatrix} m_{11} & m_{12} \\ m_{21} & m_{22} \end{bmatrix} \quad (2.4)$$

Once the characteristic matrix is known, it is then possible to calculate the reflection coefficient, r , (Eq. 4) and finally the reflectivity, R , (Eq. 5) of the multilayer.⁶

$$r = \frac{(m_{11} + m_{12}p_l)p_1 - (m_{21} + m_{22}p_l)}{(m_{11} + m_{12}p_l)p_1 + (m_{21} + m_{22}p_l)} \quad (2.5)$$

$$R = |r|^2 \quad (2.6)$$

As shown in Figure 2.7, over the range of temperatures studied, the experimental curves match very well to the simulations, with only a single adjustable parameter (the

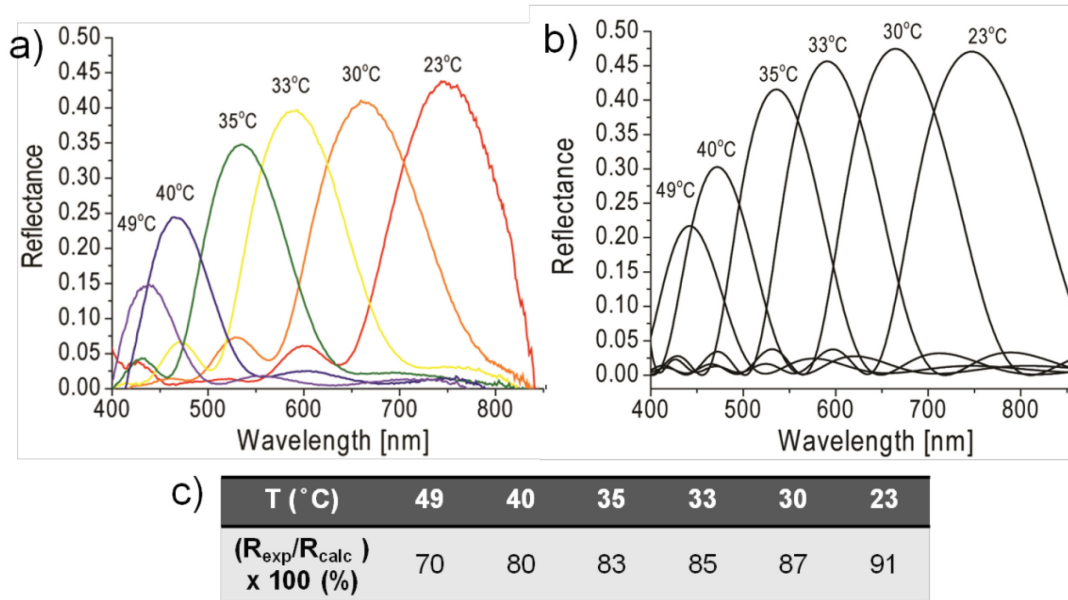


Figure 2.7 Comparison of experimental (a) and calculated (b) reflectance curves at various degrees of swelling with temperature shows c) high reflectance efficiency of thermochromic materials compared to the ideal case.

volume fraction of water) in the swelled state. The refractive indices of PpMS and PNIPAM (dry-state) were taken as 1.60 and 1.50, respectively, and dispersion was ignored. Lorentz-Lorenz theory was used to calculate the refractive index of the swelled PNIPAM layers according to Equation 2.1. 1-dimensional swelling of PNIPAM layers perpendicular to the substrate is assumed, according to Equation 2.2.

Values of ϕ_{polymer} used for calculated reflectance curves are summarized in Figure 2.8. The measured peak reflectance values range from 70% (high temperature, de-swelled

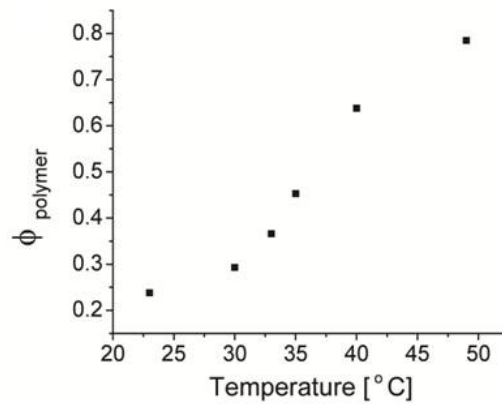


Figure 2.8 Volume fraction of polymer with temperature at various degrees of swelling used to calculate reflectance.

state) to 91% (low temperature, fully swelled state) of the calculated values. Factors such as interfacial broadening and surface roughness may contribute to slightly diminished sensor efficiency from the calculated values.

2.7 Conclusions

A simple and robust process for the fabrication of 1D photonic sensors based on sequentially spin-coated multilayers of photo-crosslinkable copolymers was demonstrated. This approach is straightforward and scalable, as the sensor size and fabrication time are limited only by the intensity and size of the UV source. Furthermore,

it offers flexibility for tailoring the properties of the photonic multilayer since it affords independent control over each layer within the stack. While temperature sensors were prepared as a convenient means to validate the platform, future chapters focus on the generalization of this technique to other geometries and stimuli simply by choosing alternative copolymer chemistries for the swellable layers.

2.8 References

1. Hirotsu, S., Hirokawa, Y. & Tanaka, T. Volume-phase transitions of ionized N-isopropylacrylamide gels. *J. Chem. Phys.* **87**, 1392 (1987).
2. Zhou, S. & Wu, C. In-Situ Interferometry Studies of the Drying and Swelling Kinetics of an Ultrathin Poly(N -isopropylacrylamide) Gel Film below and above Its Volume Phase Transition Temperature. *Macromolecules* **29**, 4998–5001 (1996).
3. Christensen, S. K., Chiappelli, M. C. & Hayward, R. C. Gelation of Copolymers with Pendent Benzophenone Photo-Cross-Linkers. *Macromolecules* **45**, 5237–5246 (2012).
4. Voronekov, V. V. & Kokorev, V. N. Synthesis of p-Alkylbenzoic Acids by One-Electron Oxidation of p-Alkyltoluenes. *J. Org. Chem. USSR* **25**, 2302–2305 (1990).
5. Chiappelli, M. C. & Hayward, R. C. Photonic multilayer sensors from photo-crosslinkable polymer films. *Adv. Mater.* **24**, 6100–4 (2012).
6. Born, M. Wolf, E. *Principles of Optics*. (Cambridge University Press, 2002).
7. Jia, J., Sarker, M., Steinmetz, M. G., Shukla, R. & Rathore, R. Photochemical elimination of leaving groups from zwitterionic intermediates generated via electrocyclic ring closure of alpha,beta-unsaturated anilides. *J. Org. Chem.* **73**, 8867–79 (2008).
8. Heller, W. Remarks on Refractive Index Mixture Rules. *J. Phys. Chem.* **69**, 1123–1129 (1965).

9. Carter, M. C. D., Sorrell, C. D. & Serpe, M. J. Deswelling Kinetics of Color Tunable Poly (N-Isopropylacrylamide). *J. Phys. Chem. B* **115**, 14359–14368 (2011).
10. Sorrell, C. D. & Serpe, M. J. Reflection order selectivity of color-tunable poly(N-isopropylacrylamide) microgel based etalons. *Adv. Mater.* **23**, 4088–92 (2011).
11. Brandrup, J., Immergut, E. H. & Grulke, E. A. *Polymer Handbook*. (John Wiley & Sons, Inc., 1999).
12. Wang, X., Qiu, X. & Wu, C. Comparison of the Coil-to-Globule and the Globule-to-Coil Transitions of a Single Poly(N-isopropylacrylamide) Homopolymer Chain in Water. *Macromolecules* **31**, 2972–2976 (1998).
13. Cheng, H., Shen, L. & Wu, C. LLS and FTIR Studies on the Hysteresis in Association and Dissociation of Poly (N-isopropylacrylamide) Chains in Water. *Macromolecules* **39**, 2325–2329 (2006).
14. Zhou, K., Lu, Y., Li, J., Shen, L., Zhang, G., Xie, Z., Wu, C. The Coil-to-Globule-to-Coil Transition of Linear Polymer Chains in Dilute Aqueous Solutions: Effect of Intrachain Hydrogen Bonding. *Macromolecules* **41**, 8927–8931 (2008).

CHAPTER 3

COLORIMETRIC RADIATION SENSING USING PHOTONIC POLYMER MULTILAYERS

3.1 Introduction

The ability to conveniently sense ionizing radiation is critical for a variety of applications including in medicine, defense, industrial food packaging, and pasteurization and sterilization techniques. Practical ranges for absorbed dose detection vary from the range of 1 Gy and below for human exposure, to upwards of hundreds of kGy for sterilization and decontamination procedures, as detailed in Table 3.1.¹

Colorimetric sensors are convenient and can offer both simple and accurate read-out. Many such detection techniques, however, rely on a change in optical density triggered by irradiation of a photo-sensitive chromophore and require external equipment for read-out in addition to stringent storage conditions to avoid device failure.² Some solution-based sensors which show clear colorimetric changes spanning a broader range of the visible spectrum provide an attractive means towards convenient, stand-alone sensors, but utilize inconvenient and toxic organic solvents.³⁻⁵ Among the many existing approaches, film-based sensing techniques are appealing for general use because they avoid potentially toxic solvents, however may also require sealed containment or have time-sensitive restrictions on read-out due to a lack of chemical stability post-irradiation.⁶⁻⁹

3.1.2 Approaches in literature

There has been extensive work in the field of radiation sensing and this section provides a brief overview of the most relevant advances and limitations in radiation

detection which similarly aim towards designing colorimetric, polymer-based sensors. Earlier work by Kojima and co-workers used leuco malachite green -containing polyvinyl chloride and polyvinyl butyral films for radiation detection. The films undergo a radiation-induced color change from colorless to green, however this system cannot stand alone as analysis by UV-vis spectrophotometry is required to determine the dose. Additionally, stability issues require rapid analysis (within 24 hr. of exposure) and device storage in a sealed, dark containment is crucial.^{6,7} A similar, film-based approach was also taken by da Silva and co-workers, utilizing colorimetric radiation sensitivity of a spin-cast polyaniline film.⁸ Upon gamma-ray exposure, the film is oxidized and transitions from blue to green with a 4 kGy dose.

Solution-based approaches toward gamma-ray radiation detection have focused on aggregation-induced emission of a fluorescent polymer-small molecule complex.⁵ The strong fluorescence intensity of a positively charged silole and negatively charged polyelectrolyte is gradually decreased to an extent detectable by eye over a dose range of 40 kGy gamma-ray radiation. However, to avoid complete degradation of the silole compound, the polymer solution alone must first be exposed and subsequently mixed with the silole for post-irradiation fluorescence analysis. Recently, Bianchi and co-workers have successfully developed easy-to-use and easy-to-read colorimetric radiation detectors based on a luminescent polymer, P(2-methoxy-5(2'-ethylhexyloxy)-p-phenylenevinylene), MEH-PPV, and a metal complex, tris-(8-hydroxyquinoline)aluminum, Alq₃.³ Radiation induced degradation promotes color changes, apparent by eye, from red to yellow to green, depending on dose. The device is portable and read-out is rapid and straight-forward; however, the solution-based nature

and requirement of storage within a sealed glass ampoule limits the practicality of the technology and poses safety concerns for general use.

Table 3.1 Electron-beam irradiation processing applications. Table reproduced and modified from E-Beam Services, Inc. http://www.ebeamservices.com/ebeam_spe_poly.htm.

Irradiation Target	Net Effect	Dose Range (kGy)
Food	Cold pasteurization	0.3-60
Medical disposable items	Sterilization	10-60
Coatings	Curing	30-160
Polyolefin foams	Crosslinking	40-80
Heat-shrinkable materials	Memory Imparted	75-250
Rubber	Vulcanization	80-400
Fluoropolymers	Degradation	500-1500
Gemstones	Coloration	10,000+

Here, a novel concept for radiation detection via colorimetric photonic sensing is described. We make use of devices based on one-dimensional photonic crystals, periodic multilayer structures that rely on the interference of light to reflect a characteristic wavelength defined by the refractive index and thickness of each layer.¹⁰ One-dimensional photonic sensors have been explored extensively for detection of a wide range of analytes, including pH, ionic strength, temperature and a variety of small molecules, as summarized in several recent reviews.¹¹⁻¹³ Previously, Chapter 2 has detailed the approach to photonic multilayers for colorimetric temperature sensing based on photo-crosslinkable polymers.¹⁴ This simple fabrication method is broadly suitable for a wide range of photonic sensors, including chemical and biological analytes, and the current chapter explores the extension to a new type of analyte, ionizing radiation.

Work presented in this chapter demonstrates that these multilayer polymer films provide a novel platform for radiation sensing, due to the radiation-induced preferential

crosslinking or dislinking of a swellable polymer gel layer within the photonic sensor. This allows for straightforward colorimetric read-out, and due to the reliance on changes in structural color, rather than absorption or emission of light by a chromophore, offers potential for the development of low cost and chemically stable radiation sensors.

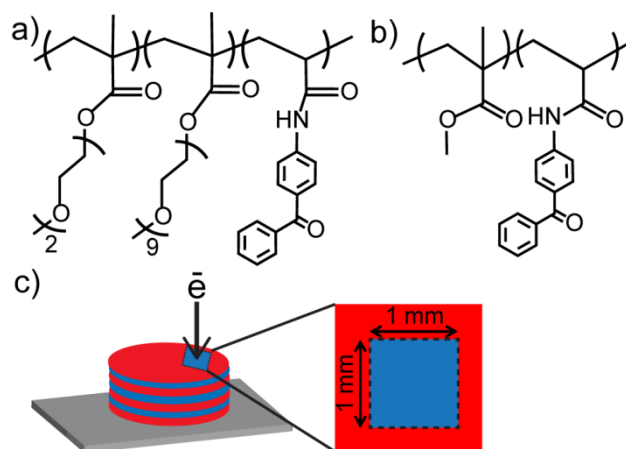


Figure 3.1 Chemical structures of responsive materials a) P(OEGMA-BP) and b) P(MMA-BP) and c) schematic of multilayer radiation exposure setup and dimensions.

3.2 Experimental methods

3.2.1 Polymer synthesis

Polymers were synthesized by conventional free radical polymerization using azobisisobutyronitrile (AIBN) (Aldrich) re-crystallized from methanol as initiator. Acrylamidobenzophenone (BP) monomer was synthesized according to a previously reported literature procedure via reaction of acryloyl chloride and 4-aminobenzophenone.¹⁵

P(p-MS-BP)

Inhibitor was removed from *p*-methylstyrene (*p*-MS) (Acros Organics) by passing through a column of basic alumina. The monomers *p*-MS (3 mL, Aldrich) and BP (0.45

g) were polymerized in 30 mL of 1,4-dioxane at 80°C for 15 h under nitrogen following three freeze-pump-thaw cycles, resulting in a copolymer containing 10 mol% of BP. The polymer was purified by precipitation into methanol, washed under vacuum filtration and dried overnight in a vacuum oven prior to use. Structure was confirmed by ¹H NMR (Bruker DPX 300).

P(OEGMA-BP)

Amounts of 2 mL of 2-(2-methoxyethoxy) ethyl methacrylate (MEO₂MA, Aldrich), 251 μL of oligoethylene glycol methyl ether methacrylate (OEGMA, $M_n = 475$ g/mol, Aldrich), 58 mg of BP and 3.4 mg of AIBN were polymerized in a 5:1 mixture of ethanol:1,4-dioxane at 80°C for 18 h under nitrogen following three freeze-pump-thaw cycles, resulting in a copolymer containing 2 mol% of BP. OEGMA and MEO₂MA were used as received. The polymer was purified by dialysis and lyophilization, and its structure confirmed by ¹H NMR.

P(MMA-BP)

Amounts of 2 g (20 mmol) of methyl methacrylate (MMA) (Sigma, purified via 3x sat. sodium bicarbonate washes followed by drying over sodium sulfate), 0.25 g (1 mmol) of acrylamide benzophenone, 8.2 mg (0.05 mmol) of AIBN (recrystallized from methanol) were dissolved in 10 mL of 1,4-dioxane and sparged with N₂ for 30 min before heating to 85 °C. The reaction was allowed to stir for 48 h and purified by precipitation into methanol, resulting in a polymer containing 5 mol% BP by ¹H NMR.

3.3 Sensor preparation & characterization

Photonic multilayers were prepared by sequential spin-coating, crosslinking and developing of polymer films as previously reported.¹⁴ Glass substrates were first cleaned

by sonication for 10 min each in acetone, ethanol and water followed by surface treatment with methacryloxypropyl trichlorosilane (Gelest) to promote substrate-polymer adhesion. Flexible Mylar substrates (McMaster-Carr) were used as received and cleaned by rinsing with water, acetone and ethanol. P(*p*-MS-BP) and P(OEGMA-BP) were cast from toluene, while P(MMA-BP) was cast from cyclohexanone. Developing solutions for the three respective copolymers were 1: 0.65 toluene: hexanes, 1: 0.53 toluene: hexanes, and chloroform. Polymer films were crosslinked using a Newport 365 nm UV light source, with a typical dose of approximately 80 J/cm², which is sufficient to fully convert the BP photo-crosslinkers. A Magellan 400 scanning electron microscope was used for all radiation exposure. As-prepared multilayers were exposed to electron beam radiation by scanning a 1 mm x 1 mm square at 150x magnification with fixed accelerating voltage of 15 kV, and current of 1.6 nA. At 15 kV, the excitation volume depth for all three polymers is in the micrometer range. Therefore, we can assume that all layers are excited and the electron beam penetrates the entire thickness of the multilayer sensors, which are $\approx 0.5 \mu\text{m}$ in total thickness. The radiation dose was varied by adjusting exposure time t , and was quantified in terms of the approximate absorbed dose according to:

$$dose \approx \frac{I * S * t}{A} \quad 3.1$$

where I is the current, S the stopping power, and A the exposure area. Values for stopping power for 15 keV kinetic energy electrons were calculated using the NIST ESTAR database based on the chemical compositions of the polymers, yielding an average value for P(*p*-MS-BP), P(OEGMA-BP) and P(MMA-BP) of 16 MeV cm²/g, which was used to estimate absorbed doses.¹⁶

The response of irradiated samples was determined by swelling in ethanol and acquiring reflectance spectra *in situ* using a reflectance probe (Semiconsoft MProbe) integrated with an upright microscope (Zeiss AxioTech). The microscope aperture was adjusted to ensure that the measured area fell entirely within the irradiated square.

3.4 Results & discussion

This approach to colorimetric radiation sensors is based on one dimensional photonic multilayers fabricated by spin-coating, photo-crosslinking, and developing of alternating layers of a high refractive index polymer, P(*p*-MS-BP) and one of two different low refractive index polymers. The layer thicknesses were chosen to reflect blue-violet light in the dry state and undergo a red-shift due to swelling of the low refractive index layers upon immersion in a mild, non-toxic solvent (in this case, ethanol). Depending on their chemical structure, polymers tend to undergo either preferential crosslinking or degradation under ionizing radiation.¹⁷ Thus, upon irradiation of the multilayers, the degree of swelling of the irradiated regions will either increase or decrease, depending on the chemical structure of the low-index layers, thereby causing a shift in the reflectance peak compared to the unexposed regions of the sample. Once irradiated and immersed in ethanol, the color change can be monitored by eye. Depending on the chemistry of the responsive polymer layers, the observer will note an apparent red or blue shift of the irradiated region compared to the non-irradiated area of the sensor. This shift can be more quantitatively monitored by using a reflectance probe to measure the reflectance spectra of the irradiated and non-irradiated regions. Once read-out is complete, the sensor can be dried and disposed of or re-used by exposing a previously non-irradiated region of the sample.

Two radiation sensor systems were designed based on polymers expected to undergo radiation-induced crosslinking or degradation, respectively, P(OEGMA-BP), Figure 1a, and P(MMA-BP), Figure 1b. The materials were copolymerized with 2-5 mol% of the photo-crosslinkable monomer BP to allow for UV crosslinking during multilayer fabrication. Mid-chain carbon-centered radicals on poly(ethylene oxide) (PEO) irradiated *in vacuo* are known to predominantly undergo crosslinking via radical recombination, particularly above 15 kGy, consistent with the dose range of our study.^{18,19} PMMA is a well-known positive resist for ion and electron beam lithography due to its degradation upon irradiation via main chain scission.^{17,19,20} PMMA films have been shown to preferentially degrade under ionizing radiation *in vacuo* at kGy doses, also comparable to the dose ranges examined in the present work.¹⁹

Upon exposure to ionizing radiation in the form of an electron beam, additional crosslinks were introduced to the P(OEGMA-BP)-based sensors, leading to a decrease in the degree of swelling and subsequently a blue shift in the wavelength of reflectance peak of the irradiated region upon swelling in ethanol (Figure 2a, b, c). This effect was evident in a ~30 nm blue shift in the reflectance spectra over exposures from 0 to 270 kGy. Conversely, irradiation induces dislinking in the P(MMA-BP) layers, leading to an increase in the degree of swelling and thus a red shift in the wavelength of reflected light. This effect was evident in a ~75 nm red shift for samples swelled in ethanol after irradiation with a dose of 325 kGy (Figure 3.2 d, e, f).

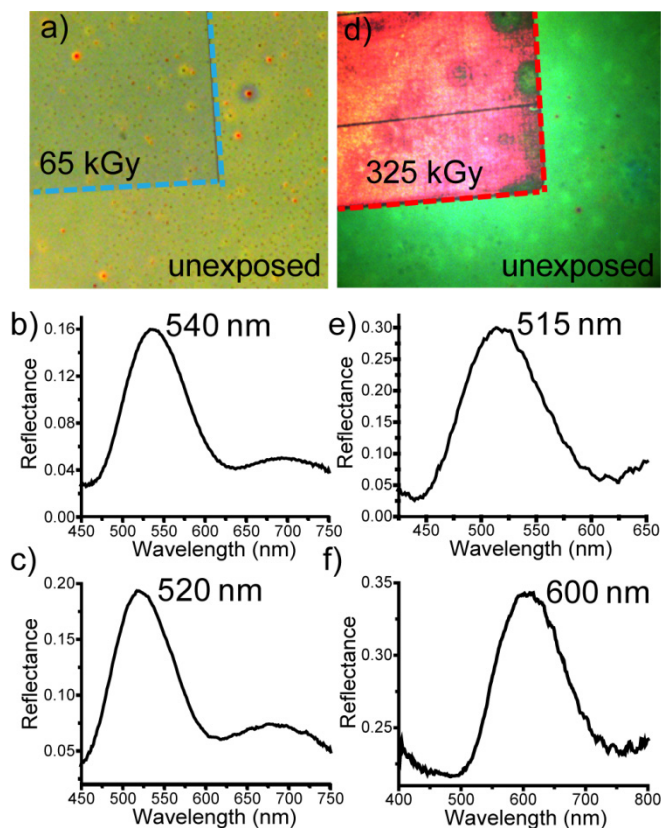


Figure 3.2 Optical micrographs of swelled multilayers after exposure to radiation within the regions denoted by the dotted square for preferentially a) crosslinking and d) degrading systems. Corresponding reflectance spectra show a c) blue shift and f) red shift from the unexposed areas (b, e) of the crosslinked and degraded sensors, respectively, upon swelling.

Figure 3.3 shows the full range of sensitivity for P(OEGMA-BP) and P(MMA-BP)-based sensors which display an increasing blue or red shift, respectively, in the wavelength of reflected light with increasing radiation dose. Preferentially crosslinking P(OEGMA-BP)-based sensors show a sharp linear decrease in λ_{\max} at doses up to approximately 50 kGy, after which there is a more gradual blue shift of λ_{\max} with increasing dose. An approximately linear dependence of λ_{\max} with increasing dose is observed for preferentially degrading PMMA-based sensors. It is noted that the P(*p*-MS-

BP) layers likely undergo additional radiation-induced crosslinking, based on previous findings showing that *para*-substituted polystyrenes tend to crosslink under ionizing radiation, presumably due to crosslinking via hydrogen abstraction from the *para*-position.¹⁷ However, ethanol is a non-solvent for P(*p*-MS-BP) and therefore these layers do not swell upon immersion in ethanol and thus do not contribute to the observed shift in reflectance.

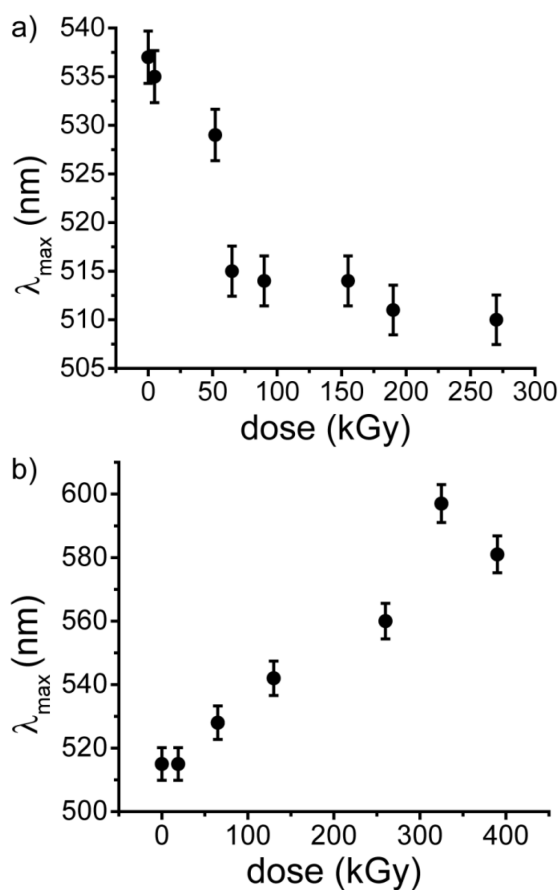


Figure 3.3 Graphs showing change in peak wavelength of reflected light with increasing radiation dose demonstrating a blue-shift for a) a preferentially crosslinking sensor and a red-shift for b) a preferentially degrading sensor. Data shown is a representative sample of sensor response with error bars depicting typical uncertainty in λ_{\max} , $\pm 0.5\%$ and $\pm 1\%$, respectively.

While the dose ranges for noticeable colorimetric changes are relatively high, they are comparable to commercial ion beam dosimetry systems, including radiochromic film systems GafChromic HD-V2, Far West Technology FWT-60 and cellulose triacetate Fujifilm FTR-125, with sensitivities of single to hundreds of kGy. Such photonic sensors could thus provide a new route towards simple and environmentally stable radiation dosimeters for food, packaging, and medical device sterilization techniques, which rely upon monitoring doses in the kGy-range.^{21,22}

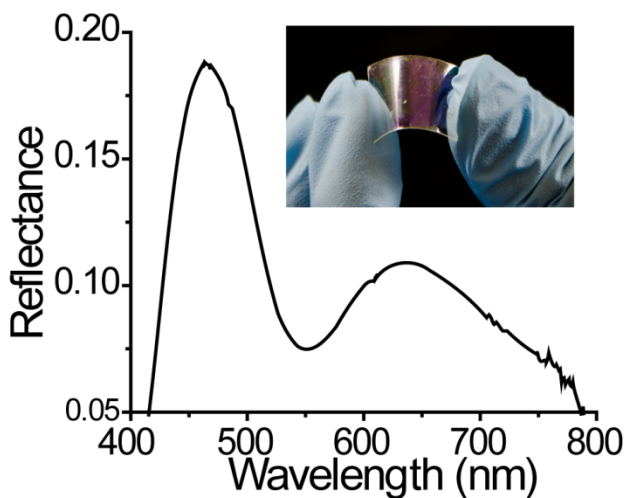


Figure 3.4 Reflectance spectrum of a 7-layer flexible sensor with a photograph (inset) showing the flexibility of such a multilayer fabricated on a Mylar sheet.

Finally, it is demonstrated that these multilayers can be effectively fabricated on flexible substrates of transparent, biaxially-oriented polyethylene terephthalate (Mylar) sheets (Figure 4). These sensors were found to maintain their structural integrity and function even after multiple swelling/de-swelling cycles. The ability to prepare these sensors on flexible substrates opens the door to use in a variety of contexts, for example, as wearable patches, or in packaging applications.

3.5 Conclusions and future outlook

This chapter describes a new approach to colorimetric radiation sensing based on photonic polymer multilayers. Preferential degradation or crosslinking of the low-index polymer layers alters the degree of swelling of the irradiated region, thereby providing a colorimetric read-out of the exposed dose. Furthermore, the process allows for the preparation of robust multilayers on polymer substrates, offering the possibility to prepare flexible sensors.

While the sensitivity of these first generation devices is in the 100 kGy range, we anticipate that further refinements to the copolymers used should enable substantial improvements in sensitivity. Improvements in sensitivity by roughly an order of magnitude can easily be envisioned by increasing the molecular weight between crosslinks in the low index layers, which would lead to a more pronounced change in the degree of swelling after irradiation—since each net dislinking event would correspond to a proportionally larger change in crosslink density—and therefore a more pronounced colorimetric response at lower doses. Further improvements should be possible through optimization of the copolymer chemistry. For example, copolymerization with methacrylic acid is known to increase the sensitivity of PMMA-based photoresists substantially, and a similar strategy could be employed here to improve the sensitivity of preferentially dislinking sensors to lower doses of radiation, i.e., by increasing the yield of dislinking reactions relative to crosslinking or other chemical reactions that do not affect backbone bonds.²³

3.6 References

1. Morehouse, K. M. & Komolprasert, V. in *Irradiat. Food Packag.* 1–11 (American Chemical Society, 2004).
2. Shani, G. *Radiation Dosimetry: Instrumentation and Methods.* (CRC Press LLC, 2001).
3. Schimitberger, T., Ferreira, G. R., Saraiva, M. F., Bianchi, a. G. C. & Bianchi, R. F. X-ray dose detector based on color changing of light-emitting polymer–metal complex hybrid material. *Sensors Actuators B Chem.* **168**, 131–137 (2012).
4. Schimitberger, T., Ferreira, G. R., Akcelrud, L. C., Saraiva, M. F. & Bianchi, R. F. X-rays sensing properties of MEH-PPV, Alq₃ and additive components: a new organic dosimeter as a candidate for minimizing the risk of accidents of patients undergoing radiation oncology. *Med. Eng. Phys.* **35**, 140–4 (2013).
5. Liu, Z., Xue, W., Cai, Z., Zhang, G. & Zhang, D. A facile and convenient fluorescence detection of gamma-ray radiation based on the aggregation-induced emission. *J. Mater. Chem.* **21**, 14487 (2011).
6. Mai, H. H., Duong, N. D. & Kojima, T. Dyed polyvinyl chloride films for use as high-dose routine dosimeters in radiation processing. *Radiat. Phys. Chem.* **69**, 439–444 (2004).
7. Mai, H. H., Solomon, H. M., Taguchi, M. & Kojima, T. Polyvinyl butyral films containing leuco-malachite green as low-dose dosimeters. *Radiat. Phys. Chem.* **77**, 457–462 (2008).
8. Laranjeira, J. M. ., Khoury, H. ., de Azevedo, W. ., de Vasconcelos, E. . & da Silva, E. . Polyaniline nanofilms as a sensing device for ionizing radiation. *Phys. E Low-dimensional Syst. Nanostructures* **17**, 666–667 (2003).
9. Soliman, Y. S., Basfar, A. A. & Msalam, R. I. A radiochromic film based on leucomalachite green for high-dose dosimetry applications. *Radiat. Meas.* **62**, 45–51 (2014).
10. Born, M. Wolf, E. *Principles of Optics.* (Cambridge University Press, 2002).
11. Ge, J. & Yin, Y. Responsive photonic crystals. *Angew. Chem. Int. Ed. Engl.* **50**, 1492–522 (2011).
12. Nair, R. V. & Vijaya, R. Photonic crystal sensors: An overview. *Prog. Quantum Electron.* **34**, 89–134 (2010).

13. Fenzl, C., Hirsch, T. & Wolfbeis, O. S. Photonic crystals for chemical sensing and biosensing. *Angew. Chem. Int. Ed. Engl.* **53**, 3318–35 (2014).
14. Chiappelli, M. C. & Hayward, R. C. Photonic multilayer sensors from photo-crosslinkable polymer films. *Adv. Mater.* **24**, 6100–4 (2012).
15. Jia, J., Sarker, M., Steinmetz, M. G., Shukla, R. & Rathore, R. Photochemical elimination of leaving groups from zwitterionic intermediates generated via electrocyclic ring closure of alpha,beta-unsaturated anilides. *J. Org. Chem.* **73**, 8867–79 (2008).
16. Berger, M.J. Coursey, J.S. Zucker, M.A. Chang, J. NIST ESTAR Database. (2005). at <<http://physics.nist.gov/PhysRefData/Star/Text/method.html>>
17. Chapiro, A. *Radiation Chemistry of Polymeric Systems*. (John Wiley & Sons, Inc., 1962).
18. Zainuddin, Albinska, J., Ulanski, P. & Rosiak, J. Radiation-induced degradation and crosslinking of poly (ethylene oxide) in solid state. *J. Radioanal. Nucl. Chem.* **253**, 339–344 (2002).
19. Shultz, A., Roth, P. & Berge, J. Radiation Degradation of Polymethacrylates . Dose Rate and Medium Effects . *J. Polym. Sci. Part A* **1**, 1651–1669 (1963).
20. Lee, E. ., Rao, G. . & Mansur, L. . LET effect on cross-linking and scission mechanisms of PMMA during irradiation. *Radiat. Phys. Chem.* **55**, 293–305 (1999).
21. Komolprasert, V. in *Packag. Non Therm. Process. Food* (Blackwell Publishing, 2007).
22. Woo, L. & Sandford, C. L. Comparison of electron beam irradiation with gamma processing for medical packaging materials. *Radiat. Phys. Chem.* **63**, 845–850 (2002).
23. *SPIE Handbook of Microlithography, Micromachining, and Microfabrication: Volume 1*. (SPIE Press, 1997).

CHAPTER 4

NANOCOMPOSITE POLYMER FILMS AND PHOTONIC MULTILAYERS WITH ENHANCED REFLECTANCE EFFICIENCY

4.1 Introduction

High refractive index polymers (HRIPs) are widely explored for a variety of applications including optics, mechanical property tunability, displays, energy and data storage.¹⁻³ Recently, new advances in photonic devices have led to an increased interest in the development of high refractive index (n) materials. A key factor in the reflectance efficiency of 1-dimensional (1-D) photonic crystals, periodic multilayers that rely on the interference of light to reflect a characteristic wavelength defined by the refractive index and thickness of each layer, is refractive index contrast between layers.^{4,5} The intensity of this characteristic wavelength can be increased by increasing the number of layers or enhancing refractive index contrast between the layers. The narrow range of refractive indices of most polymers, typically between 1.45 – 1.60, is an inherent limitation to the contrast achievable in polymer-only 1-D photonic devices.

For optical applications, one of the main obstacles of incorporating particles for transparent polymer composites is maintaining high transmittance by achieving homogenous particle dispersion and minimizing aggregation.⁶ Large aggregates, typically those greater than or equal to 40 nm, will trigger optical loss due to scattering of incident light. The intensity of scattered light rises dramatically with increasing particle size, as is well described by Rayleigh's law:

$$\frac{I}{I_0} = e^{-\left[\frac{30p_x r^3}{4\lambda^4} \left(\frac{n_p}{n_m} - 1\right)\right]} \quad 4.1$$

where I is the intensity of transmitted light, I_0 is the intensity of incident light, ϕ_p is the volume fraction of polymer, x is the optical path length, r is the radius of particles, λ the wavelength of light, n_p the refractive index of particles and n_m the refractive index of the matrix material.^{7,8}

Significant contributions have been made towards enhancing the refractive index of polymers, including via the introduction of substituent groups with high polarizability for intrinsically high refractive index polymers, as well as incorporating high refractive index metal oxide nanoparticles in polymer matrices for high- n nanocomposites.^{7,9-12} The following serves to highlight notable work in the field of fabricating polymer-nanoparticle composite films with both high transparency and enhanced refractive index. In grafting-to techniques, nanoparticle ligands contain appropriate functional groups such that polymer can be covalently attached to the particle surface. Polymers must be appropriately modified, typically end-functionalized, with a group which will react with the particle surface chemistry, thus grafting the polymer to the nanoparticle. In grafting-from techniques, polymerization is initiated from the particle surface. However, these methods are often synthetically challenging, time consuming or specific to a single materials system.

Specifically, Lü and co-workers have prepared high refractive index ZnS-polymer nanocomposite films using a grafting from technique.¹⁰ ZnS ($n = 2.36$) nanoparticles were functionalized and reacted with a UV curable urethane-methacrylate macromer (UMM), triggering immobilization of the nanoparticles in the polymer matrix upon polymerization. Resulting films exhibited low surface roughness and homogenous particle distribution, as well as excellent optical transparency and an enhanced refractive

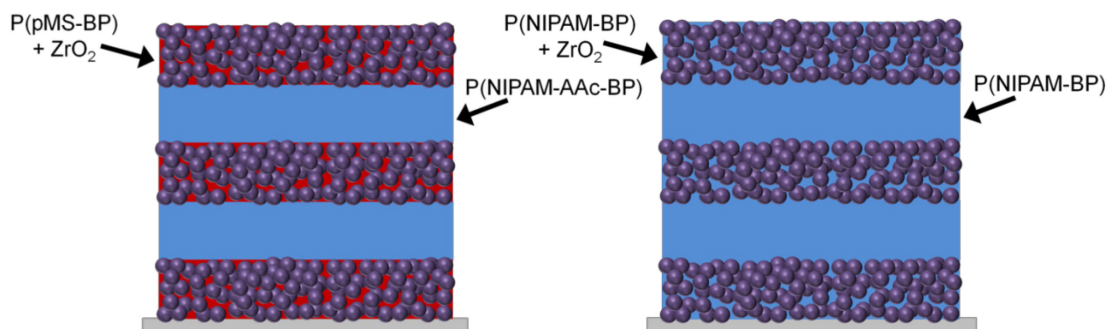
index of the composite films was from 1.645 for pure UM polymer to 1.796 with 86 wt% particle incorporation.

Early work on high refractive index thin films by Chang et. al. included the fabrication of polymer- titania ($n = 2.01$) nanocomposites using polymer, coupling agent and titania precursor via a sol-gel process.¹³ While composite films had high optical clarity as well as refractive indices as high as 1.82 for polyimide-based composites, the fabrication route is time-intensive, requiring specific polymer synthesis and modification, sol-gel processing and spin-coating followed by a multistep baking process. They have more recently developed polyimide (PI)-titania nanocomposites using a soluble fluorinated polyimide. The composite refractive index was enhanced to a larger extent, from 1.571 to 1.993, with high optical clarity, however this fabrication route also involves an extensive multistep process by which a carboxy-terminated PI undergoes esterification with titanium butoxide to form organic-inorganic bonds, followed by hydrolysis, condensation and finally thermal curing of the nanocomposite film.⁶

Ueda and co-workers have also completed in-depth studies of polymer-nanoparticle composites as well as the synthesis of polymers with inherently high refractive indices via incorporation of atoms refractive index-enhancing sulfur-containing substituents such as thioethers. Recently, these routes were combined by creating a sulfur-containing PI-titania nanocomposite with good optical transparency and an enhanced refractive index of 1.81.⁹ While a homogeneous mixture was obtained by mechanical stirring, again a multi-step procedure for polymer synthesis and composite preparation is required, including a multi-step cure followed by drying under vacuum.

Míguez and co-workers have established polymer-infiltrated nanoparticle-based photonic multilayers with high reflectance intensity as well as flexibility, however they have not been shown to be stimulus-responsive.¹⁴ Recently, Watkins and co-workers have utilized titania nanoparticles for nanocomposite-based 3-D photonic crystals and gratings, though these optical materials also do not display stimuli-responsive behavior.¹² Previous chapters have established this unique approach to photonic multilayers for colorimetric sensing of temperature and ionizing radiation.¹⁵ The following sections of this chapter describe a straight-forward route to enhance reflectance efficiency via the fabrication of homogenous nanocomposite thin films of hydrophobic and hydrophilic polymers, as well as photonic multilayers, with tunable refractive index according to the weight percent of nanoparticles in the composite.

These films are prepared by simple mixing of solutions of dispersed zirconia nanoparticles with dissolved polymer using miscible solvents for both systems. Nanocomposite photonic multilayers retain their structural integrity and thermoresponsive behavior, providing a convenient route for enhancing reflectance from a lower number of layers by enhancing refractive index contrast between layers. This technique also allows for straight-forward fabrication of “all-gel” sensors with refractive index contrast arising solely from the addition of nanoparticles to alternating layers.



Schematic 4.1 Nanocomposite photonic multilayer schematic of PNIPAM-based multilayers with a) P(pMS-BP) + 70 wt% zirconia and b) P(NIPAM-BP) + 85 wt% zirconia as the high-refractive index layers.

4.2 Experimental methods

4.2.1 Polymer synthesis

Polymers were synthesized by conventional free radical polymerization in 1,4-dioxane (Aldrich) using azobisisobutyronitrile (AIBN) (Aldrich) re-crystallized from methanol as initiator. NIPAM and acrylic acid (AAc) were purchased from Aldrich and used as received. Inhibitor was removed from *p*-methylstyrene (pMS) (Acros Organics) by passing through a column of basic alumina. Acrylamidobenzophenone (BP) monomer was synthesized according to a previously reported literature procedure via reaction of acryloyl chloride and 4-aminobenzophenone.^[15]

P(pMS-BP)

The monomers pMS (3 mL, Aldrich) and BP (0.45 g) were dissolved with AIBN (0.015 g) in 30 mL of 1,4-dioxane and polymerized at 80°C for 15 h under nitrogen following three freeze-pump-thaw cycles, yielding a copolymer containing 10 mol% of BP. The polymer was purified by precipitation into methanol, washed under vacuum

filtration and dried overnight in a vacuum oven prior to use. Structure was confirmed by ^1H NMR (Bruker DPX 300).

P(NIPAM-AAc-BP)

The monomers NIPAM (1.503 g), acrylic acid (AAc) (0.050 mL), BP (0.036 g) were dissolved with AIBN (0.005 g) in 15 mL of 1,4-dioxane and polymerized at 80°C for 15 h under nitrogen following three freeze-pump-thaw cycles, yielding a copolymer containing 5 mol% AAc and 1 mol% BP. The polymer was purified by precipitation into diethyl ether, washed over vacuum filtration and dried overnight in a vacuum oven prior to use. Structure was confirmed by ^1H NMR (Bruker DPX 300). An AAc-containing polymer was chosen to enhance the hydrophilicity and thus degree of swelling of the P(pMS-BP)/P(NIPAM-AAc-BP) multilayers.

P(NIPAM-BP)

The monomers NIPAM (2.004 g) and BP (0.232 g) were dissolved with AIBN (0.006 g) in 20 mL 1,4-dioxane and polymerized, purified and characterized using the same procedure as P(NIPAM-AAc-BP).

4.2.2 Photonic multilayer preparation & characterization

Photonic multilayers were prepared by sequential spin-coating, crosslinking and developing of polymer films as previously reported.¹⁵ Glass substrates were first cleaned by sonication for 10 min each in acetone, ethanol and water followed by surface treatment with methacryloxypropyl trichlorosilane (Gelest) to promote substrate-polymer adhesion. P(pMS-BP) and both P(NIPAM-AAc-BP) and P(NIPAM-BP) were cast from toluene and 1-propanol, respectively. Developing solutions for P(pMS-BP) and P(NIPAM-BP), and their corresponding nancomposites, were 1: 0.65 toluene: hexanes

and 2: 1 ethanol: water, respectively. Polymer films were crosslinked using a Newport 365 nm UV light source, with typical doses of approximately 80 J/cm^2 sufficient to fully convert the BP photo-crosslinkers.

Zirconia nanocrystal dispersion was purchased from Pixelligent Technologies, LLC as a $50 \pm 1 \text{ wt\%}$ ($42 \pm 2 \text{ wt\%}$ inorganic content) dispersion in propylene glycol monomethylether acetate (PGMEA) and used as received. Both NIPAM-based polymers were dissolved in PGMEA. For P(pMS-BP) composite solutions, a cloudy suspension, due to poor solubility, of polymer in PGMEA was first made, followed by dropwise addition of toluene until polymer was fully dissolved and a clear solution obtained. Sonication for 5 minutes was used to ensure complete dissolution of all polymer solutions followed by filtration through a $0.2 \mu\text{m}$ PTFE filter prior to addition of nanoparticles. Particle-polymer solutions were made by dropwise addition of an appropriate aliquot of nanoparticle dispersion to polymer solutions followed by gentle hand stirring resulting in a clear, colorless solution. Films were typically cast immediately upon mixing, however particle-containing polymer solutions were clear and stable over several weeks in most cases when sealed to avoid solvent evaporation.

All films were spin-cast at 2000 rpm for 50 s using a Headway Research spin coater. Refractive indices and thicknesses of polymer films were characterized using a variable angle spectroscopic ellipsometer (Sopra) or null ellipsometer (LSE Stokes, Gaertner). Reflectance spectra were acquired using a reflectance probe (Semiconsoft MProbe) integrated with an upright microscope (Zeiss AxioTech) with light incident normal to the sample surface and a spectral range of 400-800 nm. To monitor changes in reflectance with temperature, multilayers were placed on a temperature stage (INSTECH

HCS621V) with liquid nitrogen cooling and the sample surface fully covered with deionized water for all variable temperature experiments, allowing for 20 min equilibration at each temperature.

4.2.3 Reflectance calculations

MATLAB was used for all reflectance calculations. The transfer matrix method was employed for calculating reflectance assuming perfectly smooth interfaces parallel to the substrate and homogenous material properties (refractive index, layer thickness) through each layer of the stack in an ambient environment of air ($n = 1.00$). The refractive indices of PpMS and PNIPAM (polymer-only films) were taken as 1.57 and 1.51, respectively, and dispersion was ignored.

4.3 Results and discussion

This chapter explores a straight-forward method to enhance the refractive index of both hydrophobic and hydrophilic polymers by simple mixing with high refractive index metal oxide nanoparticles, in this case, ZrO_2 . Nanocomposite films are used to fabricate photonic multilayers with enhanced reflectance efficiency compared to their polymer-only counterparts. Solvents were chosen appropriately to optimize miscibility of polymer and nanoparticle solutions while maintaining solubility of all components.

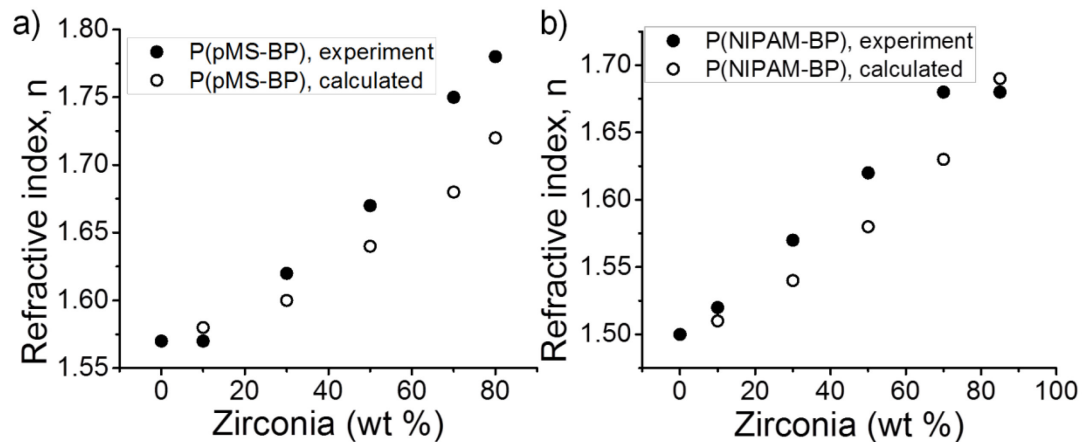


Figure 4.1 Tunability of refractive index of both a) hydrophobic PpMS and b) hydrophilic PNIPAM is achieved by adjusting weight % of zirconia.

Refractive indices of both P(pMS-BP) and P(NIPAM-BP) were increased $\sim 10\%$ (Figure 4.1) simply by adjusting the weight % incorporation of zirconia in polymer solutions prior to spin-coating. Solutions are clear and colorless for loadings up to 70 wt% zirconia in P(pMS-BP) and 85 wt% P(NIPAM-BP). AFM analysis of spin-cast films, ~ 90 nm in thickness, revealed homogenous P(pMS-BP) composites with minimal increase in rms surface roughness, 1.043 nm, compared to the polymer-only film, 0.271 (Figure 4.2 c,d). Additionally, composite films can be fully crosslinked and developed in a marginal solvent to remove uncrosslinked material, with no evidence of delamination. Homogeneous dispersion, low surface roughness and efficient crosslinking support the exploration of these composite films for photonic multilayers.

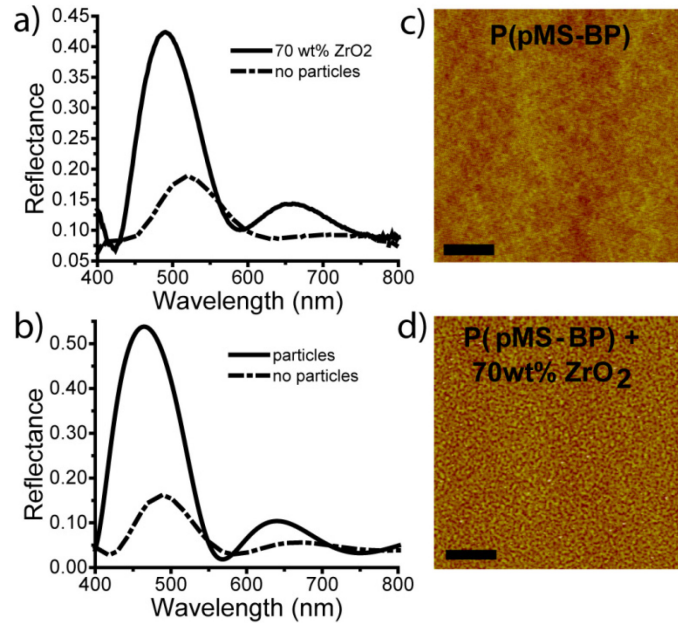


Figure 4.2 a) Experimental spectra showing enhanced reflectance of photonic multilayers with particles (solid line) versus without (dashed line) and supported by b) calculated reflectance spectra based on the experimental thickness and refractive index parameters for each system. AFM images reveal d) nanocomposite films maintain homogeneity with minimal increase in surface roughness compared to c) polymer-only film. Scale bar = 5 μm .

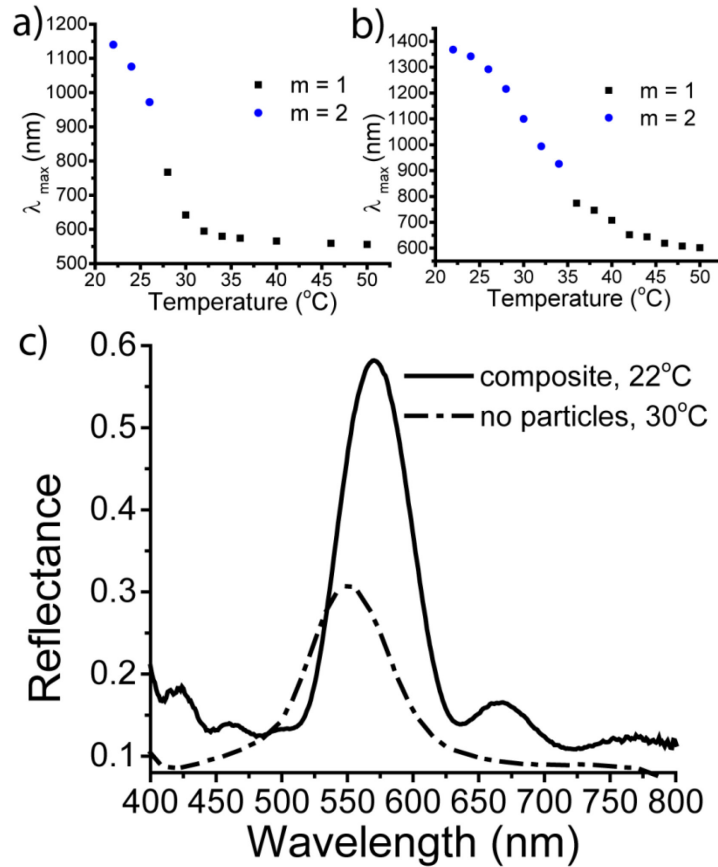


Figure 4.3 Blue shift of reflected light with increasing temperature observed for both a) P(pMS-BP) + 70 wt% ZrO₂/P(NIPAM-BP)-based nanocomposite multilayer and b) P(pMS-BP)/P(NIPAM-BP) polymer-only based multilayers in deionized water, and c) reflectance spectra at comparable degrees of swelling showing enhanced intensity of composite multilayer (solid line) versus polymer-only multilayer (dashed line). Data plotted in a,b are λ_{\max} of primary reflectance peak, $m = 1$, calculated based on the higher order harmonics, $m = 2$, if $m = 1$ was not visible in the accessible spectral range of the instrument during experiment.

In Figure 4.2 a, dry-state reflectance of P(pMS-BP)/P(NIPAM-AAc-BP) multilayers with identical optical thicknesses but different refractive index contrast between layers is compared. It was clearly observed that boosting the refractive index

contrast ~10% with the addition of 70 wt% zirconia (solid line) leads to a nearly 3-fold increase in the reflectance intensity compared to an equivalent polymer-only multilayer (dashed line). Comparison of experimental spectra to calculations (Figure 4.2b) of perfectly uniform systems with zero roughness but equivalent optical properties (refractive index and physical thickness of layers), reveals high reflectance efficiency, ~70%, is maintained in the nanocomposite system compared to the polymer-only system, ~85%. Small differences between the λ_{\max} of the calculated and experimental reflectance spectra may be attributed to slight variations in nanocomposite film thickness through the multilayer stack. Furthermore, in addition to multilayers with higher reflectance intensity, this also allows for the fabrication of multilayers with sufficiently high reflectance for detection by eye from a reduced number of layers, and thus a faster fabrication time.

Responsive behavior of these multilayers arises from the temperature sensitive behavior of PNIPAM, which de-swells due to a volume phase transition above a lower critical solution temperature ~32°C in water. Layer thicknesses were chosen to reflect blue-violet light in the dry state and undergo a red-shift through the visible spectrum due to swelling of the low refractive index NIPAM-based layers upon immersion in deionized water. In the swelled state, nanocomposite multilayers retain their structural integrity, thermochromic response and enhanced reflectance efficiency as demonstrated in Figure 4.3.

Tunability of the refractive index of our responsive material, P(NIPAM-BP), allows for the fabrication of all-gel photonic multilayers containing 85 wt% loading P(NIPAM-BP) as high refractive index layers and show a well defined reflectance peak

in the dry state at only 7 layers (Figure 4.4a). When swelled in water, these all-gel composites also retain structural integrity and temperature-responsive behavior. In addition, the use of only gel materials allows for a greater degree of swelling and thus

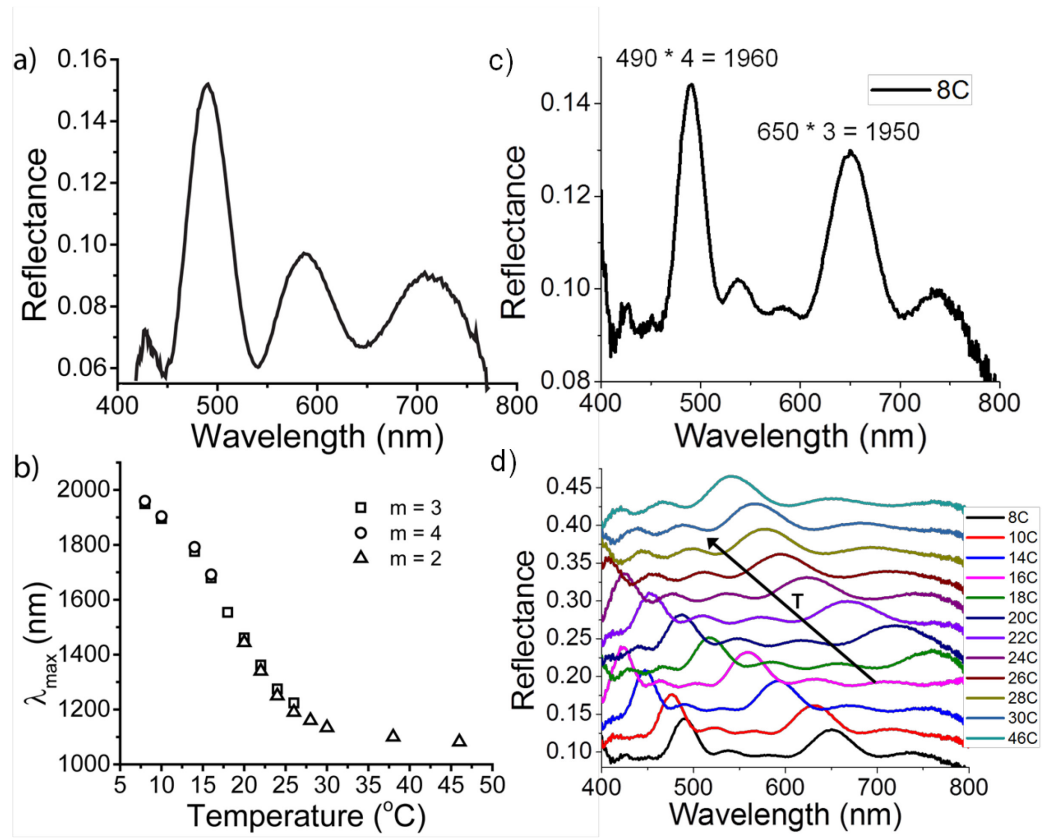


Figure 4.4 Reflectance spectra of an all-gel P(NIPAM-BP)-based composite photonic multilayer in the dry state. b) Plot showing blue shift of reflected light with increasing temperature for all-gel composite immersed in deionized water. $m = 2,3,4$ corresponds to the harmonic used to calculate λ_{\max} of primary peak, $m = 1$. Data plotted are λ_{\max} of primary reflectance peak, $m = 1$, calculated based on c) the higher order harmonics, $m = 2,3,4$, visible in d) the accessible spectral range of the instrument during experiment.

accessibility to an even wider range of wavelengths in the UV, visible and IR portions of the spectrum. By eliminating the brittle P(pMS-BP) layers, these all-gel composite multilayers also hold promise for use as colorimetric strain sensors.

Notably, there is a shift in transition temperature to lower temperature with the presence of zirconia. For polymer-only multilayers, an expected transition temperature of 32°C, near the lower critical solution temperature of P(NIPAM), is observed. This transition is lowered to 27°C for 70 wt% loading of a P(pMS-BP)/P(NIPAM-AAc-BP) multilayer, and again lower, 18°C, for the 85 wt% P(NIPAM-BP)/P(NIPAM-BP) all-gel multilayer. To understand if this trend could be attributed to stronger van der Waals interactions upon addition of inorganic particles, we calculate the interaction potential, W , for two infinitely parallel half-spaces separated by 60 nm water, PS-water-PS and ZrO₂-water-ZrO₂ and find W of ZrO₂-water-ZrO₂, 1×10^{-6} N/m, is an order of magnitude larger than PS-water-PS, 1×10^{-7} N/m. This change in W , however, is insignificant when considering the osmotic pressure, on the order of hundreds of kPa, of the hydrated gel compared to the considerably smaller disjoining pressure taken from the derivative of W with respect to the half-space separation distance. While the ligand chemistry of the commercially supplied zirconia nanoparticles in this work is proprietary, it is possible that thermoresponsive behavior of the ligands as well as ligand-ligand, ligand-polymer and ligand-solvent interactions may also influence the onset of the multilayer transition temperature. This phenomenon may be further exploited to tune the transition temperature of thermoresponsive materials, and its mechanism is under continued investigation.

4.4 Conclusions and outlook

For photonic applications, a careful balance must be maintained to ensure enhanced reflectance efficiencies by increasing refractive index contrast are not consequentially negated by a large extent of roughness at the layer interfaces. Nanoparticles with higher refractive indices but which do not absorb greatly in the visible wavelengths, such as ZnS ($n = 2.36$) and TiO₂ ($n_{\text{rutile}} = 2.70$), may also be of interest for refractive index enhancement.^{1,2,3} The ability to fabricate homogenous nanoparticle-polymer composites in a simple, straight-forward manner would prove beneficial to a broader range of fields beyond photonics, including, but certainly not limited to, optoelectronics, sensing, displays and coatings. In this chapter, the fabrication of all-gel composite multilayers was described. This technique holds promise for future use as a colorimetric strain sensor. For example, if the multilayer could be fabricated on a sacrificial layer and transferred to a flexible, elastomeric substrate, such as poly(dimethyl siloxane) (PDMS), one may envision a blue-shift or red-shift of λ_{max} when placed in tension or compression, respectively.^{16,17}

4.6 References

1. Caseri, W. Nanocomposites of polymers and metals or semiconductors: Historical background and optical properties. *Macromol. Rapid Commun.* **21**, 705–722 (2000).
2. Althues, H., Henle, J. & Kaskel, S. Functional inorganic nanofillers for transparent polymers. *Chem. Soc. Rev.* **36**, 1454–65 (2007).
3. Hanemann, T. & Szabó, D. V. *Polymer-Nanoparticle Composites: From Synthesis to Modern Applications. Material.* **3**, 3468–3517 (2010).
4. Born, M. Wolf, E. *Principles of Optics.* (Cambridge University Press, 2002).
5. Guldin, S., Kolle, M., Stefik, M., Langford, R., Eder, D., Wiesner, U., Steiner, U. Tunable mesoporous bragg reflectors based on block-copolymer self-assembly. *Adv. Mater.* **23**, 3664–8 (2011).
6. Chang, C.-M., Chang, C.-L. & Chang, C.-C. Synthesis and Optical Properties of Soluble Polyimide/Titania Hybrid Thin Films. *Macromol. Mater. Eng.* **291**, 1521–1528 (2006).
7. Liu, J. & Ueda, M. High refractive index polymers: fundamental research and practical applications. *J. Mater. Chem.* **19**, 8907 (2009).
8. Zimmermann, L., Weibel, M., Caseri, W., Suter, U. & Walther, R. High refractive index films of polymer nanocomposites. *J. Mater. Res.* **8**, 1742–1748 (1993).
9. Liu, J., Nakamura, Y., Ogura, T., Shibasaki, Y., Ando, S., Ueda, M. Optically Transparent sulfur containing polyimide-TiO₂ nanocomposite films with high refractive index and negative pattern formation from poly (amic acid) -TiO₂ nanocomposite film. *Chem. Mater.* 273–281 (2008).
10. Lü, C., Cheng, Y., Liu, Y., Liu, F. & Yang, B. A Facile Route to ZnS–Polymer Nanocomposite Optical Materials with High Nanophase Content via γ -Ray Irradiation Initiated Bulk Polymerization. *Adv. Mater.* **18**, 1188–1192 (2006).
11. Lu, C., Cui, Z., Wang, Y., Zuo, L., Guan, C., Yang, B., Shen, J. Preparation and characterization of ZnS-polymer nanocomposite films with high refractive index. *J. Mater. Chem.* **13**, 2189 (2003).
12. Beaulieu, M. R., Hendricks, N. R. & Watkins, J. J. Large-Area Printing of Optical Gratings and 3D Photonic Crystals Using Solution-Processable Nanoparticle/Polymer Composites. *ACS Photonics* **1**, 799–805 (2014).

13. Chang, C. & Chen, W. High-Refractive-Index Thin Films Prepared from Dianhydride – Titania Hybrid Materials. 3419–3427 (2001).
14. Calvo, M. E., Sánchez Sobrado, O., Lozano, G. & Míguez, H. Molding with nanoparticle-based one-dimensional photonic crystals: a route to flexible and transferable Bragg mirrors of high dielectric contrast. *J. Mater. Chem.* **19**, 3144 (2009).
15. Chiappelli, M. C. & Hayward, R. C. Photonic multilayer sensors from photo-crosslinkable polymer films. *Adv. Mater.* **24**, 6100–4 (2012).
16. Haque, M. A., Kurokawa, T., Kamita, G., Yue, Y. & Gong, J. P. Rapid and Reversible Tuning of Structural Color of a Hydrogel over the Entire Visible Spectrum by Mechanical Stimulation. *Chem. Mater.* **23**, 5200–5207 (2011).
17. Yue, Y. *et al.* Mechano-actuated ultrafast full-colour switching in layered photonic hydrogels. *Nat. Commun.* **5**, 4659 (2014).

CHAPTER 5

KINETIC RESPONSE OF PHOTONIC POLYMER MULTILAYERS

5.1 Introduction

It is important to better understand and ultimately control the response kinetics of photonic multilayers for them to be useful in practical applications. Many studies have examined the swelling behavior of surface-attached hydrogel films, but often with less focus on the kinetics.¹⁻³ It was apparent in Chapter 2 that the kinetics of swelling for the P(NIPAM-AAc-BP)-based multilayer thermochromic materials are quite slow, which can possibly be attributed to several causes: de-aggregation of hydrophobic benzophenone moieties, inter- and intra-molecular hydrogen bonding, or limitations of mass transport through the thickness of the multilayer. In this chapter, possible causes for limited swelling kinetics are hypothesized and explored experimentally by studying alternative photo-crosslinkable copolymers as well as examining the kinetics at short time scales in the earliest stages of swelling.

To better understand the factors influencing the kinetics of thermochromic multilayers, three additional temperature responsive copolymers: OEGMA, DEAM, and uncharged NIPAM, were considered. To do so, a copolymer of 93 mol% 2-(2-methoxyethoxy)ethyl methacrylate, 5 mol% oligo(ethylene glycol)methacrylate and 2 mol% AAmBP, P(MEO₂MA-OEGMA-AAmBP), was synthesized. This particular composition was chosen based on work by Lutz and co-workers in which MEO₂MA-OEGMA copolymers were investigated as an alternative to the PNIPAM which shows hysteresis in LCST.⁴⁻⁶ It was found that a copolymer containing 95 mol% MEO₂MA and 5% OEGMA has an LCST most similar to PNIPAM, 32 °C, and thus we chose a similar

molar composition to be able to study temperature responsiveness in a range comparable to that of the PNIPAM-based sensors.

To further investigate the effect of hydrogen bonding on sensor response kinetics, *N,N*-diethylacrylamide (DEAM) was also copolymerized with BP and used to fabricate a multilayer with a comparable number of layers and thickness for a direct kinetic comparison of swelling and de-swelling in water. Wu and co-workers have shown that PDEAM, unlike PNIPAM, does not exhibit hysteresis in the coil-to-globule-to-coil transition.⁷⁻¹¹ This is attributed to the absence of a hydrogen bond donor in the DEAM moiety, while PNIPAM is capable of forming inter- and intra- molecular hydrogen bonds due to the presence of an -NH. While there is a variety of N-substituted acrylamides, PDEAM is a suitable choice for comparison because it also displays an LCST near to that of PNIPAM (~32 °C) and thus can be tested in a similar temperature range. This study will help elucidate if hydrogen bonding is the main source of the slow kinetics in PNIPAM-based temperature sensors.

Schmaljohann and co-workers have in fact observed that surface attached, crosslinked DEAM and NIPAM show two time ranges of swelling, characterized as a fast 'dynamic' swelling and a slow 'equilibrium' swelling, for films as thin as 10-20 nm in the dry state.¹² The fast 'dynamic' range was found to occur within minutes or less, and the slow 'equilibrium' swelling over the course of several days. While these time scales are significantly longer than the results presented in this chapter, they, too, note the slow swelling results are in contrast to the fast response time expected for thin hydrogel films. It should also be noted that the system of Schmaljohann and co-workers also includes the additional presence of poly(ethylene glycol) side chains pendent to DEAM and NIPAM

backbones, which is suggested to slow the swelling further due to added hydrogen bonding interactions.

5.2 Experimental methods

P(OEGMA-MEO₂MA-BP)

This polymer was synthesized as described in Chapter 3 and spin cast from toluene. Amounts of 2 mL of 2-(2-methoxyethoxy) ethyl methacrylate (MEO₂MA, Aldrich), 251 μ L of oligoethylene glycol methyl ether methacrylate (OEGMA, $M_n = 475$ g/mol, Aldrich), 58 mg of BP and 3.4 mg of AIBN were polymerized in a 5:1 mixture of ethanol:1,4-dioxane at 80°C for 18 h under nitrogen following three freeze-pump-thaw cycles, resulting in a copolymer containing 2 mol% of BP. OEGMA and MEO₂MA were used as received. The polymer was purified by dialysis and lyophilization, and its structure confirmed by ¹H NMR. M_n of 73 kg/mol with a PDI of 1.94 was determined by THF GPC against PMMA standards. Differential scanning calorimetry (DSC) revealed a glass transition temperature (T_g) of -40°C.

P(DEAM-BP)

Amounts of 2.15 mL of diethylacrylamide (DEAM, Aldrich), 227 mg of BP and 5.9 mg of AIBN were polymerized in 25 mL 1,4-dioxane at 80°C for 18 h under nitrogen following three freeze-pump-thaw cycles, resulting in a copolymer containing 5 mol% of BP. DEAM was used as received. The polymer was purified by precipitation into stirring hexanes and its structure confirmed by ¹H NMR. Differential scanning calorimetry (DSC) revealed a glass transition temperature (T_g) of 80°C. P(DEAM-BP) showed good solubility in 1-propanol, toluene and chloroform. A solution of 11:10 water:1-propanol

was used for developing crosslinked polymer films. For multilayers, solutions of 12 mg/mL P(DEAM-BP) in 1-propanol were spin-cast at 2000 rpm for 50 s.

P(NIPAM-BP)

Amounts of 2.004 g NIPAM, 232 mg of BP and 6 mg of AIBN were polymerized in 20 mL 1,4-dioxane at 80°C for 18 h under nitrogen following three freeze-pump-thaw cycles, resulting in a copolymer containing 5 mol% of BP. NIPAM was used as received. The polymer was purified by precipitation into stirring diethyl ether and its structure confirmed by ¹H NMR. Charge-containing P(NIPAM-5%AAc-1%BP) was synthesized and used as described in Chapter 2.

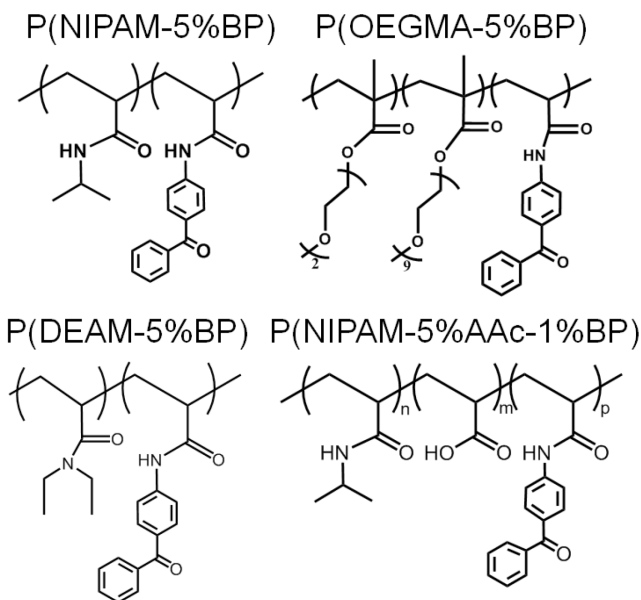


Figure 5.1 Chemical structures of responsive monomers used for kinetics studies of temperature sensitive systems.

5.3 Results and discussion

This chapter describes a more detailed analysis of swelling kinetics comparing polymer chemistries with (poly(N-isopropylacrylamide –BP) (PNIPAM)) and without (poly(N,N-diethyl acrylamide) (PDEAM), poly(oligo ethylene glycol methacrylate) (POEGMA)) a hydrogen bond donating group, specifically the N-H amide present only in PNIPAM.

Table 5.1 Range of swelling for non-charge containing responsive multilayers, from $\lambda_{\max}(\text{dry})$ to $\lambda_{\max}(\text{swell, RT water})$.

Composition	Swelling range in RT water (nm)
P(DEAM-BP)	70
P(NIPAM-BP)	100
P(OEGMA-MEO ₂ MA-BP)	115

Multilayers were fabricated as described in 1.2.1 and designed to have equivalent optical thicknesses such that each reflects blue-violet in the dry state. Upon initial swelling of P(MEO₂MA-OEGMA-AAmBP)-based multilayer in deionized water, peak reflectance wavelength shifted approximately 115 nm (from blue to yellow) and an equilibrium study of peak reflectance with temperature showed a blue-shift of approximately 80 nm in wavelength over a 50 °C temperature change (20 to 70 °C). Neutral P(NIPAM-BP) and P(DEAM-BP)-based multilayers have a λ_{\max} range of 100 nm and 70 nm, respectively, when swelled in deionized water at room temperature.

When initially swelled in room temperature water from the dry state, both P(DEAM-BP) and P(OEGMA-MEO₂MA-BP)-based multilayers display faster swelling kinetics than either neutral or charged PNIPAM, as well as monoexponential fits for both

swelling and deswelling (Table 5.2). The swelling of both neutral and charge-containing PNIPAM multilayers is best fit with a biexponential (Table 5.2). This initial swelling from the dry state is shown in Figure 5.2. Since the degree of swelling of each polymer differs slightly, λ_{\max} values for each sample are normalized between 0 (dry state) and 1 (fully swelled state) to allow for clearer comparison between systems. This result supports the possibility of inter- and intra- molecular hydrogen bonding as a source for slow kinetics in PNIPAM-based sensors. This also demonstrates that the slow swelling kinetics of PNIPAM are material dependent rather than an inherent drawback to this fabrication process.

Deswelling time constants for all neutral multilayers were comparatively quite fast, best fit with a monoexponential with a time constant, $\tau \sim 10$ s. Deswelling for these neutral materials may perhaps be limited by mass transport as water molecules are expelled from gel layers above the lower critical solution temperature.¹³⁻¹⁶ Acrylic acid-containing PNIPAM-based multilayers show a far slower monoexponential deswelling time constant, $\tau \sim 180$ s, possibly due to added electrostatic repulsion of charged moieties upon collapse of the gel above LCST and enhanced hydrophilicity compared to the neutral materials.

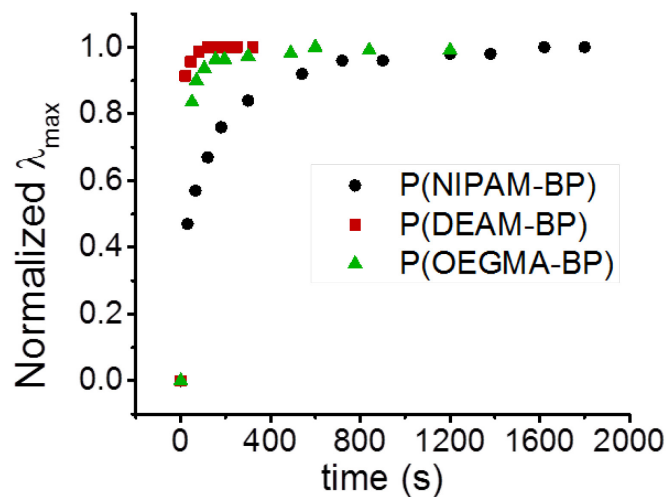


Figure 5.2 Monitoring change in λ_{\max} for multilayers of equivalent optical thickness with different temperature responsive layers based on, P(NIPAM-BP), P(DEAM-BP) or P(OEGMA-BP), swelled in deionized water from the dry state.

Beyond monitoring reflectance spectra upon initial hydration from the dry state, further studies were conducted to monitor the dynamic swelling and de-swelling behavior of multilayers triggered by rapidly changing temperature. A new experimental setup of rapidly transferring the multilayer between water baths of heated and room

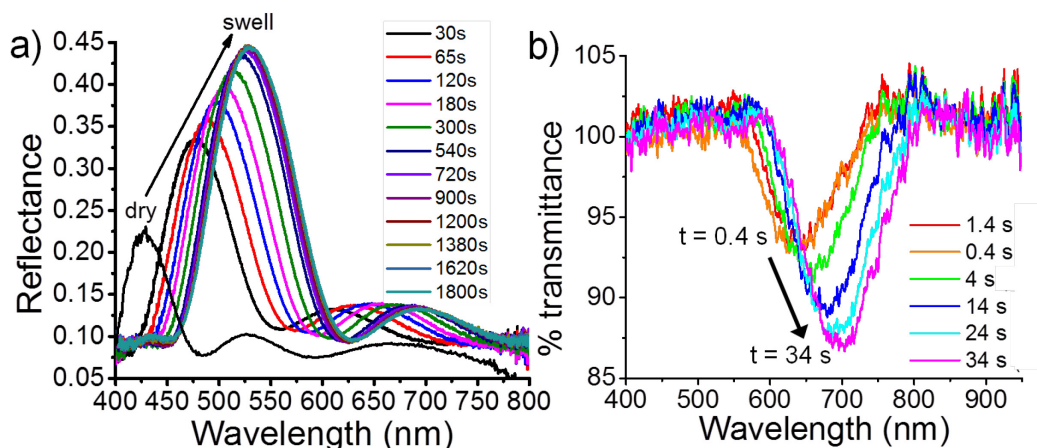


Figure 5.3 a) Reflectance spectra of P(NIPAM-BP)-based multilayer swelling in water at room temperature. For analysis of initial swelling at shorter time scales, b) transmittance spectra of swelling P(NIPAM-5%AAc-1%BP)-based multilayer are shown. A well-defined characteristic Bragg peak is observed at all time points, which is red-shifted with increasing degree of swelling.

temperature deionized water to de-swell and re-swell, respectively, was developed to lessen limitations of heat transfer present when using a temperature stage, used in Chapter 2, to heat and cool the sample. It was found that all three polymers show similarly rapid temperature triggered de-swelling kinetics, with a time constant of $\tau \sim 10$ s. POEGMA and PDEAM show comparable swelling kinetics, while the slower PNIPAM swelling is best fit using a bi-exponential, of the form $y = A_1 e^{-t/\tau_1} + A_2 e^{-t/\tau_2}$, with time constant τ_1 similar to that of PDEAM and POEGMA, as well as a second time constant, τ_2 , one order of magnitude slower, providing evidence that the slow response kinetics of PNIPAM-based sensors may be due to the breaking of hydrogen bonds during swelling cycles. (Table 5.2) Fits using a bi-exponential show nearly equivalent contributions from both the A_1 and A_2 coefficient terms.

Next, swelling at short times for initial hydration of NIPAM-based multilayers is examined, as shown in Figure 5.3. A well-defined characteristic Bragg peak is observed at all time points. This peak is red-shifted with increasing degree of swelling. The

Table 5.2 Time constants for λ_{\max} vs. time curves best fit with either a single or bi-exponential.

	P(NIPAM-BP)	P(OEGMA-BP)	P(DEAM-BP)	P(NIPAM-AAc-BP)
initial swell (τ, s)	$\tau_1 = 170$ $\tau_2 = 1400$	30	20	$\tau_1 = 720$ $\tau_2 = 60$
de-swell (τ, s)	10	10	10	180
re-swell (τ, s)	$\tau_1 = 60$ $\tau_2 = 335$	$\tau_1 = 20$ $\tau_2 = 150$	$\tau = 60$	$\tau_1 = 820$ $\tau_2 = 65$

intensity of the peak also intensifies as the refractive index contrast is enhanced with swelling and the optical thicknesses of the periodic layers become closer to the ideal conditions for maximum reflectance intensity of a quarter-wave film stack. The uniform growth of these peaks suggests that the multilayer swells homogeneously with time, even at short time scales, on the order of single seconds, not previously accessible using the microscope-integrated reflectometer with typical acquisition times on the order of 15 s. A disordered spectra lacking a characteristic reflectance peak would be expected if the multilayer were to swell non-uniformly, for instance due to limitations of mass transport of water through the thickness of the stack.^{17,18} Additionally, swelling of a single film of P(NIPAM-AAc-BP), ~ 250 nm thick, also shows a similarly swelling response with fast initial swelling and a slower equilibration, on the order of 15 min, as monitored by reflectometry.¹⁹ Therefore, these data, along with the rapid swelling in ethanol, a larger molecule than water, observed in Chapter 2, all suggest the swelling of these photonic multilayers is not limited due to limitations of through-thickness mass transport. Upon

swelling, the de-aggregation of hydrophobic benzophenone moieties, hydrogen bonding and electrostatic interactions (for charge-containing films), all likely contribute to the slow kinetics observed. Temperature induced re-swelling of P(OEGMA-BP)-based multilayers is best fit with a bi-exponential. The longer time constant may be due to the presence of hydrogen bond acceptor ether oxygens present in the OEGMA side chains, which are entirely absent in DEAM. Additionally, though we have greatly reduced hydrogen bond affinity through the use of DEAM and OEGMA, we note that these materials do still contain some small percentage of hydrogen bond donors present in the acrylamide functionality of the acrylamidobenzophenone crosslinkers.

This chapter also explores the salt-responsive swelling kinetics of a highly charged polymer, poly(sulfopropyl methacrylate-BP), P(SPMA-BP), previously utilized in Chapter 6 for its selective salt-sensitivity, fast response and high degree of swelling. PSPMA-based multilayers exhibit fast swelling kinetics which become slower with

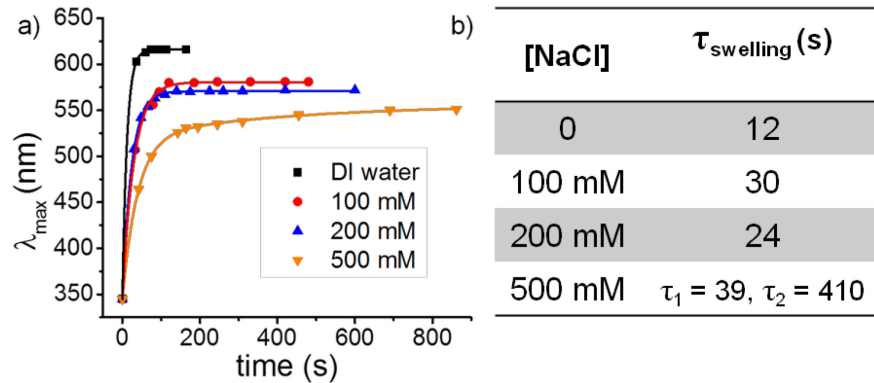


Figure 5.4 a) Monitoring swelling of λ_{\max} with time in various salt concentrations and b) corresponding time constants for kinetic data best fit with either a single or bi-exponential shows fast kinetic response which slows with increasing salt concentration.

increasing salt concentration. The data presented in Figure 5.4 shows λ_{\max} with time upon swelling of a PSPMA-based multilayer for deionized water and a range of salt concentrations. Response is fastest in deionized water, fit with a monoexponential with $\tau \sim 12$ s. This response slows slightly with increasing salt concentrations of 100 mM and 200 mM, both fit with a monoexponential. Swelling in 500 mM NaCl solution, however, is best fit with a bi-exponential, displaying slower time constants of $\tau_1 \sim 39$ s and $\tau_2 \sim 410$ s. (Figure 5.4) This material displays both salt sensitivity as well as a high degree of swelling, making it suitable for Bragg mirror or filter sensors which can span a broad range of wavelengths.

Careful examination of the surface of multilayers after multiple swelling cycles in certain cases revealed evidence of localized delamination (Figure 5.5). Even after several swelling/de-swelling cycles, multilayer films remain adhered to the substrate and exhibit strong reflectance. Optical microscopy and profilometry reveal areas of localized delamination do not propagate globally across the surface, which would likely lead to device failure or a significant decrease in reflectance intensity. Optical profilometry was used to analyze the surface in-situ during de-swelling, triggered by slow removal of a

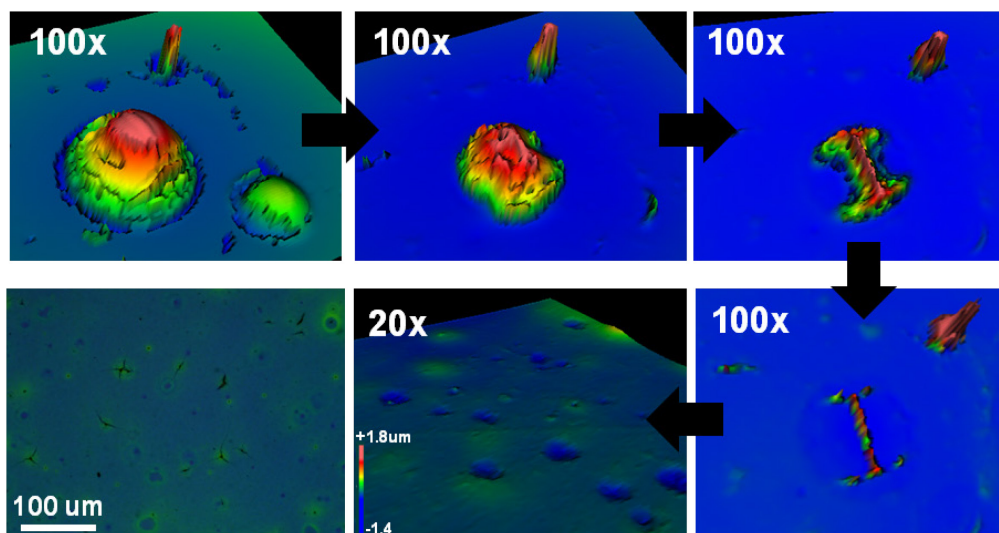


Figure 5.5 Optical profilometry showing the surface morphology of a de-swelling P(OEGMA)-based multilayer. Similar delamination scars are evident on a dried P(SPMA)-based multilayer (bottom left).

large water droplet. In the initial states of de-swelling, rounded areas of $\sim 30 \mu\text{m}$ diameter can be observed protruding through the top, rigid P(pMS-BP) layer. These protrusions of underlying gel recede as the sample dries until the surface is again nearly flat, with small remaining depressions indicative of these delamination sites. By optical microscopy, it is evident that these gel protrusions leave a permanent scar in the top P(pMS-BP) layers

(Figure 5.4, bottom left). It is possible these delamination points nucleate at pinholes in the P(pMS-BP) films which form during the spin-coating process.

5.4 Conclusions and future outlook

Understanding the kinetic response is crucial in allowing for the design of photonic multilayers with predictable responses. In some instances, slower kinetics may be desirable, for example in the case of monitoring exposure to an analyte with time, perhaps useful in smart packaging applications where an item cannot be exposed to a particular level of humidity or solvent vapor atmosphere for a prolonged period of time. Additionally, the ability to tune response time with polymer chemistry demonstrates that the slow swelling kinetics of PNIPAM-based multilayers are material dependent rather than an inherent drawback to this fabrication process. In this chapter, results demonstrate that adjusting the responsive copolymer chemistry by using temperature-sensitive polymers with a lower affinity for hydrogen bonding allows for the fabrication of multilayers with improved response times.

Much can be learned from a future study of the composition drift of benzophenone in the polymers presented in this thesis. It is possible large clusters of hydrophobic benzophenone moieties hinder the swelling kinetics, and can perhaps be more evenly distributed using controlled radical polymerization techniques. Another alternative is the exploration of crosslinkable monomers with less hydrophobic character, to minimize any possible aggregation of hydrophobic moieties. Future work will also include careful studies of the swelling kinetics of single, thin gel films. Additionally, the work presented in this thesis has so far only considered transport of small molecules

(water and, to some extent, salt), but it will be important to understand how larger analytes, such as biomolecules, will diffuse into multilayers as well.

5.5 References

1. Toomey, R., Freidank, D. & R  he, J. Swelling Behavior of Thin, Surface-Attached Polymer Networks. *Macromolecules* **37**, 882–887 (2004).
2. Alf, M. E., Hatton, T. A. & Gleason, K. K. Insights into Thin, Thermally Responsive Polymer Layers Through Quartz Crystal Microbalance with Dissipation. 10691–10698 (2011).
3. Patra, L. & Toomey, R. Viscoelastic response of photo-cross-linked poly(N-isopropylacrylamide) coatings by QCM-D. *Langmuir* **26**, 5202–7 (2010).
4. Hoth, A. & Lutz, J.-F. Preparation of Ideal PEG Analogues with a Tunable Thermosensitivity by Controlled Radical Copolymerization of 2-(2-Methoxyethoxy)ethyl Methacrylate and Oligo(ethylene glycol)Methacrylate. *Macromolecules* **39**, 893–896 (2006).
5. Lutz, J.-F., Akdemir, O. & Hoth, A. Point by point comparison of two thermosensitive polymers exhibiting a similar LCST: is the age of poly(NIPAM) over? *J. Am. Chem. Soc.* **128**, 13046–7 (2006).
6. Lutz, J.-F. Thermo-Switchable Materials Prepared Using the OEGMA-Platform. *Adv. Mater.* **23**, 2237–2243 (2011).
7. Wang, X., Qiu, X. & Wu, C. Comparison of the Coil-to-Globule and the Globule-to-Coil Transitions of a Single Poly(N-isopropylacrylamide) Homopolymer Chain in Water. *Macromolecules* **31**, 2972–2976 (1998).
8. Pang, X. & Cui, S. Single-Chain Mechanics of Poly(N,N-diethylacrylamide) and Poly(N-isopropylacrylamide): Comparative Study Reveals the Effect of Hydrogen Bond Donors. *Langmuir* **29**, 12176–12182 (2013).
9. Zhou, K. *et al.* The Coil-to-Globule-to-Coil Transition of Linear Polymer Chains in Dilute Aqueous Solutions: Effect of Intrachain Hydrogen Bonding. *Macromolecules* **41**, 8927–8931 (2008).
10. Cheng, H., Shen, L. & Wu, C. LLS and FTIR Studies on the Hysteresis in Association and Dissociation of Poly (N-isopropylacrylamide) Chains in Water. *Macromolecules* **39**, 2325–2329 (2006).

11. Lu, Y., Zhou, K., Ding, Y., Zhang, G. & Wu, C. Origin of hysteresis observed in association and dissociation of polymer chains in water. *Phys. Chem. Chem. Phys.* **12**, 3188–94 (2010).
12. Schmaljohann, D., Beyerlein, D., Nitschke, M. & Werner, C. Thermo-reversible swelling of thin hydrogel films immobilized by low-pressure plasma. *Langmuir* **20**, 10107–14 (2004).
13. Zhou, S. & Wu, C. In-Situ Interferometry Studies of the Drying and Swelling Kinetics of an Ultrathin Poly(N -isopropylacrylamide) Gel Film below and above Its Volume Phase Transition Temperature. *Macromolecules* **29**, 4998–5001 (1996).
14. Yoon, J. A., Kowalewski, T. & Matyjaszewski, K. Comparison of Thermoresponsive Deswelling Kinetics of Poly (oligo (ethylene oxide) methacrylate) -Based Thermoresponsive Hydrogels Prepared by “ Graft-from ” ATRP. *Macromolecules* 2261–2268 (2011).
15. Carter, M. C. D., Sorrell, C. D. & Serpe, M. J. Deswelling Kinetics of Color Tunable Poly (N-Isopropylacrylamide). *J. Phys. Chem. B* **115**, 14359–14368 (2011).
16. Patra, L., Vidyasagar, A. & Toomey, R. The effect of the Hofmeister series on the deswelling isotherms of poly(N-isopropylacrylamide) and poly(N,N-diethylacrylamide). *Soft Matter* **7**, 6061 (2011).
17. Lim, H. S., Lee, J.-H., Walsh, J. J. & Thomas, E. L. Dynamic swelling of tunable full-color block copolymer photonic gels via counterion exchange. *ACS Nano* **6**, 8933–9 (2012).
18. Born, M. Wolf, E. *Principles of Optics*. (Cambridge University Press, 2002).
19. Zhang, X., Guan, Y. & Zhang, Y. Ultrathin hydrogel films for rapid optical biosensing. *Biomacromolecules* **13**, 92–7 (2012).

CHAPTER 6

NEW GEOMETRIES AND SENSOR DESIGNS: DYNAMIC FILTERS, MIRRORS AND ARRAYS

6.1 Introduction and motivation

Thus far, the photonic multilayers presented in this thesis have been Bragg mirrors, or periodic dielectric multilayers which reflect a characteristic wavelength of light. Bragg filters transmit a characteristic wavelength of light and can be described as having maximum transmittance for a cavity layer of optical thickness, $2d$, sandwiched between two Bragg mirrors with each layer of optical thickness, d .^{1,2} One of the main advantages of the sequential layer deposition process is the ability to control the thickness and material properties of each individual layer. This chapter describes the expansion of

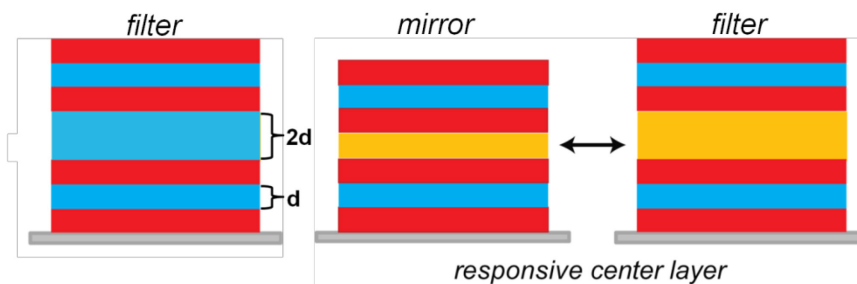


Figure 6.1 Schematic of a Bragg filter geometry (left) and a dynamic mirror-filter multilayer achieved by tuning the chemistry of the central layer to selectively swell (mirror, center) or de-swell (filter, right) in response to a particular analyte.

our multilayer fabrication approach to create new geometries, including Bragg filters, as well as arrays, or multiple sensors on a single substrate.

Previously, Ruhe and co-workers used sequentially spin-cast polymer films to create Bragg filters.³ In this case, the Bragg filter was not dynamic, and this multilayer was fixed in the filter geometry. Transitioning between a Bragg filter and mirror on a

single responsive photonic multilayer has not been demonstrated. Such sensors may not exhibit a broad range of colorimetric response but instead could be used as an “on/off” detector, with high intensity reflectance potentially signifying the presence of the analyte. This switchable nature would serve a unique purpose as an alternate form of sensor read-out or as a functional film in optical applications including displays, thermal and light management.⁴⁻⁶

In addition to new geometries, this chapter will also describe how the photo-patternable, layer-by-layer approach lends itself easily to the creation of sensor arrays, or multiple sensors on a single substrate. The idea of arrays serves to both 1) decrease fabrication time by eliminating the need for several independent coating steps for layers that are common to all components of the array, and 2) to allow for multi-functional sensors which can detect multiple analytes on a single substrate either by changing color or changing the characteristic reflectance spectrum, *i.e.* mirror-to-filter transition.

Photonic sensor arrays are especially of interest in areas where high-throughput sensing is desirable, particularly in rapid detection of small molecules or probes for medical diagnostics.⁷ Ozin and co-workers, for example, have pioneered the “photonic nose” as a novel platform for detection of volatile small molecules and bacteria.⁸ Li and co-workers have developed molecular recognition sensor arrays based on a combination of colloidal crystal templating and molecular printing to create molecularly imprinted inverse opal photonic polymers. These sensor arrays display high sensitivity and selectivity to a range of analytes, yet their fabrication does require a multi-step process and can potentially suffer from cross-contamination.⁹

6.2 Experimental methods

All polymers were synthesized by conventional free-radical polymerization as described in earlier chapters. Prior to spin coating, all polymer solutions were first sonicated for 10 min followed by filtration through a 0.2 μm PTFE filter. Solutions of polymer when spin-cast, cross-linked using 365 nm UV light and developed as described previously. All spin coating was completed at 2000 rpm for 50 s with a 1000 rpm ramp. P(pMS-BP) and P(NIPAM-BP) were synthesized as described in earlier chapters.

P(SPMA-BP)

Amounts of 1 g sulfopropyl methacrylate (SPMA, Aldrich), 53.6 mg of BP and 2 mg of AIBN were polymerized in a 10:3:1 mixture of methanol:1,4-dioxane:water at 80°C for 18 h under nitrogen following three freeze-pump-thaw cycles, resulting in a copolymer containing 5 mol% of BP. Water was necessary to fully dissolve SPMA, which was used as received. The polymer was purified by dialysis against 10:3:1 methanol:1,4-dioxane:water and several cycles of water, followed by lyophilization, and its structure confirmed by ^1H NMR. P(SPMA-BP) displays high solubility in water and weak to poor solubility in all other polar solvents tested. To dissolve this polymer in a suitable solvent system for spin-coating, a milky suspension of 15 mg/mL in trifluoroethanol (TFE) was first created. Polymer was completely dissolved upon addition of 0.5 vol% water, forming a clear solution. Spin-coating of homogenous films yielded as-cast thicknesses of 92 ± 3 nm and 77 ± 1 nm after crosslinking at 80 mW/cm² and developing in 0.5 vol% water in methanol.

P(OEGMA-MAA-BP)

Amounts of 2.728 mL OEGMA ($M_w = 475$ g/mol), 2.03 mL of methacrylic acid (MAA, Aldrich), 390 mg BP and 8 mg of AIBN were polymerized in 40 mL of a 1:1 mixture of methanol:1,4-dioxane at 80°C for 18 h under nitrogen following three freeze-pump-thaw cycles, resulting in a copolymer containing 48 mol% OEGMA, 48 mol% MAA and 4 mol% of BP. OEGMA and MAA were used as received. The polymer was purified by dialysis against 1:1 methanol:1,4-dioxane and several cycles of water followed by lyophilization, and its structure confirmed by ^1H NMR. Polymer was spin-cast from TFE at 12 mg/mL.

P(NIPAM-MPC-BP)

Amounts of 2 g NIPAM, 340 mg MPC, 325 mg BP and 4 mg of AIBN were stirred in 1,4-dioxane and methanol was added dropwise until all monomers were fully dissolved. The reaction mixture was polymerized at 80°C for 18 h under nitrogen following three freeze-pump-thaw cycles, resulting in a copolymer containing 5 mol% of BP. MPC and NIPAM were used as received. The polymer was purified by dialysis against 1:1 methanol:1,4-dioxane and several cycles of water followed by lyophilization, and its structure confirmed by ^1H NMR. Polymer was spin-cast from 1-propanol at 12 mg/mL. Spin-coating of homogenous films yielded as-cast thicknesses of 79 +/- 4 nm and 70 +/- 2 nm after crosslinking and developing in 1:4 water:1-propanol.

6.3 Results and discussion

6.3.1 Demonstration of tunable Bragg filter

The first demonstration of a tunable Bragg filter was achieved by fabricating a multilayer with alternating layers of high- n P(pMS-BP) and low- n P(NIPAM-BP) with a P(pMS-BP) cavity layer of thickness $2d_h$. This multilayer was designed to exhibit a

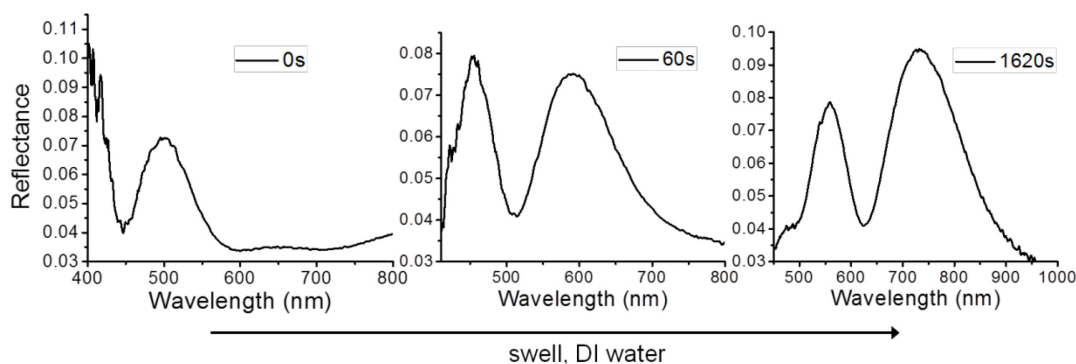


Figure 6.2 Demonstration of a Bragg filter with a high refractive index central cavity layer. The filter character is retained with swelling, and the transmittance peak shifts with swelling of the P(NIPAM-BP) responsive layers in room temperature water.

transmittance peak ~ 450 nm, as seen in the 0 s time point of Figure 6.2. When swelled in DI water, the transmittance peak red-shifts as P(NIPAM-BP) layers swell. Maximum filter character is evident at ~ 60 s of swelling, indicating the optical thickness of the low and high refractive index layers are most equal at this degree of swelling.

This concept was expanded upon to create a multilayer with reversible mirror and filter character depending upon degree of swelling. To do so, a responsive, hydrophilic polymer was chosen for the cavity layer, to allow for selective swelling of this layer as a triggering mechanism for the transition between filter (fully swelled cavity) and mirror (de-swelled cavity). A charged polymer, poly(OEGMA-48%MAA-4%BP) was selected

for its hydrophilicity and salt responsivity due to the presence of charged functionality. P(NIPAM-BP) was selected for the low-n layers in the stack due to its hydrophilicity but lack of salt sensitivity due to the absence of charged groups. This configuration allows

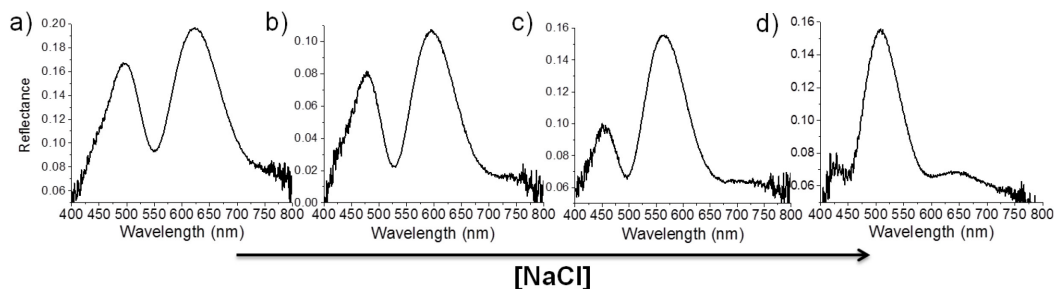


Figure 6.3 Reflectance spectra showing the transition from filter to mirror with increasing salt concentration from a) DI water, b) 0.05 M, c) 0.3 M to d) 4M.

for the selective swelling or de-swelling of the central layer by varying salt concentration, as seen in Figure 6.3. As salt concentration is increased, this triggers the de-swelling of the central cavity layer, which de-swells and eventually matches the optical thickness of the remaining layers in the stack, creating a Bragg mirror. This geometry is tunable and reversible with salt concentration.

6.3.2 Multifunctional sensors and arrays

In this chapter, multifunctional sensors with capabilities for independent sensing of salt and temperature are studied, and their response optimized by adjusting the chemistry of the responsive polymers to maximize dynamic swelling response while maintaining selective sensitivity to either temperature or salt. To enhance the extent of swelling of polymer multilayers while retaining selective sensitivity to either salt or temperature independently, poly(sulfopropyl methacrylate-5%BP) P(SPMA-BP) was utilized as a salt-sensitive material. As a highly charged polyelectrolyte, PSPMA not only

demonstrates salt sensitivity, but also fast kinetics and a high degree of swelling in water, with PSPMA-based multilayers swelling through the visible spectrum in less than one minute (Figure 6.4).

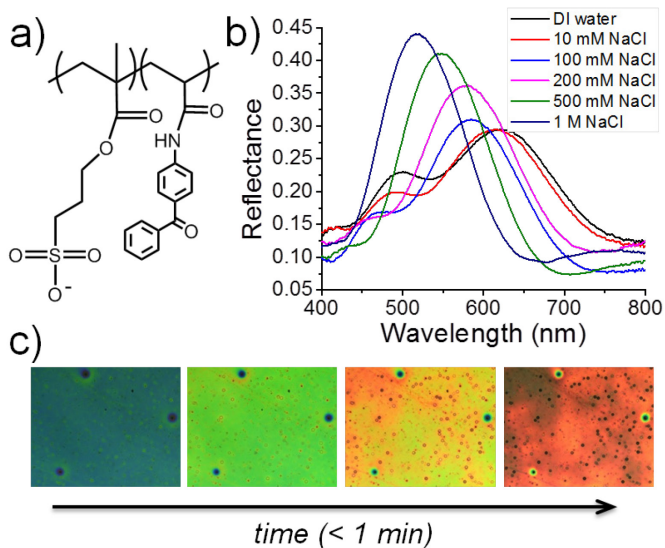


Figure 6.4 a) Structure of polyelectrolyte, P(SPMS-BP), used as b) a salt-sensitive material for multilayers with c) rapid response time through the visible spectrum.

Neutral poly(NIPAM-BP) (Figure 6.5a) was explored as a first-generation salt-insensitive, temperature responsive polymer. This material does display salt insensitivity due to the lack of charge, however this also limits its degree of swelling. To enhance the degree of swelling without imparting salt sensitivity, 5 mol% of the highly hydrophilic zwitterionic co-monomer methacryloyloxyethyl phosphorocholine (MPC) was incorporated, yielding a copolymer of P(NIPAM-5%MPC-5%BP) (Figure 6.5b).¹⁰

Multilayers of equal optical thicknesses with dry-state reflectance peaks of $\lambda_{\text{max}} \sim 425 \text{ nm}$ were fabricated with either P(NIPAM-BP) or P(NIPAM-MPC-BP) as the responsive low-index layers. Comparison of each multilayer swelled in water, as seen in

Figure 6.5b, reveals the introduction of MPC improves the range of λ_{\max} two-fold upon

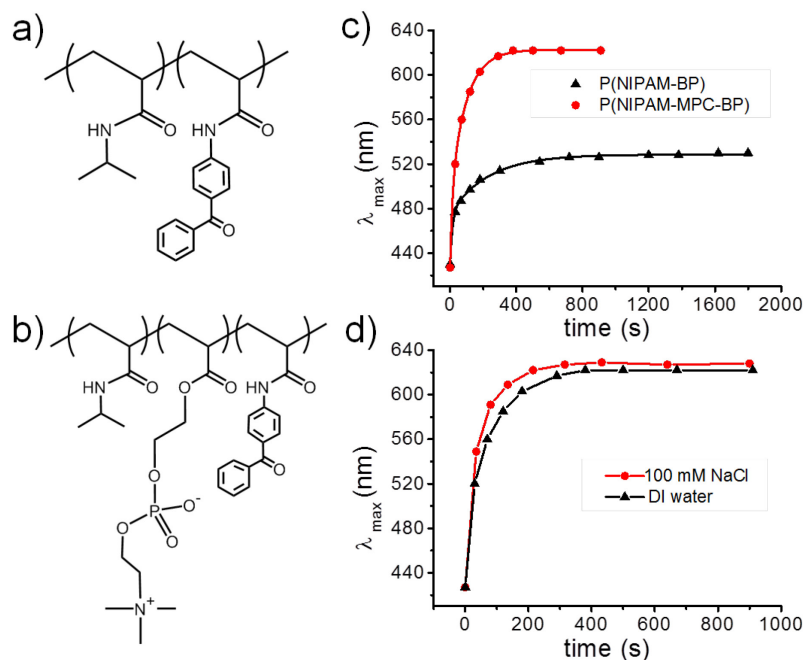


Figure 6.5 Structure of a) neutral and b) MPC-containing PNIPAM. Addition of zwitterionic MPC c) enhances the degree of swelling two-fold d) without imparting any salt sensitivity to multilayers when swelled in up to 100 mM salt.

swelling in water, allowing for a wider range of accessible wavelengths and colors from a single sensor.

Photo-masks can be used to fabricate an array of sensors with varying sensitivity or geometry on a single substrate as depicted in Figure 6.6. A photo-mask was used to selectively irradiate and crosslink specific areas of the substrate with the high refractive index layer for all cases being P(pMS-BP). This sensor was designed to reflect entirely as a Bragg mirror with a design wavelength of $\lambda_{\max} \sim 450$ nm in the dry state. Swelling in

water triggers a shift to either a Bragg filter (Figure 6.6, left) or a red-shifted Bragg mirror which reflects 550 nm (green) light (Figure 6.6, right). This demonstration reveals

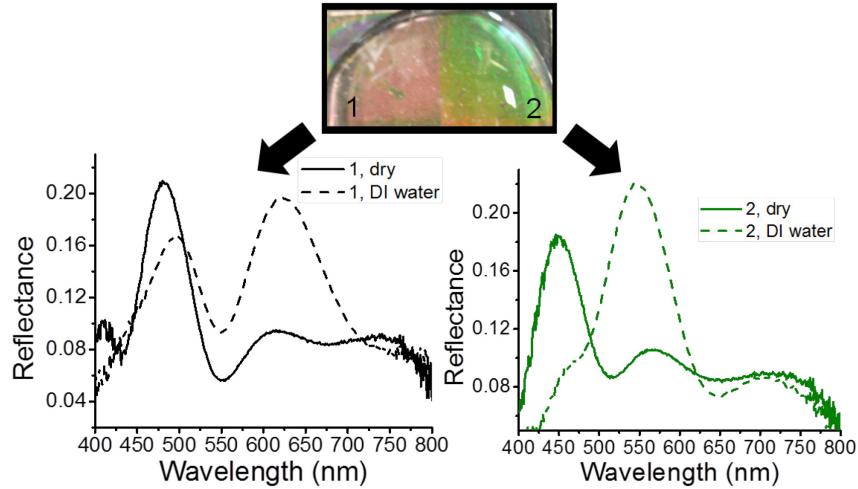


Figure 6.6 Two sensors patterned in parallel on a single substrate are Bragg mirrors in the dry state (solid lines) and transition to a filter (left) or mirror (right) with a design wavelength of 550 nm upon swelling in water.

not only can multiple sensors be patterned on a single substrate, they can also display tunable geometries upon swelling.

6.4 Conclusions and future directions

This chapter has demonstrated the flexibility of the fabrication approach to be used in the straight-forward preparation of dynamic and tunable Bragg mirrors, filters, and arrays. Scaling up the sensor size as well as decreasing fabrication time is also possible due to the straight-forward nature of the multilayer fabrication process which is limited only by the size and intensity of the UV light source. The use of arrays expands this platform to be able to conveniently sense multiple analytes simultaneously on a single substrate. Patterning multilayers in parallel allows for decreased fabrication time

and the realization of multifunctional sensor arrays by optimizing materials chemistry for selectivity to particular analytes. Here, selective sensitivity to salt or temperature is optimized utilizing the chemistry of a polyelectrolyte, P(SPMA-BP), for salt responsiveness, and a zwitterion-containing P(NIPAM-MPC-BP) for temperature responsiveness. While the work presented in this chapter has focused on salt and temperature, one can envision this approach to be expanded to a wide variety of analytes and functional systems according the multilayer geometry and materials chemistry of the responsive layers. Future work will focus on expanding the range of analytes by exploring new responsive polymer chemistries. Photo-patterning will be employed to fabricate arrays with a greater number of sensors.

6.5 References

1. Born, M. Wolf, E. *Principles of Optics*. (Cambridge University Press, 2002).
2. Joannopoulos, J. D., Villeneuve, P. R. & Fan, S. Photonic crystals: putting a new twist on light. *Nature* **386**, 143–149 (1997).
3. Mönch, W., Dehnert, J., Prucker, O., Rühle, J. & Zappe, H. Tunable Bragg filters based on polymer swelling. *Appl. Opt.* **45**, 4284–90 (2006).
4. Weber, M., Stover, C., Gilbert, L., Nevitt, T. & Ouderkirk, A. Giant birefringent optics in multilayer polymer mirrors. *Science* **287**, 2451–6 (2000).
5. Ma, H., Jen, A. K.-Y. & Dalton, L. R. Polymer-Based Optical Waveguides: Materials, Processing, and Devices. *Adv. Mater.* **14**, 1339–1365 (2002).
6. Paquet, C. & Kumacheva, E. Nanostructured polymers for photonics. *Mater. Today* **11**, 48–56 (2008).
7. Liu, Q., Tian, H., Yang, D., Zhou, J., Yeng, Y., Ji, Y. Nanoscale radius-graded photonic crystal sensor arrays using interlaced and symmetrical resonant cavities for biosensing. *Sensors Actuators A Phys.* **216**, 223–230 (2014).

8. Bonifacio, L. D., Puzzo, L.P., Breslav, S., Willey, B.M., McGeer, A., Ozin, G.A. Towards the photonic nose: a novel platform for molecule and bacteria identification. *Adv. Mater.* **22**, 1351–4 (2010).
9. Xu, D., Zhu, W., Wang, C., Tian, T., Cui, J., Li, J., Wang, H., Li, G. Molecularly imprinted photonic polymers as sensing elements for the creation of cross-reactive sensor arrays. *Chemistry* **20**, 16620–5 (2014).
10. Shimizu, T., Goda, T., Minoura, N., Takai, M. & Ishihara, K. Super-hydrophilic silicone hydrogels with interpenetrating poly(2-methacryloyloxyethyl phosphorylcholine) networks. *Biomaterials* **31**, 3274–80 (2010).

CHAPTER 7

ELECTROCHROMIC RESPONSE OF PHOTONIC MULTILAYER FILMS

7.1 Introduction and motivation

Electrochromic (EC) materials display a color change triggered by an applied electric field. Particularly useful applications of electrochromic materials are displays, optical coatings, and smart windows, mirrors, glasses or paper.¹⁻⁴ Reversible control over light-reflective or light-transmissive properties is particularly of interest for thermal management, materials camouflage and optical information and storage devices.^{5,6} Electrochromic polymers are especially of interest due to their processability, cost efficiency, ease of tunability, stability and flexibility compared to small molecule or inorganic counterparts.⁷ EC polymers typically rely on reduction-oxidation (redox) reactions to trigger color change, and many can generate multiple colors due to the presence of more than two redox states.⁸ To date, EC polymer systems have widely focused on the chemistry and derivatives of conjugated polymers including polythiophenes, polypyrroles and polyanilines, yet they often face drawbacks of low thermal stability, poor mechanical properties, and complicated syntheses often requiring the use of environmentally toxic solvents. Recently, polyimide, polyamide and polynorbornene-based EC polymers showed greater thermal stability, mechanical properties and reversibility. However, these systems still rely on the presence of an electroactive chromophore, making them susceptible to photo- or oxidative degradation and thus may require careful protection from their external environment or operational

restrictions to a narrow range of potentials to avoid permanent oxidation and thus irreversibility.

As was detailed in Chapter 3, photonic materials are an excellent stable alternative to the use of electroactive chromophores due to their reliance on structural-color. The electrochromic phenomenon has been recognized in photonic materials including the three-dimensional periodically porous inverse opal gels designed by Watanabe and Takeoka.^{9,10} The electrochromic behavior of block copolymers has also been explored. Zhang and co-workers utilized quaternized polystyrene-*b*-poly(2-vinyl pyridine) (PS-*b*-P2VP) block copolymers to create periodic lamellar assemblies with sub-second electrochromic response times, attributed to charging of the P2VP.^{11,12} Thomas and co-workers have expanded their platform of self-assembled PS-P2VP photonic materials for use as tunable electrochromic gels. An electrochemical reaction between trifluoroethanol solvent and P2VP domains is relied upon to trigger a de-swelling of the multilayer, leading to a blue-shift in λ_{\max} with applied voltage.¹³ Kang and co-workers have also utilized PS-*b*-P2VP lamellar photonic gels for photonic pixels, with potential use in e-paper applications, by controlling the hysteresis strength and the position of pH, both of which are highly dependent on the species of anions pairing with pyridinium groups in P2VP blocks.¹⁴ Continued development of electrochromic photonic gels is a promising route for the advancement of smart, switchable EC materials due to their flexibility, chemical stability, convenient preparation, and potentially high tunability and dynamic range of reflected or transmitted wavelengths.

This chapter details preliminary findings of the electrochromic response of acrylic acid-containing PNIPAM-based multilayers. First, it is demonstrated that responsive

photonic gel multilayers can be successfully fabricated on a conducting transparent substrate. An applied potential, in this case 3V, triggers the de-swelling of the multilayer, leading to a blue-shift in λ_{max} . When the voltage is removed, the process is fully reversible and the multilayer re-swells to its initial wavelength.

7.2 Experimental methods

Alternating layers of P(NIPAM-5%AAc-1%BP) and P(pMS-BP) were prepared on a transparent conductive substrate, Indium Tin Oxide (ITO, Nanocs, 100 Ω /sq)- coated glass. P(NIPAM-5%AAc-1%BP) and P(pMS-BP) were synthesized as described in Chapter 2. ITO-coated glass substrates were prepared by first sonicating 10 minutes successively in water, ethanol and acetone. Substrates were next treated with methacryloxypropyltrichlorsilane (Gelest) to promote polymer substrate-adhesion in the same manner as described in Chapter 2. Thirteen layers were spin cast on ITO by sequential spin-coating, crosslinking and developing of 20mg/mL P(pMS-BP) in toluene and 12 mg/mL P(NIPAM-5%AAc-1%BP) in 1-propanol. Multilayers were designed to reflect blue-violet light (\sim 475 nm) in the dry state and red-shift through the visible spectrum upon swelling in deionized water.

To test swelling and electrochromic response, the ITO-multilayer surface was covered nearly entirely with deionized water, leaving a dry portion for electrode connection. First, structural and optical integrity of an ITO-based multilayer was tested by monitoring the reflectance of the sample in room temperature water. For electrochromic measurements, a platinum counter electrode suspended in the droplet of water, above the ITO surface. A gold conductive clamp was used to connect a dry portion

of the ITO surface to the (+) electrode lead. A potential of 3V was applied across the sample, with zero current flow.

7.3 Results and discussion

Prior to testing the electrochromic behavior of photonic multilayers, it was first necessary to demonstrate feasibility of device fabrication on a new type of substrate, glass coated with a transparent electrode, ITO. Indeed, responsive multilayers with well-defined Bragg peaks could be successfully fabricated on ITO, displaying reversible red-shifts upon swelling in room temperature DI water as seen in Figure 7.1, with no evidence of delamination.

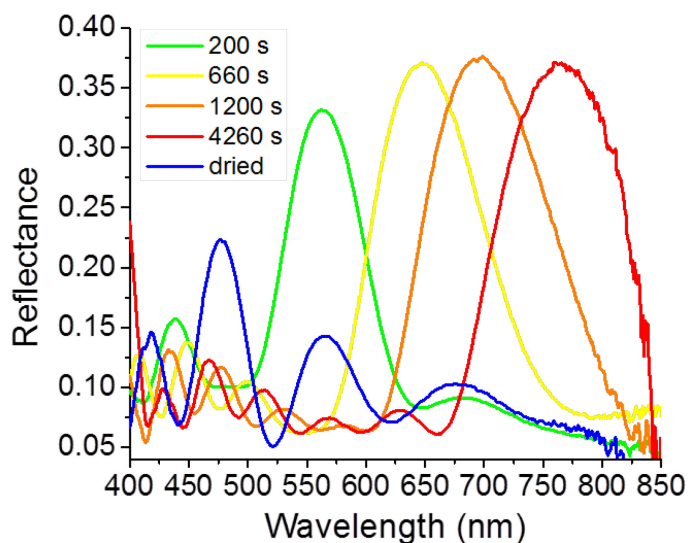


Figure 7.1 Demonstration of photonic multilayers successfully fabricated and swelled on silane-treated ITO substrate with well defined reflectance peaks and no evidence of delamination.

Next, a potential of 3V is applied across the ITO-multilayer, with a platinum counter electrode immersed in a droplet of water swelling the photonic gel. A positive

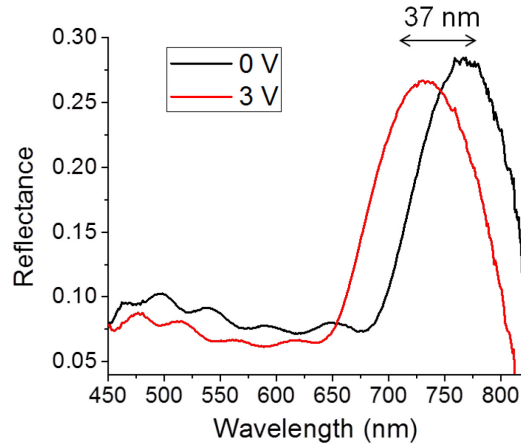


Figure 7.2 Reflectance spectra reveal multilayers fabricated on ITO do demonstrate a reversible blue-shift in λ_{\max} under an applied voltage of 3V, indicating the voltage-induced de-swelling of P(NIPAM-AAc-BP) layers in the film stack. potential is applied to the ITO substrate, triggering the de-swelling of the negatively charged P(NIPAM-5%AAc-1%BP) layers and a blue-shift of λ_{\max} as demonstrated in Figure 7.2. Applying an anodic potential to the ITO leads to the buildup of positive

charges on the ITO surface which attracts the negatively charged AAc moieties in the solvated PNIPAM layers. Typical shifts in λ_{\max} ($\Delta\lambda(\text{cycle})$) between the “on” (3V) and “off” (0V) states are $\Delta\lambda(\text{cycle}) = 36 \pm 10$ nm. Osada and co-workers found that a

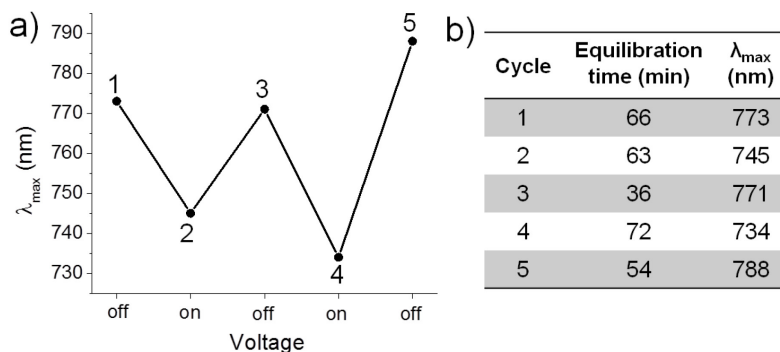


Figure 7.3 a) Reversibility of electrochromic behavior where 3V triggers a blue-shift in the “on” state with b) typical equilibration times for “on” and “off” cycles on the order of tens of minutes.

voltage applied across an anionic polyelectrolyte gel will induce contraction of the gel at the anode due to electro-kinetic mechanism, a process reversible upon removal of the applied field.¹⁵ It is concluded that gel contraction can be attributed to the transport of hydrated ions and water in the network. When a field is applied across the gel system both the covalently incorporated anions and the dissociated H^+ counter-ions experience electrical forces in opposite directions. H^+ counter-ions are thought to migrate to the platinum cathode, where they are reduced, while a build-up of positive charge at the anode triggers contraction of the overall negatively charged multilayer. Though a similar electrochromic response of de-swelling with anodic potential is observed, unlike Osada’s studies, the experiments presented in this chapter were not conducted under an applied dc current.

Thomas and co-workers conclude that the electrochromic response of PS-P2VP photonic gels is triggered by applying a positive, anodic potential to the substrate electrode, which leads to electrostatic repulsion of the partially (2 mol%) positively charged P2VP layers, and thus a red-shift in λ_{\max} . This red-shift is enhanced at a critical voltage $\sim 1.5V$, above which P2VP chain disentanglement coupled with electrostatic repulsion is thought to contribute to pronounce swelling. In the work presented herein, the multilayers contain 5 mol% negatively charged acrylic acid moieties and therefore, similar to Thomas' predictions, a blue-shift in λ_{\max} is observed with applied positive potential to the ITO substrate, triggering de-swelling in this case which may be due to electrostatic attraction of opposite charges in the NIPAM layers and the anode. Thomas and co-workers also observe slow voltage-induced swelling and de-swelling kinetics, on the order of tens of minutes, similar to the trend observed in this chapter. It is thought this response can be made faster with the introduction of a higher percentage of charged groups, which is indeed the case for a fully quarternized P2VP-containing photonic block copolymer electrochromic gel.¹³

The electrochromic response is reversible as demonstrated in Figure 7.3a. As was seen in Chapter 5, the response kinetics in both the “on” and “off” modes are relatively

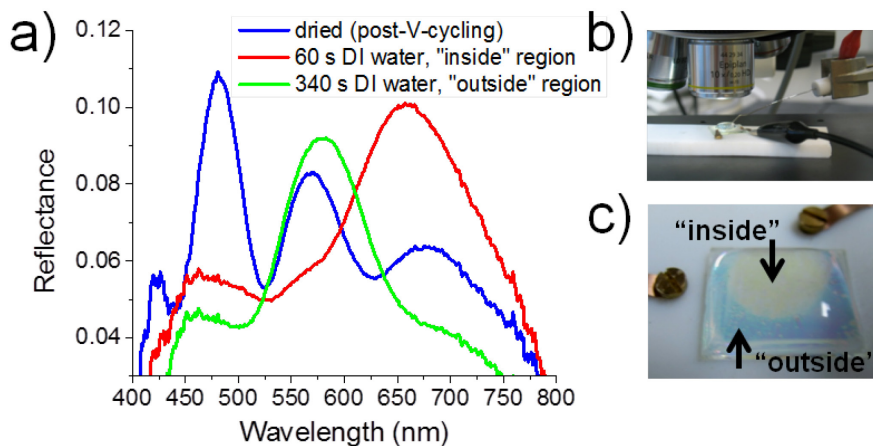


Figure 7.4 a) Reflectance spectra reveal faster swelling in regions to which voltage was previously applied according to the setup in b). After voltage-cycling, swelling of the previously cycled region shows fast kinetics, displaying a further red-shift (yellow color) than the outside region (blue-green) not previously cycled.

slow, on the order of tens of minutes (Figure 7.3 b) for full equilibration. While the accessible range of responsive swelling demonstrated here is narrower than that of the thermochromic materials, it is still sufficient for optical detection.

After V-cycling, the multilayer was allowed to dry, and subsequently the entire sample was swelled in DI water. Figure 7.4 shows the difference in color and kinetics of the “inside” region of the multilayer, which was previously under an applied field during swelling in water, compared to the “outside” region, which remained dry throughout the entire V-cycling process. The swelling kinetics of the “inside” region are significantly faster than the “outside”, swelling to a λ_{max} of more than 650 nm in 60 s, whereas it takes

nearly six times as long for the “outside” region to swell to only 575 nm. The mechanism responsible for this phenomenon will be the subject of future investigations.

7.4 Conclusions and future directions

Electrochromic materials have a wide variety of applications, particularly for use in smart films and coatings, which will continue to be explored and optimized. Many existing technologies can display tunable and reversible colors with rapid response, yet rely on environmentally sensitive redox reactions and require synthetically challenging routes utilizing toxic solvents and materials. This chapter has demonstrated that photonic polymer multilayers hold promise for use in electrochromic systems as tunable, reversible and cost-efficient materials. Future work will involve optimizing the percent composition of charge and the chemistry of the charged moiety in the responsive polymer layers to broaden the dynamic range of swelling/de-swelling, and thus reflected wavelengths, under an applied electric field. Careful engineering of the multilayer can allow for reversibly light-transmissive (filter) or light-reflective (mirror) films by using an applied field to control the degree of swelling of the center layer. Here, the concept was demonstrated using P(NIPAM-AAc-BP), however the electrochromic effect is not limited to the chemistry of this system and one can envision using a wide variety of charged, hydrophilic polymers, or adjusting the ratio of AAc in similar NIPAM-based systems, in future devices.

7.5 References

1. Granqvist, C. G. Electrochromics for smart windows: Oxide-based thin films and devices. *Thin Solid Films* **564**, 1–38 (2014).
2. Thakur, V. K., Ding, G., Ma, J., Lee, P. S. & Lu, X. Hybrid materials and polymer electrolytes for electrochromic device applications. *Adv. Mater.* **24**, 4071–96 (2012).
3. Tieke, B. Coordinative supramolecular assembly of electrochromic thin films. *Curr. Opin. Colloid Interface Sci.* **16**, 499–507 (2011).
4. Hilsun, C. Flat-panel electronic displays: a triumph of physics, chemistry and engineering. *Philos. Trans. A. Math. Phys. Eng. Sci.* **368**, 1027–82 (2010).
5. Runnerstrom, E. L., Llordés, A., Lounis, S. D. & Milliron, D. J. Nanostructured electrochromic smart windows: traditional materials and NIR-selective plasmonic nanocrystals. *Chem. Commun.* **50**, 10555–72 (2014).
6. Kanu, S. S. & Binions, R. Thin films for solar control applications. *Proc. R. Soc. A Math. Phys. Eng. Sci.* **466**, 19–44 (2009).
7. Abidin, T., Zhang, Q., Wang, K.-L. & Liaw, D.-J. Recent advances in electrochromic polymers. *Polymer.* **55**, 5293–5304 (2014).
8. Argun, A. A., Aubert, P.-H., Thompson, B.C., Schwendeman, I., Gaupp, C.L., Hwang, J., Pinto, N.J., Tanner, D.B., MacDiarmid, A.G., Reynolds, J.R. Multicolored Electrochromism in Polymers: Structures and Devices. *Chem. Mater.* **16**, 4401–4412 (2004).
9. Ueno, K., Sakamoto, J., Takeoka, Y. & Watanabe, M. Electrochromism based on structural colour changes in a polyelectrolyte gel. *J. Mater. Chem.* **19**, 4778 (2009).
10. Ueno, K., Matsubara, K., Watanabe, M. & Takeoka, Y. An Electro- and Thermochromic Hydrogel as a Full-Color Indicator. *Adv. Mater.* **19**, 2807–2812 (2007).
11. Lu, Y., Xia, H., Zhang, G. & Wu, C. Electrically tunable block copolymer photonic crystals with a full color display. *J. Mater. Chem.* **19**, 5952 (2009).
12. Lu, Y., Meng, C., Xia, H., Zhang, G. & Wu, C. Fast electrically driven photonic crystal based on charged block copolymer. *J. Mater. Chem. C* **1**, 6107 (2013).

13. Walish, J. J., Kang, Y., Mickiewicz, R. a. & Thomas, E. L. Bioinspired Electrochemically Tunable Block Copolymer Full Color Pixels. *Adv. Mater.* **21**, 3078–3081 (2009).
14. Hwang, K, Kwak, D., Kang, C., Kim, D., Ahn, Y., Kang, Y. Electrically tunable hysteretic photonic gels for nonvolatile display pixels. *Angew. Chem. Int. Ed.* **50**, 6311–4 (2011).
15. Kaneko, D., Gong, J. P. & Osada, Y. Polymer gels as soft and wet chemomechanical systems:an approach to artificial muscles. *J. Mater. Chem.* **12**, 2169–2177 (2002).

CHAPTER 8

SUMMARY AND OUTLOOK

This thesis serves to establish and explore a unique approach to the fabrication and utilization of polymer-based multilayers as responsive and tunable 1D photonic films. A library of photo-crosslinkable copolymers containing pendent benzophenone crosslinkers was synthesized and utilized to fabricate multilayers in a straight-forward manner with independent control over the layer thicknesses and materials chemistry of each layer via sequential spin-coating, crosslinking and developing. Surface and through-thickness structural uniformity of the multilayers was confirmed using atomic force microscopy and dynamic secondary ion mass spectrometry. Thermochromic, electrochromic and radiation-sensitive multilayers were studied by tuning the chemistry of the responsive layers. Radiation-sensitive photonic multilayers are a novel approach to colorimetric radiation sensing and do not rely on commonly utilized oxygen or light sensitive chromophores. The kinetic response of multilayers was studied by exploring the swelling and de-swelling response of different polymers as multilayer and single-films. Multilayer reflectance efficiency was improved by introducing high refractive index metal oxide nanoparticles to enhance refractive index contrast between layers. The incorporation of nanoparticles into composite polymer films allowed for straight-forward tunability of refractive indices of both hydrophobic and hydrophilic, responsive polymers by adjusting nanoparticle content. This control over refractive index also allowed for the fabrication of all-gel photonic multilayers based entirely on temperature responsive poly(N-isopropylacrylamide). The photo-crosslinkable system and sequential layer

platform was also expanded upon to build sensor arrays and dynamic Bragg filters which can reversibly transition to mirrors, providing an additional read-out mechanism.

Photonic materials will continue to serve an important purpose in a variety of applications, including displays, sensors, responsive surfaces and opto-electronic devices. One may envision the responsive photonic multilayers explored in this thesis to have potential future use, for example, as “erasable” photonic paper, perhaps using solvents of varying polarity as a source of several inks, with different colors triggered due to a change in degree of swelling with solvent strength for the responsive layers. The incorporation of magnetic particles may also provide a new route towards reversible and selective patterning by differential swelling or de-swelling of photonic gel multilayers.

Alternative fabrication approaches, including coextrusion or ink-jet printing, may be explored to optimize fabrication time or allow for a wider array of sensors, material chemistries or device designs. While the current method of crosslinking using benzophenone has proved effective, new chemistries with faster crosslinking kinetics, such as phenyl-azide, may also be examined.

Finally, these photonic multilayers may also be explored as a route towards convenient and rapid sensing of biomolecules. One may envision the responsive copolymer functionalized with a moiety capable of bio-recognition via complexation, subsequently triggering a change in degree of swelling and thus color. Such a rapid and convenient method would be useful in water quality testing and medical diagnostics.

BIBLIOGRAPHY

- Abidin, T., Zhang, Q., Wang, K.-L. & Liaw, D.-J. Recent advances in electrochromic polymers. *Polymer (Guildf)*. **55**, 5293–5304 (2014).
- Alf, M. E., Hatton, T. A. & Gleason, K. K. Insights into Thin , Thermally Responsive Polymer Layers Through Quartz Crystal Microbalance with Dissipation. 10691–10698 (2011).
- Althues, H., Henle, J. & Kaskel, S. Functional inorganic nanofillers for transparent polymers. *Chem. Soc. Rev.* **36**, 1454–65 (2007).
- Argun, A. A., Aubert, P.-H., Thompson, B.C., Schwendeman, I., Gaupp, C.L., Hwang, J., Pinto, N.J., Tanner, D.B., MacDiarmid, A.G., Reynolds, J.R. Multicolored Electrochromism in Polymers: Structures and Devices. *Chem. Mater.* **16**, 4401–4412 (2004).
- Asher, S.A., Kimble, K. W. & Walker, J. P. Enabling Thermoreversible Physically Cross-Linked Polymerized Colloidal Array Photonic Crystals. *Chem. Mater.* **20**, 7501–7509 (2008).
- Beaulieu, M. R., Hendricks, N. R. & Watkins, J. J. Large-Area Printing of Optical Gratings and 3D Photonic Crystals Using Solution-Processable Nanoparticle/Polymer Composites. *ACS Photonics* **1**, 799–805 (2014).
- Berger, M.J. Coursey, J.S. Zucker, M.A. Chang, J. NIST ESTAR Database. (2005). at <<http://physics.nist.gov/PhysRefData/Star/Text/method.html>>
- Bonifacio, L. D., Puzzo, L.P., Breslav, S., Willey, B.M., McGeer, A., Ozin, G.A. Towards the photonic nose: a novel platform for molecule and bacteria identification. *Adv. Mater.* **22**, 1351–4 (2010).
- Born, M. Wolf, E. *Principles of Optics*. (Cambridge University Press, 2002).
- Brandrup, J., Immergut, E. H. & Grulke, E. A. *Polymer Handbook*. (John Wiley & Sons, Inc., 1999).
- Calvo, M. E., Sánchez Sobrado, O., Lozano, G. & Míguez, H. Molding with nanoparticle-based one-dimensional photonic crystals: a route to flexible and transferable Bragg mirrors of high dielectric contrast. *J. Mater. Chem.* **19**, 3144 (2009).
- Carter, M. C. D., Sorrell, C. D. & Serpe, M. J. Deswelling Kinetics of Color Tunable Poly (N-Isopropylacrylamide). *J. Phys. Chem. B* **115**, 14359–14368 (2011).

- Caseri, W. Nanocomposites of polymers and metals or semiconductors: Historical background and optical properties. *Macromol. Rapid Commun.* **21**, 705–722 (2000).
- Chang, C. & Chen, W. High-Refractive-Index Thin Films Prepared from Dianhydride – Titania Hybrid Materials. *J. Poly. Sci. A.* 3419–3427 (2001).
- Chang, C.-M., Chang, C.-L. & Chang, C.-C. Synthesis and Optical Properties of Soluble Polyimide/Titania Hybrid Thin Films. *Macromol. Mater. Eng.* **291**, 1521–1528 (2006).
- Chapiro, A. *Radiation Chemistry of Polymeric Systems*. (John Wiley & Sons, Inc., 1962).
- Cheng, H., Shen, L. & Wu, C. LLS and FTIR Studies on the Hysteresis in Association and Dissociation of Poly (N-isopropylacrylamide) Chains in Water. *Macromolecules* **39**, 2325–2329 (2006).
- Chiappelli, M. C. & Hayward, R. C. Photonic multilayer sensors from photocrosslinkable polymer films. *Adv. Mater.* **24**, 6100–4 (2012).
- Choi, S. Y., Mamak, M., von Freymann, G., Chopra, N. & Ozin, G. a. Mesoporous bragg stack color tunable sensors. *Nano Lett.* **6**, 2456–61 (2006).
- Christensen, S. K., Chiappelli, M. C. & Hayward, R. C. Gelation of Copolymers with Pendent Benzophenone Photo-Cross-Linkers. *Macromolecules* **45**, 5237–5246 (2012).
- Colodrero, S., Ocaña, M. & Míguez, H. Nanoparticle-based one-dimensional photonic crystals. *Langmuir* **24**, 4430–4 (2008).
- Colodrero, S., Ocaña, M., González-Elipe, A.R. & Míguez, H. Response of nanoparticle-based one-dimensional photonic crystals to ambient vapor pressure. *Langmuir* **24**, 9135–9 (2008).
- Dorman, G. & Prestwich, G. D. Benzophenone Photophores in Biochemistry. *Biochemistry* **33**, (1994).
- Doytcheva, M., Dotcheva, D., Stamenova, R., Orahovats, A. & Leder, J. Ultraviolet-Induced Crosslinking of Solid Poly(ethylene oxide). *J. Appl. Polym. Sci.* **64**, 2299–2307 (1996).
- Fenzl, C., Hirsch, T. & Wolfbeis, O. S. Photonic crystals for chemical sensing and biosensing. *Angew. Chem. Int. Ed. Engl.* **53**, 3318–35 (2014).
- Ge, J. & Yin, Y. Responsive photonic crystals. *Angew. Chem. Int. Ed. Engl.* **50**, 1492–522 (2011).

- Goponenko, A. V & Asher, S.A. Modeling of stimulated hydrogel volume changes in photonic crystal Pb²⁺ sensing materials. *J. Am. Chem. Soc.* **127**, 10753–9 (2005).
- Granqvist, C. G. Electrochromics for smart windows: Oxide-based thin films and devices. *Thin Solid Films* **564**, 1–38 (2014).
- Griller, D., Howard, J. A., Marriott, P. R. & Scaiano, J. C. Absolute Rate Constants for the Reactions of tert-Butoxyl, tert-Butylperoxyl, and Benzophenone Triplet with Amines: The Importance of a Stereoelectronic Effect. *J. Am. Chem. Soc.* **103**, 619–623 (1981).
- Guldin, S., Kolle, M., Stefik, M., Langford, R., Eder, D., Wiesner, U., Steiner, U. Tunable mesoporous bragg reflectors based on block-copolymer self-assembly. *Adv. Mater.* **23**, 3664–8 (2011).
- Hanemann, T. & Szabó, D. V. *Polymer-Nanoparticle Composites: From Synthesis to Modern Applications. Materials (Basel)*. **3**, 3468–3517 (2010).
- Haque, M. A., Kurokawa, T., Kamita, G., Yue, Y. & Gong, J. P. Rapid and Reversible Tuning of Structural Color of a Hydrogel over the Entire Visible Spectrum by Mechanical Stimulation. *Chem. Mater.* **23**, 5200–5207 (2011).
- Heller, W. Remarks on Refractive Index Mixture Rules. *J. Phys. Chem.* **69**, 1123–1129 (1965).
- Higuchi, H., Yamashita, T., Horie, K. & Mitai, I. Photo-Cross-Linking Reaction of Benzophenone-Containing Polyimide and Its Model Compounds. *Chem. Mater.* **3**, 188–194 (1991).
- Hilsum, C. Flat-panel electronic displays: a triumph of physics, chemistry and engineering. *Philos. Trans. A. Math. Phys. Eng. Sci.* **368**, 1027–82 (2010).
- Hirotsu, S., Hirokawa, Y. & Tanaka, T. Volume-phase transitions of ionized N-isopropylacrylamide gels. *J. Chem. Phys.* **87**, 1392 (1987).
- Holtz, J. H. & Asher, S. a. Polymerized colloidal crystal hydrogel films as intelligent chemical sensing materials. *Nature* **389**, 829–32 (1997).
- Hoth, A. & Lutz, J.-F. Preparation of Ideal PEG Analogues with a Tunable Thermosensitivity by Controlled Radical Copolymerization of 2-(2-Methoxyethoxy)ethyl Methacrylate and Oligo(ethylene glycol)Methacrylate. *Macromolecules* **39**, 893–896 (2006).
- Hwang, K., Kwak, D., Kang, C., Kim, D., Ahn, Y., Kang, Y. Electrically tunable hysteretic photonic gels for nonvolatile display pixels. *Angew. Chem. Int. Ed.* **50**, 6311–4 (2011).

- Jia, J., Sarker, M., Steinmetz, M. G., Shukla, R. & Rathore, R. Photochemical elimination of leaving groups from zwitterionic intermediates generated via electrocyclic ring closure of alpha,beta-unsaturated anilides. *J. Org. Chem.* **73**, 8867–79 (2008).
- Joannopoulos, J. D., Villeneuve, P. R. & Fan, S. Photonic crystals: putting a new twist on light. *Nature* **386**, 143–149 (1997).
- Kaneko, D., Gong, J. P. & Osada, Y. Polymer gels as soft and wet chemomechanical systems: an approach to artificial muscles. *J. Mater. Chem.* **12**, 2169–2177 (2002).
- Kang, C, Kim, E., Baek, H., Hwang, K., Kwak, D., Kang, Y., Thomas, E.L. Full color stop bands in hybrid organic/inorganic block copolymer photonic gels by swelling-freezing. *J. Am. Chem. Soc.* **131**, 7538–9 (2009).
- Kang, Y., Walish, J. J., Gorishnyy, T. & Thomas, E. L. Broad-wavelength-range chemically tunable block-copolymer photonic gels. *Nat. Mater.* **6**, 957–60 (2007).
- Kanu, S. S. & Binions, R. Thin films for solar control applications. *Proc. R. Soc. A Math. Phys. Eng. Sci.* **466**, 19–44 (2009).
- Kim, E., Kang, C. Baek, H., Hwang, K., Kwak, D., Lee, E., Kang, Y., Thomas, E.L. Control of Optical Hysteresis in Block Copolymer Photonic Gels: A Step Towards Wet Photonic Memory Films. *Adv. Funct. Mater.* **20**, 1728–1732 (2010).
- Kim, J., Hanna, J.A., Byun, M., Santangelo, C. D. & Hayward, R. C. Designing Responsive Buckled Surfaces by Halftone Gel Lithography. *Science*. **335**, 1201–1205 (2012).
- Kim, J., Hanna, J.A., Hayward, R. C. & Santangelo, C. D. Thermally responsive rolling of thin gel strips with discrete variations in swelling. *Soft Matter* **8**, 2375 (2012).
- Kobler, J., Lotsch, B. V, Ozin, G.A, Bein, T. Vapor-sensitive bragg mirrors and optical isotherms from mesoporous nanoparticle suspensions. *ACS Nano* **3**, 1669–76 (2009).
- Komolprasert, V. in *Packag. Non Therm. Process. Food* (Blackwell Publishing, 2007).
- Lu, C., Cui, Z., Wang, Y., Zuo, L., Guan, C., Yang, B., Shen, J. Preparation and characterization of ZnS-polymer nanocomposite films with high refractive index. *J. Mater. Chem.* **13**, 2189 (2003).
- Laranjeira, J. M., Khoury, H., de Azevedo, W., de Vasconcelos, E. & da Silva, E. Polyaniline nanofilms as a sensing device for ionizing radiation. *Phys. E Low-dimensional Syst. Nanostructures* **17**, 666–667 (2003).

- Lee, E., Rao, G., Mansur, L. LET effect on cross-linking and scission mechanisms of PMMA during irradiation. *Radiat. Phys. Chem.* **55**, 293–305 (1999).
- Lee, K. & Asher, S. A. Photonic Crystal Chemical Sensors: pH and Ionic Strength. *J. Am. Chem. Soc.* **122**, 9534–9537 (2000).
- Lim, H. S., Lee, J.-H., Walish, J. J. & Thomas, E. L. Dynamic swelling of tunable full-color block copolymer photonic gels via counterion exchange. *ACS Nano* **6**, 8933–9 (2012).
- Lim, H. S., Lee, J.-H., Walish, J. J. & Thomas, E. L. Dynamic swelling of tunable full-color block copolymer photonic gels via counterion exchange. *ACS Nano* **6**, 8933–9 (2012).
- Liu, J. & Ueda, M. High refractive index polymers: fundamental research and practical applications. *J. Mater. Chem.* **19**, 8907 (2009).
- Liu, J., Nakamura, Y., Ogura, T., Shibasaki, Y., Ando, S., Ueda, M. Optically Transparent sulfur containing polyimide-TiO₂ nanocomposite films with high refractive index and negative pattern formation from poly (amic acid) -TiO₂ nanocomposite film. *Chem. Mater.* 273–281 (2008).
- Liu, Q., Tian, H., Yang, D., Zhou, J., Yeng, Y., Ji, Y. Nanoscale radius-graded photonic crystal sensor arrays using interlaced and symmetrical resonant cavities for biosensing. *Sensors Actuators A Phys.* **216**, 223–230 (2014).
- Liu, Z., Xue, W., Cai, Z., Zhang, G. & Zhang, D. A facile and convenient fluorescence detection of gamma-ray radiation based on the aggregation-induced emission. *J. Mater. Chem.* **21**, 14487 (2011).
- Lotsch, B. V., Scotognella, F., Moeller, K., Bein, T. & Ozin, G.A. Stimuli-responsive Bragg stacks for chemo-optical sensing applications. **7713**, 77130V–77130V–10 (2010).
- Lü, C., Cheng, Y., Liu, Y., Liu, F. & Yang, B. A Facile Route to ZnS–Polymer Nanocomposite Optical Materials with High Nanophase Content via γ -Ray Irradiation Initiated Bulk Polymerization. *Adv. Mater.* **18**, 1188–1192 (2006).
- Lu, Y., Meng, C., Xia, H., Zhang, G. & Wu, C. Fast electrically driven photonic crystal based on charged block copolymer. *J. Mater. Chem. C* **1**, 6107 (2013).
- Lu, Y., Xia, H., Zhang, G. & Wu, C. Electrically tunable block copolymer photonic crystals with a full color display. *J. Mater. Chem.* **19**, 5952 (2009).

- Lu, Y., Zhou, K., Ding, Y., Zhang, G. & Wu, C. Origin of hysteresis observed in association and dissociation of polymer chains in water. *Phys. Chem. Chem. Phys.* **12**, 3188–94 (2010).
- Lutz, J.-F. Thermo-Switchable Materials Prepared Using the OEGMA-Platform. *Adv. Mater.* **23**, 2237–2243 (2011).
- Lutz, J.-F., Akdemir, O. & Hoth, A. Point by point comparison of two thermosensitive polymers exhibiting a similar LCST: is the age of poly(NIPAM) over? *J. Am. Chem. Soc.* **128**, 13046–7 (2006).
- Ma, H., Jen, A. K.-Y. & Dalton, L. R. Polymer-Based Optical Waveguides: Materials, Processing, and Devices. *Adv. Mater.* **14**, 1339–1365 (2002).
- Mai, H. H., Duong, N. D. & Kojima, T. Dyed polyvinyl chloride films for use as high-dose routine dosimeters in radiation processing. *Radiat. Phys. Chem.* **69**, 439–444 (2004).
- Mai, H. H., Solomon, H. M., Taguchi, M. & Kojima, T. Polyvinyl butyral films containing leuco-malachite green as low-dose dosimeters. *Radiat. Phys. Chem.* **77**, 457–462 (2008).
- Mönch, W., Dehnert, J., Prucker, O., Rühle, J. & Zappe, H. Tunable Bragg filters based on polymer swelling. *Appl. Opt.* **45**, 4284–90 (2006).
- Morehouse, K. M. & Komolprasert, V. in *Irradiat. Food Packag.* 1–11 (American Chemical Society, 2004).
- Nair, R. V. & Vijaya, R. Photonic crystal sensors: An overview. *Prog. Quantum Electron.* **34**, 89–134 (2010).
- Pang, X. & Cui, S. Single-Chain Mechanics of Poly(N,N-diethylacrylamide) and Poly(N-isopropylacrylamide): Comparative Study Reveals the Effect of Hydrogen Bond Donors. *Langmuir* **29**, 12176–12182 (2013).
- Paquet, C. & Kumacheva, E. Nanostructured polymers for photonics. *Mater. Today* **11**, 48–56 (2008).
- Patra, L. & Toomey, R. Viscoelastic response of photo-cross-linked poly(N-isopropylacrylamide) coatings by QCM-D. *Langmuir* **26**, 5202–7 (2010).
- Patra, L., Vidyasagar, A. & Toomey, R. The effect of the Hofmeister series on the deswelling isotherms of poly(N-isopropylacrylamide) and poly(N,N-diethylacrylamide). *Soft Matter* **7**, 6061 (2011).

- Rabek, J. F. *Mechanisms of Photophysical Processes and Photochemical Reactions in Polymers: Theory and Applications*. (John Wiley & Sons, Inc., 1987).
- Redel, E., Mirtchev, P., Huai, C., Petrov, S. & Ozin, G.A. Nanoparticle films and photonic crystal multilayers from colloidally stable, size-controllable zinc and iron oxide nanoparticles. *ACS Nano* **5**, 2861–9 (2011).
- Reese, E., Baltusavich, M. E., Keim, J. P. & Asher, S. a. Development of an intelligent polymerized crystalline colloidal array colorimetric reagent. *Anal. Chem.* **73**, 5038–42 (2001).
- Runnerstrom, E. L., Llordés, A., Lounis, S. D. & Milliron, D. J. Nanostructured electrochromic smart windows: traditional materials and NIR-selective plasmonic nanocrystals. *Chem. Commun. (Camb)*. **50**, 10555–72 (2014).
- Schimitberger, T., Ferreira, G. R., Akcelrud, L. C., Saraiva, M. F. & Bianchi, R. F. X-rays sensing properties of MEH-PPV, Alq3 and additive components: a new organic dosimeter as a candidate for minimizing the risk of accidents of patients undergoing radiation oncology. *Med. Eng. Phys.* **35**, 140–4 (2013).
- Schimitberger, T., Ferreira, G. R., Saraiva, M. F., Bianchi, A. G. C. & Bianchi, R. F. X-ray dose detector based on color changing of light-emitting polymer–metal complex hybrid material. *Sensors Actuators B Chem.* **168**, 131–137 (2012).
- Schmaljohann, D., Beyerlein, D., Nitschke, M. & Werner, C. Thermo-reversible swelling of thin hydrogel films immobilized by low-pressure plasma. *Langmuir* **20**, 10107–14 (2004).
- Shani, G. *Radiation Dosimetry: Instrumentation and Methods*. (CRC Press LLC, 2001).
- Shimizu, T., Goda, T., Minoura, N., Takai, M. & Ishihara, K. Super-hydrophilic silicone hydrogels with interpenetrating poly(2-methacryloyloxyethyl phosphorylcholine) networks. *Biomaterials* **31**, 3274–80 (2010).
- Shoute, L. C. T. & Huie, R. E. Reactions of Triplet Decafluorobenzophenone with Alkenes . A Laser Flash Photolysis Study. **5639**, 3467–3471 (1997).
- Shultz, A., Roth, P. & Berge, J. Radiation Degradation of Polymethacrylates . Dose Rate and Medium Effects . *J. Polym. Sci. Part A* **1**, 1651–1669 (1963).
- Soliman, Y. S., Basfar, A. A. & Msalam, R. I. A radiochromic film based on leucomalachite green for high-dose dosimetry applications. *Radiat. Meas.* **62**, 45–51 (2014).
- Sorrell, C. D. & Serpe, M. J. Reflection order selectivity of color-tunable poly(N-isopropylacrylamide) microgel based etalons. *Adv. Mater.* **23**, 4088–92 (2011).

- SPIE Handbook of Microlithography, Micromachining, and Microfabrication: Volume 1.* (SPIE Press, 1997).
- Thakur, V. K., Ding, G., Ma, J., Lee, P. S. & Lu, X. Hybrid materials and polymer electrolytes for electrochromic device applications. *Adv. Mater.* **24**, 4071–96 (2012).
- Tieke, B. Coordinative supramolecular assembly of electrochromic thin films. *Curr. Opin. Colloid Interface Sci.* **16**, 499–507 (2011).
- Toomey, R., Freidank, D. & R  he, J. Swelling Behavior of Thin, Surface-Attached Polymer Networks. *Macromolecules* **37**, 882–887 (2004).
- Ueno, K., Matsubara, K., Watanabe, M. & Takeoka, Y. An Electro- and Thermochromic Hydrogel as a Full-Color Indicator. *Adv. Mater.* **19**, 2807–2812 (2007).
- Ueno, K., Sakamoto, J., Takeoka, Y. & Watanabe, M. Electrochromism based on structural colour changes in a polyelectrolyte gel. *J. Mater. Chem.* **19**, 4778 (2009).
- Voronekov, V. V. & Kokorev, V. N. Synthesis of p-Alkylbenzoic Acids by One-Electron Oxidation of p-Alkyltoluenes. *J. Org. Chem. USSR* **25**, 2302–2305 (1990).
- Walish, J. J., Kang, Y., Mickiewicz, R. a. & Thomas, E. L. Bioinspired Electrochemically Tunable Block Copolymer Full Color Pixels. *Adv. Mater.* **21**, 3078–3081 (2009).
- Walker, J. P. & Asher, S. A. Nerve Agent Sensing Photonic Crystal (PCCA) photonic crystal sensing material that senses the. *Test* **77**, 1596–1600 (2005).
- Wang, X., Qiu, X. & Wu, C. Comparison of the Coil-to-Globule and the Globule-to-Coil Transitions of a Single Poly(N-isopropylacrylamide) Homopolymer Chain in Water. *Macromolecules* **31**, 2972–2976 (1998).
- Wang, X., Qiu, X. & Wu, C. Comparison of the Coil-to-Globule and the Globule-to-Coil Transitions of a Single Poly(N-isopropylacrylamide) Homopolymer Chain in Water. *Macromolecules* **31**, 2972–2976 (1998).
- Weber, M., Stover, C., Gilbert, L., Nevitt, T. & Ouderkirk, A. Giant birefringent optics in multilayer polymer mirrors. *Science* **287**, 2451–6 (2000).
- Weissman, J., Sunkara, H., Tse, A. & Asher, S. Thermally Switchable Periodicities and Diffraction from Mesoscopically Ordered Materials. *Science* **274**, 959–60 (1996).
- Winn, J. N., Fink, Y., Fan, S. & Joannopoulos, J. D. Omnidirectional reflection from a one-dimensional photonic crystal. *Opt. Lett.* **23**, 1573–5 (1998).

- Woo, L. & Sandford, C. L. Comparison of electron beam irradiation with gamma processing for medical packaging materials. *Radiat. Phys. Chem.* **63**, 845–850 (2002).
- Xu, D., Zhu, W., Wang, C., Tian, T., Cui, J., Li, J., Wang, H., Li, G. Molecularly imprinted photonic polymers as sensing elements for the creation of cross-reactive sensor arrays. *Chemistry* **20**, 16620–5 (2014).
- Yoon, J. A., Kowalewski, T. & Matyjaszewski, K. Comparison of Thermoresponsive Deswelling Kinetics of Poly (oligo (ethylene oxide) methacrylate) -Based Thermoresponsive Hydrogels Prepared by “ Graft-from ” ATRP. *Macromolecules* 2261–2268 (2011).
- Yoon, J., Lee, W. & Thomas, E. L. Thermochromic Block Copolymer Photonic Gel. *Macromolecules* **41**, 4582–4584 (2008).
- Yue, Y., Kurokawa, T., Haque, M.A., Nakajima, T., Nonoyama, T., Li, X., Kajiwara, I., Gong, J.P. Mechano-actuated ultrafast full-colour switching in layered photonic hydrogels. *Nat. Commun.* **5**, 4659 (2014).
- Zainuddin, Albinska, J., Ulanski, P. & Rosiak, J. Radiation-induced degradation and crosslinking of poly (ethylene oxide) in solid state. *J. Radioanal. Nucl. Chem.* **253**, 339–344 (2002).
- Zhang, X., Guan, Y. & Zhang, Y. Ultrathin hydrogel films for rapid optical biosensing. *Biomacromolecules* **13**, 92–97 (2012).
- Zhou, K., Lu, Y., Li, J., Shen, L., Zhang, G., Xie, Z., Wu, C. The Coil-to-Globule-to-Coil Transition of Linear Polymer Chains in Dilute Aqueous Solutions: Effect of Intrachain Hydrogen Bonding. *Macromolecules* **41**, 8927–8931 (2008).
- Zhou, S. & Wu, C. In-Situ Interferometry Studies of the Drying and Swelling Kinetics of an Ultrathin Poly(N -isopropylacrylamide) Gel Film below and above Its Volume Phase Transition Temperature. *Macromolecules* **29**, 4998–5001 (1996).
- Zimmermann, L., Weibel, M., Caseri, W., Suter, U. & Walther, R. High refractive index films of polymer nanocomposites. *J. Mater. Res.* **8**, 1742–1748 (1993).